ALL ROADS LEAD TO ERGOSTEROL: HOW STEROLS ARE CRITICAL FOR SPORULATION AND NI TOLERANCE IN *CRYPTOCOCCUS NEOFORMANS*

by

AMBER R. MATHA

(Under the Direction of Xiaorong Lin)

ABSTRACT

Cryptococcus neoformans is a ubiquitous environmental fungus and opportunistic human fungal pathogen. Due to the range of environments this fungus can be exposed to, C. neoformans has many mechanisms in place to tolerate environmental stressors. The plasma membrane is the primary site of response to extracellular stimuli. The lipids and proteins that compose the plasma membrane can be rearranged based on the needs of the cell. Lipids in particular are important for processes such as prospore formation and endocytosis in the yeast Saccharomyces cerevisiae. I found that the spores of C. neoformans are enriched in ergosterol, the main fungal sterol, and that deletion of the transcription factor involved in regulating ergosterol biosynthesis (SRE1) was defective at producing spores. We determined that overexpression of ergosterol biosynthesis genes in this deletion mutant restored sporulation frequencies. I also found that nickel (Ni), a common soil contaminant, reduces cellular ergosterol content and that the SRE1 deletion mutant was extremely sensitive to media supplemented with Ni. The inability of $srel\Delta$ to express ergosterol biosynthesis pathway (EBP) genes is likely the cause of the Ni sensitivity phenotype. I found that overexpression of ERG25, a component of the EBP, was capable of rescuing the $sre 1\Delta$ phenotype. Erg25 is known to bind iron and site-directed mutagenesis of the histidine

residues predicted to interact with the iron ion abolished the ability of the ERG25 overexpression strain to rescue the growth defect of $sre1\Delta$ on Ni. The reduction of sterols by Ni is conserved in mammalian lung epithelial cells. The maintenance of ergosterol is critical for cell survival and understanding of the stimuli and/or cellular processes that cause changes in ergosterol are

important for understanding the biology of this fungus as a whole.

INDEX WORDS:

Cryptococcus neoformans, ergosterol, mating, sporulation, nickel

ALL ROADS LEAD TO ERGOSTEROL: HOW STEROLS ARE CRITICAL FOR SPORULATION AND NI TOLERANCE IN *CRYPTOCOCCUS NEOFORMANS*

by

AMBER R. MATHA

BS, Mercyhurst University, 2018

A Dissertation Submitted to the Graduate Faculty of The University of Georgia in Partial Fulfillment of the Requirements for the Degree

DOCTOR OF PHILOSOPHY

ATHENS, GEORGIA

2024

© 2024

Amber R. Matha

All Rights Reserved

ALL ROADS LEAD TO ERGOSTEROL: HOW STEROLS ARE CRITICAL FOR SPORULATION AND NI TOLERANCE IN *CRYPTOCOCCUS NEOFORMANS*

by

AMBER R. MATHA

Major Professor: Committee: Xiaorong Lin Zachary Lewis Karl Lechtreck Robert Maier

Electronic Version Approved:

Ron Walcott Vice Provost for Graduate Education and Dean of the Graduate School The University of Georgia December 2024

ACKNOWLEDGEMENTS

First and foremost, I would like to thank my P.I., Dr. Xiaorong Lin. When I had a hard time seeing my potential and had low self-confidence, she never ceased to believe in me.

Next, I would like to thank my committee members past and present, Dr. Zachary Lewis, Dr. Karl Lechtreck, Dr. Chang Hyun Khang, and Dr. Robert Maier. I will be forever grateful for their patience, helpful comments, and suggestions. It is a time commitment to serve on a graduate student's committee and I am thankful for their time spent on me.

The Lin Lab is like a family and I would be remiss if I neglected to thank all past and present lab members that I have interacted with. From their suggestions and feedback on manuscript drafts and during lab meetings, to creating friendships at the break room table, I am so glad to have been a part of such a congenial lab.

Lastly, but certainly not least, I would like to thank my family; specifically, my husband Noah and my parents, for always believing in me and for being my biggest cheerleaders through arguably one of the most challenging chapters of my life.

TABLE OF CONTENTS

	Pag	e
ACKNO	WLEDGEMENTS i	V
LIST OF	TABLESv	ii
LIST OF	FIGURESvi	ii
CHAPTI	ER	
1	INTRODUCTION AND LITERATURE REVIEW	1
	Purpose of the study	1
	Human Fungal Pathogen and Environmental Fungus Cryptococcus neoformans	1
	The plasma membrane as a control center for intracellular communication	2
	Mating in C. neoformans	3
	Ergosterols wide-ranging impact on cell biology	4
	References	7
2	ERGOSTEROL IS CRITICAL FOR SPOROGENESIS IN CRYPTOCOCCUS	
	NEOFORMANS1	5
	Abstract1	6
	Introduction1	7
	Materials and methods1	9
	Results2	4
	Discussion	0
	References 3	3

53
54
55
57
70
73
82
118

LIST OF TABLES

Page
Table S2.1: Fungal strains used in this study
Table S2.2: Plasmids and primers used in this study
Table S3.1: Differentially expressed genes H99 Ni vs H99 RPMI
Table S3.2: Differentially expressed genes H99 DMG vs H99 RPMI112
Table S3.3: Differentially expressed genes H99 Hypoxia vs H99 normoxia112
Table S3.4: Differentially expressed genes $srel \Delta$ Ni vs H99 Ni
Table S3.5: Differentially expressed genes $sre1\Delta$ Hypoxia vs H99 Hypoxia112
Table S3.6: Differentially expressed genes shared between H99 Ni vs H99 RPMI and H99
hypoxia vs H99 normoxia data sets
Table S3.7: Fungal strains used in this study
Table S3.8: Primers and plasmids used in this study

LIST OF FIGURES

Page
Figure 1.1: Diagram of the ergosterol biosynthesis pathway in <i>C. neoformans</i> 14
Figure 2.1: Ergosterol is enriched in spores and basidia based on filipin staining40
Figure 2.2: $srel\Delta$ has a sporulation defect in both unilateral and bilateral crosses41
Figure 2.3: Meiosis is occurring in the basidia generated by $sre1\Delta$ crosses
Figure 2.4: Deletion of EBP genes negatively impacts mating
Figure 2.5: Overexpressed ergosterol biosynthetic genes are functional and can restore successful
sporulation in the $srel\Delta$ mutant
Figure S2.1: Impact of $srel\Delta$ on Serotype D mating
Figure S2.2: RT-PCR confirmation of <i>ERG</i> gene overexpression
Figure 3.1: $sre1\Delta$ growth defect is specific to Ni
Figure 3.2: Ni causes increased expression of multiple genes in the ergosterol biosynthesis
pathway95
Figure 3.3: Overexpression of ERG25, but not other ERG genes tested, causes drastically
increased tolerance to Ni in both WT and $sre1\Delta$
Figure 3.4: Ni causes alteration of sterol profiles
Figure 3.5: Mutating histidine enriched pocket abolishes the ability of Erg25 to confer Ni
tolerance
Figure 3.6: Overexpression of Ure7 does not confer Ni tolerance to <i>sre1</i> \(\Delta\)

Figure 3.7: Ni causes a decrease in membrane sterols in A549 lung epithelial cells10	2
Figure S3.1: Urease is not required for Ni tolerance	13
Figure S3.2: Metal accumulation does not dictate metal sensitivity	4
Figure S3.3: Ni and hypoxia have distinct impacts in $sre1\Delta$ and limited similarities in H9910	15
Figure S3.4: Ni and Co elicit overlapping and different effects	6
Figure S3.5: The $sre1\Delta$ sensitivity to Ni is not due to iron starvation	7
Figure S3.6: Neither <i>ERG3</i> nor <i>ERG4</i> is required for cryptococcal tolerance of Ni	8
Figure S3.7: ERG25 is required for tolerance of Co and ERG overexpression can partially restore	·e
the growth defect of $srel \Delta$ in hypoxia	19
Figure S3.8: Erg25 protein sequence contains histidine residues in predicted metal binding	
regions11	0
Figure S3.9: $URE7$ is overexpressed in both wildtype and $sre1\Delta$ backgrounds	1

CHAPTER 1

INTRODUCTION AND LITERATURE REVIEW

Purpose of the study

This study focuses on the fungus *Cryptococcus neoformans*, an environmental fungus and opportunistic human fungal pathogen. The ubiquitous nature of this organism, as well as its ability to cause human disease in immunocompromised individuals, result in this organism being a public health threat. Understanding the cellular biology of this organism can inform future research on treatments to better patient outcomes. In this dissertation, I summarize my work on investigating the role of ergosterol during mating and in the response of *C. neoformans* to metals encountered in the natural environment.

Human fungal pathogen and environmental fungus: Cryptococcus neoformans

Cryptococcus neoformans is a ubiquitous environmental fungus and opportunistic human fungal pathogen that is the cause of death for hundreds of thousands of people every year [1, 2]. The natural reservoirs for *C. neoformans* are pigeon guano, soils, and trees [3]. Humans are exposed to this organism via the inhalation of desiccated yeasts and spores that exist free floating in the air [4]. Immunocompetent individuals are capable of clearing the fungus, or the fungus can remain dormant in the lungs of these individuals without causing disease [5, 6], however, in immunocompromised hosts, this fungus is capable of causing serious disease. *C. neoformans* can disseminate via the bloodstream from the lungs, across the blood-brain barrier, to cause meningitis [7-9]. Without proper treatment, *C. neoformans* infection is uniformly fatal.

As stated previously, *C. neoformans* primarily exists in the environment [10] associated with trees [11], pigeon guano [12], and soil [13]. The natural environment can impose harsh growth conditions and *C. neoformans* has developed mechanisms such as melanin production and capsule formation to tolerate stressful environmental conditions. One way that fungi in general respond to nutrient limited conditions is by undergoing sexual reproduction to produce spores, which are better capable of resisting harsh conditions [14]. Under inductive conditions for mating [15-17] *C. neoformans* can undergo a yeast-to-hypha transition which can allow for nutrient scavenging. Sexual mating can occur both unisexually or bisexually, where unisexual reproduction involves an organism(s) of the same mating type [14, 18], and bisexual mating involving the fusion of two yeast cells of opposite mating types [14, 19]. *C. neoformans* can complete its sexual cycle in pigeon guano [20]. Undergoing mating in the natural environment allows *C. neoformans* to disseminate via the air allowing the fungus increased opportunity to come in contact with a human host [21]. Indeed, spores and desiccated yeasts are small (1-5 μm in diameter), and are able to enter the alveoli of the lungs [21].

The plasma membrane as a control center for intracellular communication

C. neoformans needs to respond to environmental cues in order to survive. The signals that the fungus commonly responds to in the environment are: heat, UV radiation, and low glucose, to name a few. The C. neoformans cell envelope consists of three layers. A polysaccharide capsule, a defining feature and virulence factor for this fungus, is the outermost layer of the cell. The capsule protects the cell body from radiation, desiccation, and other environmental stressors [22]. Another function of the capsule is to mask the cell wall, since the cell wall presents a large number of antigens on its surface. Without capsule, C. neoformans is typically avirulent [23-25]. The cell wall, constructed primarily of β-glucans, chitin, and

chitosan, is a dynamic structure that changes depending on external signals from the environment [26]. The third layer, the plasma membrane (PM), is the location of many sensors that respond to stressful conditions [27]. In addition, the dynamic nature of the PM allows the cells to respond to a variety of stimuli from both outside and inside the cell [28].

Although the cell wall and the capsule are critical for keeping stressors away from the cell body, without transmembrane sensors and receptors, the cell would be unable to adapt to its environment [29]. Indeed, various plasma membrane components are responsible for tolerance to stressors in yeast. *S. cerevisiae* has been found to modify the membrane proteome as a result of osmotic stress [30]. Membrane remodeling has also been observed in *C. neoformans* in response to CO₂, a stress that the fungus must tolerate in order to survive in the human host [31].

Since proteins are typically the biomolecules responsible for signal transduction and environmental sensing, changes to the plasma membrane proteome occur rapidly. However, non-protein components of the cell membrane have proven to be equally as important for responding to environmental stimuli. *S. cerevisiae* utilizes lipid modifications in order to better tolerate heat and salt stress [32, 33]. Both lipids and proteins present in cell membranes are critical for the ability for a cell to maintain membrane potential. In fact, perturbation of sterols in the membrane decreases activities of other proteins in the membrane. For example, deletion of ergosterol biosynthesis pathway (EBP) genes causes a reduction in the activity of Pdr5, a multidrug transporter in *S. cerevisiae* [34]. Sterol content has also been implicated in the ability for the yeast to be able to undergo endocytosis [35].

Mating in C. neoformans

The plasma membrane is critical for signal transduction cascades and one of the most important signaling cascades attributed to virulence and stress response in *C. neoformans* is that

of the yeast to hyphal transition during mating. Pheromone production is the initial signal of the mating pathway in *C. neoformans* and can stimulate hyphal morphogenesis via paracrine as well as autocrine signaling mechanisms [36]. A MAP kinase cascade, stimulated by pheromone sensing, has been shown to regulate the ability for *C. neoformans* to undergo cell-cell fusion [37].

The plasma membrane naturally undergoes changes as a result of budding and also the yeast to hyphal transition. Sterol-rich domains (SRDs), for example, have been observed via filipin staining at the site of bud formation, septa sites, as at the leading edge of conjugation tubes prior to cell fusion [38]. In *S. cerevisiae* the leading edge of a budding cell is highly concentrated with SRDs [39, 40]. Lipid droplets are necessary for successful prospore plasma membrane and cell wall development in *S. cerevisiae* [41]. Indeed, ergosterol depletion inhibits pheromone signaling and plasma membrane fusion [42].

Ergosterol's wide-ranging impact on cell biology

Ergosterol is the fungal equivalent of human cholesterol and is critical for maintaining membrane fluidity. Ergosterol biosynthesis is completed by a long biosynthetic pathway composed of 24 proteins (Figure 1.1 [43]). The ergosterol biosynthesis pathway (EBP) consists of two parts: the mevalonate pathway and the late pathway. The mevalonate pathway starts with the input of Acetyl-CoA and ends with the production of farnesyl pyrophosphate (FPP). FPP can be used as a progenitor for the biosynthesis of other important biomolecules [44]. Two molecules of FPP are used to generate squalene, the starting substrate for the late pathway.

The late pathway is specific for the production of ergosterol; converting squalene to ergosterol. Branching off of the late pathway is an alternative pathway which is activated when Erg11 is inactivated by azole drugs such as fluconazole [45]. The alternative pathway results in

the formation of a fungistatic compound called 14α methylergosta 8-24 (28) dienol. Of all of the EBP genes in the late pathway, seven are non-essential in *S. cerevisiae*. These genes are *ERG24*, *ERG28*, *ERG6*, *ERG2*, *ERG3*, *ERG5*, *ERG4*, and all function during the final biosynthetic steps of the pathway (Figure 1.1).

Mutation of ergosterol biosynthesis pathway genes have far-reaching impacts in fungal cell biology, outside of just diminishing the production of ergosterol end product (reviewed in [46]). Ergosterol deletion mutants are capable of reducing membrane trafficking, defects in mating, increasing tolerance to high temperatures, and fragmenting of vacuoles. Overexpression of EBP genes also impacts cell biology. For example, the overexpression of nine EBP genes in *S. cerevisiae* causes doubling time to increase and all but three EBP overexpression strains had a sensitivity to calcium starvation [43]. Most overexpression strains (19/25) also had reduced growth in high salt [43].

Changes in EBP genes, whether deletion or overexpression, cause changes to the normal cell biology in filamentous fungi as well. In *Aspergillus fumigatus*, *ERG24*, *ERG5*, and *ERG4* are required for successful conidiation [47-49]. The essentiality of *ERG4* for conidiation is conserved in plant pathogens *Penicillium expansum*, *Fusarium graminearum*, and *Magnaporthe oryzae* [50-52]. Not only is conidiation reduced in the *MoERG4* mutant, but the strain also shows a defect in appressorium formation and effector protein secretion, which are both critical for the virulence of this fungus [52].

Deletion of *ERG27* in *S. cerevisiae* induces a petite phenotype, which is caused by a loss of the mitochondrial DNA (mtDNA) [53]. *ERG27* is essential in most other fungal species, however, the ability for *S. cerevisiae* to survive in the absence of mtDNA allows for *ERG27* deletion. Blockage of the EBP by azole drugs and statins also impact the stability of mtDNA by

inducing petite colonies [53, 54]. In addition, in *S. cerevisiae* the presence or absence of mtDNA determines the localization of Erg27 either to lipid droplets or the endoplasmic reticulum, respectively. Loss of mtDNA also reduced the amount of ergosterol present in cell membranes [53]. This shows that not only can ergosterol impact the ability of the plasma membrane to resist stress, but can also impact other organelles.

Here, in this dissertation, I will discuss the role of ergosterol on the successful mating of *C. neoformans* in Chapter 2. Chapter 3 will discuss the impact environmental metals have on ergosterol content in the cells.

References

- 1. Rajasingham R, Smith RM, Park BJ, Jarvis JN, Govender NP, Chiller TM, et al. Global burden of disease of HIV-associated cryptococcal meningitis: an updated analysis. The Lancet infectious diseases. 2017;17(8):873-81.
- 2. Zhao Y, Ye L, Zhao F, Zhang L, Lu Z, Chu T, et al. *Cryptococcus neoformans*, a global threat to human health. *Infectious Diseases of Poverty*. 2023;12(1):20.
- 3. Passoni LC. Wood, animals and human beings as reservoirs for human *Cryptococcus* neoformans infection. Revista Iberoamericana de Micologia. 1999;16(2m):77-81.
- 4. Bahn Y-S, Sun S, Heitman J, Lin X. Microbe profile: *Cryptococcus neoformans* species complex. *Microbiology*. 2020;166(9):797.
- 5. Alanio A. Dormancy in *Cryptococcus neoformans*: 60 years of accumulating evidence.

 The Journal of clinical investigation. 2020;130(7):3353-60.
- 6. Dromer F, Ronin O, Dupont B. Isolation of *Cryptococcus neoformans* var. gattii from an Asian patient in France: evidence for dormant infection in healthy subjects. *Journal of Medical and Veterinary Mycology*. 1992;30(5):395-7.
- 7. Perfect JR, Casadevall A. Cryptococcosis. *Infectious Disease Clinics*. 2002;16(4):837-74.
- 8. Nielsen K, Cox GM, Litvintseva AP, Mylonakis E, Malliaris SD, Benjamin DK, Jr., et al. *Cryptococcus neoformans* a strains preferentially disseminate to the central nervous system during coinfection. *Infect Immun*. 2005;73(8):4922-33. PubMed PMID: 16041006.
- 9. Dromer F, Levitz SM. Invasion of *Cryptococcus* into the central nervous system.

 *Cryptococcus: From Human Pathogen to Model Yeast. 2010:465-71.

- 10. Levitz SM. The ecology of *Cryptococcus neoformans* and the epidemiology of cryptococcosis. *Reviews of infectious diseases*. 1991;13(6):1163-9.
- 11. Lazera M, Pires F, Camillo-Coura L, Nishikawa M, Bezerra C, Trilles L, et al. Natural habitat of *Cryptococcus neoformans* var. neoformans in decaying wood forming hollows in living trees. *Journal of medical and veterinary mycology*. 1996;34(2):127-31.
- 12. Cafarchia C, Romito D, Iatta R, Camarda A, Montagna MT, Otranto D. Role of birds of prey as carriers and spreaders of *Cryptococcus neoformans* and other zoonotic yeasts.

 *Medical Mycology. 2006;44(6):485-92.
- 13. Emmons CW. Isolation of *Cryptococcus neoformans* from soil. *Journal of bacteriology*. 1951;62(6):685-90.
- 14. Fu C, Sun S, Billmyre RB, Roach KC, Heitman J. Unisexual versus bisexual mating in *Cryptococcus neoformans*: Consequences and biological impacts. *Fungal Genetics and Biology*. 2015;78:65-75.
- 15. Kwon-Chung K. A new genus, Filobasidiella, the perfect state of *Cryptococcus neoformans*. *Mycologia*. 1975;67(6):1197-200.
- 16. Kwon-Chung K. Morphogenesis of *Filobasidiella neoformans*, the sexual state of *Cryptococcus neoformans*. *Mycologia*. 1976;68(4):821-33.
- 17. Alspaugh JA, Davidson RC, Heitman J. Morphogenesis of *Cryptococcus neoformans*.

 Contributions to microbiology. 2000;5:217-38.
- 18. Wang L, Lin X. Mechanisms of unisexual mating in *Cryptococcus neoformans*. Fungal Genetics and Biology. 2011;48(7):651-60.

- 19. Zhao Y, Lin J, Fan Y, Lin X. Life Cycle of *Cryptococcus neoformans*. *Annu Rev Microbiol*. 2019;73:17-42. Epub 2019/05/15. doi: 10.1146/annurev-micro-020518-120210. PubMed PMID: 31082304.
- 20. Nielsen K, De Obaldia AL, Heitman J. *Cryptococcus neoformans* mates on pigeon guano: implications for the realized ecological niche and globalization. *Eukaryotic cell*. 2007;6(6):949-59.
- 21. Velagapudi R, Hsueh Y-P, Geunes-Boyer S, Wright JR, Heitman J. Spores as infectious propagules of *Cryptococcus neoformans*. *Infection and immunity*. 2009;77(10):4345-55.
- 22. O'Meara TR, Alspaugh JA. The *Cryptococcus neoformans* capsule: a sword and a shield. *Clinical microbiology reviews*. 2012;25(3):387-408.
- 23. Chang YC, Kwon-Chung K. Complementation of a capsule-deficient mutation of *Cryptococcus neoformans* restores its virulence. *Molecular and cellular biology*. 1994;14(7):4912-9.
- 24. Chang YC, Penoyer LA, Kwon-Chung K. The second capsule gene of *Cryptococcus* neoformans, CAP64, is essential for virulence. *Infection and immunity*. 1996;64(6):1977-83.
- 25. Moyrand F, Fontaine T, Janbon G. Systematic capsule gene disruption reveals the central role of galactose metabolism on *Cryptococcus neoformans* virulence. *Molecular microbiology*. 2007;64(3):771-81.
- 26. O'Meara TR, Holmer SM, Selvig K, Dietrich F, Alspaugh JA. *Cryptococcus neoformans*Rim101 is associated with cell wall remodeling and evasion of the host immune responses. *MBio*. 2013;4(1):10.1128/mbio. 00522-12.

- 27. Rutherford JC, Bahn Y-S, Van Den Berg B, Heitman J, Xue C. Nutrient and stress sensing in pathogenic yeasts. *Frontiers in Microbiology*. 2019;10:442.
- 28. Marguet D, Lenne PF, Rigneault H, He HT. Dynamics in the plasma membrane: how to combine fluidity and order. *The EMBO journal*. 2006;25(15):3446-57.
- 29. Brown SM, Campbell LT, Lodge JK. *Cryptococcus neoformans*, a fungus under stress. *Current opinion in microbiology*. 2007;10(4):320-5.
- 30. Szopinska A, Degand H, Hochstenbach J-F, Nader J, Morsomme P. Rapid response of the yeast plasma membrane proteome to salt stress. *Molecular & Cellular Proteomics*. 2011;10(11).
- 31. Ristow LC, Jezewski AJ, Chadwick BJ, Stamnes MA, Lin X, Krysan DJ. *Cryptococcus neoformans* adapts to the host environment through TOR-mediated remodeling of phospholipid asymmetry. *Nature communications*. 2023;14(1):6587.
- 32. Chatterjee MT, Khalawan SA, Curran BP. Cellular lipid composition influences stress activation of the yeast general stress response element (STRE). *Microbiology*. 2000;146(4):877-84.
- 33. Carratù L, Franceschelli S, Pardini CL, Kobayashi GS, Horvath I, Vigh L, et al.

 Membrane lipid perturbation modifies the set point of the temperature of heat shock
 response in yeast. *Proceedings of the National Academy of Sciences*. 1996;93(9):3870-5.
- 34. Kodedová M, Sychrová H. Changes in the sterol composition of the plasma membrane affect membrane potential, salt tolerance and the activity of multidrug resistance pumps in Saccharomyces cerevisiae. *PLoS One*. 2015;10(9):e0139306.

- 35. Degreif D, Cucu B, Budin I, Thiel G, Bertl A. Lipid determinants of endocytosis and exocytosis in budding yeast. *Biochimica Et Biophysica Acta (BBA)-Molecular and Cell Biology of Lipids*. 2019;1864(7):1005-16.
- 36. Shen W-C, Davidson RC, Cox GM, Heitman J. Pheromones stimulate mating and differentiation via paracrine and autocrine signaling in *Cryptococcus neoformans*. *Eukaryotic cell*. 2002;1(3):366-77.
- 37. Lin X, Jackson JC, Feretzaki M, Xue C, Heitman J. Transcription factors Mat2 and Znf2 operate cellular circuits orchestrating opposite-and same-sex mating in *Cryptococcus neoformans*. *PLoS genetics*. 2010;6(5):e1000953.
- 38. Nichols CB, Fraser JA, Heitman J. PAK kinases Ste20 and Pak1 govern cell polarity at different stages of mating in *Cryptococcus neoformans*. *Molecular biology of the cell*. 2004;15(10):4476-89.
- 39. Alvarez FJ, Douglas LM, Konopka JB. Sterol-rich plasma membrane domains in fungi. *Eukaryotic cell*. 2007;6(5):755-63.
- 40. Athanasopoulos A, Andre B, Sophianopoulou V, Gournas C. Fungal plasma membrane domains. *FEMS microbiology reviews*. 2019;43(6):642-73.
- Hsu T-H, Chen R-H, Cheng Y-H, Wang C-W. Lipid droplets are central organelles for meiosis II progression during yeast sporulation. *Molecular biology of the cell*. 2017;28(3):440-51.
- 42. Jin H, McCaffery JM, Grote E. Ergosterol promotes pheromone signaling and plasma membrane fusion in mating yeast. *The Journal of cell biology*. 2008;180(4):813-26.

- 43. Bhattacharya S, Esquivel BD, White TC. Overexpression or deletion of ergosterol biosynthesis genes alters doubling time, response to stress agents, and drug susceptibility in *Saccharomyces cerevisiae*. *MBio*. 2018;9(4):10.1128/mbio. 01291-18.
- 44. Albertsen L, Chen Y, Bach LS, Rattleff S, Maury J, Brix S, et al. Diversion of flux toward sesquiterpene production in *Saccharomyces cerevisiae* by fusion of host and heterologous enzymes. *Applied and Environmental Microbiology*. 2011;77(3):1033-40.
- 45. Jordá T, Puig S. Regulation of ergosterol biosynthesis in *Saccharomyces cerevisiae*. *Genes*. 2020;11(7):795.
- 46. Johnston EJ, Moses T, Rosser SJ. The wide-ranging phenotypes of ergosterol biosynthesis mutants, and implications for microbial cell factories. *Yeast*. 2020;37(1):27-44.
- 47. Long N, Xu X, Zeng Q, Sang H, Lu L. Erg4A and Erg4B are required for conidiation and azole resistance via regulation of ergosterol biosynthesis in *Aspergillus fumigatus*.

 Applied and environmental microbiology. 2017;83(4):e02924-16.
- 48. Long N, Zhong G. The C-22 sterol desaturase Erg5 is responsible for ergosterol biosynthesis and conidiation in *Aspergillus fumigatus*. *Journal of Microbiology*. 2022;60(6):620-6.
- 49. Li Y, Dai M, Zhang Y, Lu L. The sterol C-14 reductase Erg24 is responsible for ergosterol biosynthesis and ion homeostasis in *Aspergillus fumigatus*. *Applied Microbiology and Biotechnology*. 2021;105:1253-68.
- 50. Han Z, Zong Y, Zhang X, Gong D, Wang B, Prusky D, et al. Erg4 is involved in ergosterol biosynthesis, conidiation and stress response in *Penicillium expansum*. *Journal of Fungi*. 2023;9(5):568.

- 51. Liu X, Jiang J, Yin Y, Ma Z. Involvement of FgERG4 in ergosterol biosynthesis, vegetative differentiation and virulence in *Fusarium graminearum*. *Molecular plant pathology*. 2013;14(1):71-83.
- 52. Guo Z, Liu X, Wang N, Mo P, Shen J, Liu M, et al. Membrane component ergosterol builds a platform for promoting effector secretion and virulence in *Magnaporthe oryzae*.

 New Phytologist. 2023;237(3):930-43.
- 53. Cirigliano A, Macone A, Bianchi MM, Oliaro-Bosso S, Balliano G, Negri R, et al. Ergosterol reduction impairs mitochondrial DNA maintenance in S. cerevisiae. Biochimica et Biophysica Acta (BBA)-Molecular and Cell Biology of Lipids. 2019;1864(3):290-303.
- 54. Cirigliano A, Amelina A, Biferali B, Macone A, Mozzetta C, Bianchi MM, et al. Statins interfere with the attachment of *S. cerevisiae* mtDNA to the inner mitochondrial membrane. *Journal of Enzyme Inhibition and Medicinal Chemistry*. 2020;35(1):129-38.

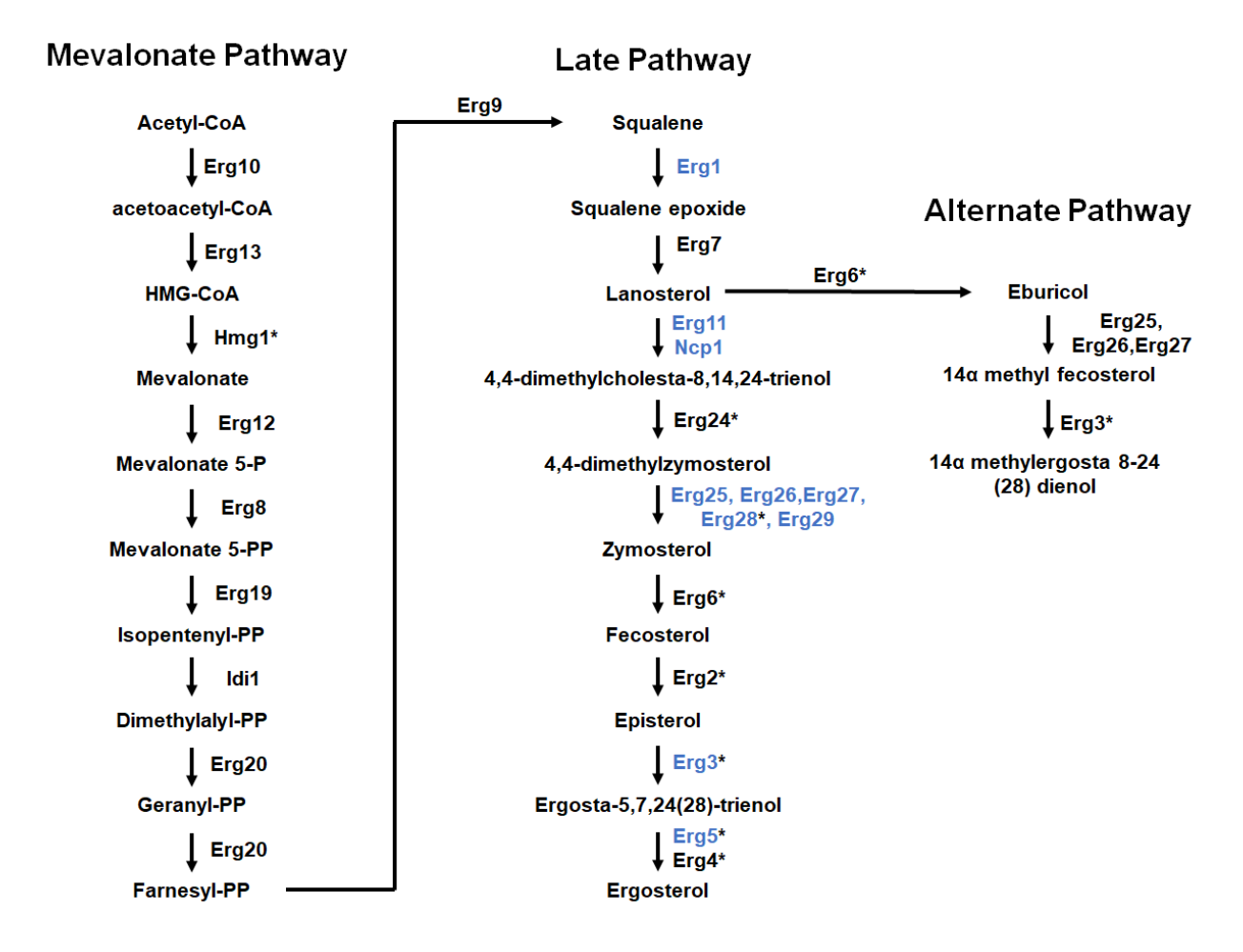


Figure 1.1: Diagram of the ergosterol biosyntheis pathway in C. neoformans

Enzymes written in blue require oxygen for their enzymatic step. Enzymes labeled with an asterisk are non-essential genes.

CHAPTER 2

ERGOSTEROL IS CRITICAL FOR SPOROGENSIS IN CRYPTOCOCCUS NEOFORMANS

¹ Amber R. Matha, Xiaofeng Xie, and Xiaorong Lin*. 2024. *Journal of Fungi*. © 2024 by the authors. Licensee MDPI, Basel, Switzerland. Reprinted here with permission of publisher

Abstract

Microbes, both bacteria and fungi, produce spores to survive stressful conditions. Spores produced by the environmental fungal pathogen Cryptococcus neoformans serve as both surviving and infectious propagules. Because of their importance in disease transmission and pathogenesis, factors necessary for cryptococcal spore germination are being actively investigated. However, little is known about nutrients critical for sporogenesis in this pathogen. Here, we found that ergosterol, the main sterol in fungal membranes, is enriched in spores relative to yeasts and hyphae. In C. neoformans, the ergosterol biosynthesis pathway (EBP) is upregulated by the transcription factor Sre1 in response to conditions that demand elevated ergosterol biosynthesis. Although the deletion of SRE1 enhances the production of mating hyphae, the $srel\Delta$ strain is deficient at producing spores even when crossed with a wild-type partner. We found that the defect of the $sre1\Delta$ strain is specific to sporogenesis, not meiosis or basidium maturation preceding sporulation. Consistent with the idea that sporulation demands heightened ergosterol biosynthesis, EBP mutants are also defective in sporulation. We discovered that the overexpression of some EBP genes can largely rescue the sporulation defect of the $sre1\Delta$ strain. Collectively, we demonstrate that ergosterol is a critical component in cryptococcal preparation for sporulation.

Key words

Cryptococcus neoformans, mating, sporulation, ergosterol

Introduction

Sporulation is a cell survival strategy employed by prokaryotic and eukaryotic microbes to survive in harsh conditions that, otherwise, inhibit vegetative growth. Bacteria, such as Bacillus, can produce endospores via asymmetric cell division, which results in the production of a spore developing inside the mother cell [1]. These spores are resistant to various types of stress that the mother cells are sensitive to, allowing the spores to persist [2].

One defining feature distinguishing eukaryotes from prokaryotes is that spores can be produced in the former organisms via sexual reproduction with meiosis. One of the model species for studying sexual reproduction is the pathogenic basidiomycete fungus *Cryptococcus neoformans*. This fungus was first characterized in 1894 [3] and has been recognized as an asexual yeast with mitotic divisions both in the environment and the host. The sexual cycle of *C. neoformans*, with its characteristic morphological changes from yeasts to hyphae and to fruiting bodies, was not defined until the 1970s by Dr. June-Kwon Chung [4,5]. In addition to producing resilient sexual spores, the morphological transition to hyphae better allows for nutrient scavenging and protection against predation by soil amoeba [6,7].

Given the fact that spores are resistant to stressful environments and are infectious agents that can cause fatal cryptococcal meningitis [8,9], several groups, including the pioneers Dr. June-Kwon Chung and Dr. Joseph Heitman, have dedicated their work to dissecting the mating process [5,10-15]. Two modes of sexual reproduction are discovered in this fungus: unisexual and bisexual reproduction [4,16]. Unisexual reproduction is mainly achieved via cells of a single mating type generating hyphae and spores after endoduplication to double its DNA content prior to meiosis [14]. By contrast, bisexual mating occurs when cells of two mating types, α and a, conjugate with each other in response to pheromones, forming a dumbbell-shaped zygote [13]

(Figure 2.1A). The zygote then grows polarly as dikaryotic hyphae with two parental nuclei migrating in synchronization without nuclear fusion. Hyphal extension can occur indefinitely until unknown stimuli cause the aerial hyphal tip to swell and become a basidium. Here, the two parental nuclei fuse, undergoing meiosis and repeated rounds of mitosis to give rise to four haploid spore chains that bud off the surface of the basidium (Figure 2.1A) [4,10,17].

Spores are markedly reduced in metabolic activities compared to other cell types [8,18,19]. Because of this, spores must come packaged with much of the cellular material necessary for germination, since the generation of major biomolecules requires the transcription and translation of the enzymes to build them. Ergosterol is a major component of the cell membrane, responsible for membrane rigidity and integrity. Current antifungal drugs used to treat cryptococcosis, such as amphotericin B or fluconazole, target ergosterol directly or the EBP pathway. Consequently, the EBP mutants show increased sensitivity to these antifungals [20,21]. Spores are particularly resistant to antifungal drug exposure [22]. Thus, we hypothesize that the EBP pathway is important in sexual reproduction, especially sporulation.

The main transcription factor that upregulates the transcription of EBP genes is Sre1. Previously, Sre1 or its homologues have primarily been investigated for their role in response to hypoxia in humans and fungi [23,24]. Little research has been conducted to investigate other roles this transcription factor might have during normal cellular development. Given the critical nature of cholesterol for oogenesis in mammals [25–27], we postulate that ergosterol is important during sexual reproduction in lower eukaryotes like fungi.

Analyzing recently published RNA-seq data indicates that *SRE1* is upregulated (almost four-fold increase) on mating-inducing V8 media compared to rich YPD media favorable for vegetative yeast growth [28]. The transcript level of *SRE1* is further increased over time on V8

media [29], suggesting that this transcription factor might be more critical for the later step(s) of the mating process. Surprisingly, a previous study reported that the $sre1\Delta$ mutant showed enhanced mating based on visual observation of increased filamentation [30]. However, the potential role of Sre1 in the later steps of the mating process has not been thoroughly investigated. In this study, we found that although the $sre1\Delta$ mutant indeed showed enhanced filamentation when crossed with a wild-type partner compared to a wild-type cross during bisexual mating, the mutant cross was deficient at sporulation. As we demonstrate in this paper, this defect is tightly linked to the role of Sre1 in increasing EBP genes.

Materials and Methods

Strains and Growth Conditions

The *C. neoformans* strains used in this study are listed in Table S1. Strains were stored at 80 °C in glycerol stocks and freshly streaked out prior to experimentation. Cells were maintained on YPD medium at 30 °C unless stated otherwise.

Mating

Mating was conducted on V8 pH = 5 agar media for serotype A crosses and V8 pH = 7 agar media for serotype D crosses [11]. Equal number of cells of both mating partners (OD600 = 3) were mixed together, and 10 μ L of this mixture was spotted onto the plate. The mating crosses were carried out at 21 °C in the dark for approximately two weeks.

Growth Assays

To examine vegetative yeast growth, the tested strains were grown in a YPD liquid medium overnight at 30 $^{\circ}$ C with shaking. Cells were washed with sterile water and adjusted to a cell density of OD600 = 0.1. The cell suspensions were then inoculated into a 96-well plate

incubated at 30 °C for two days in an Epoch 2 plate reader. OD₆₀₀ was read every hour for the duration of the experiment.

To examine fluconazole sensitivity, the tested strains were grown in YPD liquid medium overnight at 30 °C with shaking. Cells were washed with sterile water, adjusted to a cell density of $OD_{600} = 1$, and serially diluted in 10-fold increments. The prepared cells were spotted onto YNB agar media as well as YNB agar media with the indicated concentration of fluconazole.

Gene Manipulation

For gene deletion, the SRE1 deletion cassette was amplified from genomic DNA (gDNA) of a *sre1*Δ mutant, which is part of the C. neoformans transcription factor deletion library generated by Dr. Yong-Sun Bahn and colleagues [30]. All primers used in this study are listed in Table S2. To generate the sgRNA for the *SRE1* deletion, the U6 promoter and sgRNA scaffold were amplified from JEC21 gDNA and the plasmid pDD162, using primer pairs Linlab4627/Linlab7751 and Linlab4628/Linlab7752, respectively. The U6 promoter and sgRNA scaffold pieces were fused together by overlap PCR with primers Linlab4594/Linlab4595 to generate the final sgRNA construct as described previously [31,32].

For gene overexpression, open reading frames (ORFs) were amplified via PCR using the genomic DNA of C. neoformans H99 as the template and cloned into vectors containing either the *TEF1* (pLinlab995) or the *GPD1* (pLinlab1059) promoter. The resulting plasmids were confirmed via restriction enzyme digestion. M13F and M13R primers were used to amplify the donor DNA for Transient CRISPR-Cas9 coupled with electroporation (TRACE) [33], and constructs were inserted into the safe haven *SH2* region [34].

Overexpression and deletion constructs were transformed into the indicated *C. neoformans* strains via TRACE [31,32]. Transformants were selected on YPD medium with 100

μg/mL of nourseothricin (NAT), 100 μg/mL of neomycin (NEO), or 200 μg/mL of hygromycin (HYG), depending on the drug marker used.

The successful deletion of *SRE1* was screened via diagnostic PCR. Primers 8488 and 4897, which lie on the *SRE1* open reading frame, were used to ensure that the ORF was missing. Primer pairs 4895 (a *SRE1* promoter forward) and 3792 (an inside NAT reverse primer) were used to ensure that the NAT cassette was inserted into the *SRE1* original locus. The successful integration of EBP gene overexpression constructs into the *SH2* region was screened via 3-primer PCR [35]. Since the construct can be inserted into the *SH2* region in either the forward or the reverse direction, primer 5936, a reverse primer on the overexpression construct, was paired with *SH2* sequencing primers 4814 and 4815. Regardless of the direction in which the construct was inserted into the *SH2* site, or whether it was not inserted at all, a band would amplify with the three primer PCRs, and the size of the band indicated which of the three situations had occurred in the tested transformants.

All primers and plasmids used in this study are listed in Table S2.

RNA Extraction and Real-Time PCR

Real Time PCR (RT-PCR) was used to confirm the ergosterol biosynthesis gene overexpression. Cells were grown in YPD liquid cultures with shaking at 30 °C overnight. They were collected, flash-frozen with liquid nitrogen, and lyophilized overnight. Desiccated cells were manually disrupted with glass beads, and total RNA was extracted using the PureLink RNA Mini Kit (Invitrogen, Waltham, MA, USA) according to the instruction of the manufacturer. To remove DNA contamination, samples were treated with DNase using the TURBO DNA-free Kit (Invitrogen). First strand cDNA was synthesized using the GoScript Reverse Transcription System (Promega, Madison, WI, USA) following the manufacturer's instructions. Power SYBR

Green (Invitrogen) was used for all RT-PCR reactions. *TEF1* was used as an endogenous control for all RNA samples. All RT-PCR primers used are listed in Table S2. Relative transcript level was determined using the $\Delta\Delta$ Ct method as we described previously [37], and statistical significance was determined using Student's t-test.

Microscopy

For fluorescence observation of filipin stainingor Dmc1-mCherry, samples were observed with a Zeiss Imager M2 microscope equipped with an AxioCam 506 mono camera. The mNG signal was visualized using the filter FL filter set 38 HE GFP (Carl Zeiss Microscopy, Munich, Germany). Filipin was visualized with the FL Filter Set 49 DAPI (Carl Zeiss Microscopy). The mCherry signal was visualized with the FL filter set 43 HE cy3 (Carl Zeiss Microscopy). All fluorescence images except field of view images were taken with a Zeiss 63x apochromat oil objective with a numerical aperture of 1.4. The field-of-view images were taken with the Zeiss 40x Plan-Neofluar objective lens with a numerical aperture of 0.75.

The fluorescence intensity, cell length, and cell diameter were quantified via Zen Pro software (Carl Zeiss Microscopy). Yeast and basidial surface areas were estimated by calculating the surface area of a sphere:

$$SA_{\text{yeast/basidium}} = 4\pi r^2 \tag{1}$$

Hyphal and spore surface areas were estimated by calculating the surface area of a cylinder:

$$SA_{hypha/spore} = 2\pi r(r+h)$$
 (2)

For mating colony imaging, a SZX16 stereoscope (Olympus) was used to observe whole colony and colony edge morphologies. Images were captured with an AxioCam 305 camera (Carl Zeiss Microscopy) and acquired using the Zen Pro software (Carl Zeiss Microscopy).

For imaging of basidia still on the V8 agar, a CX41 light microscope (Olympus) equipped with an AxioCam 305 camera (Carl Zeiss Microscopy) was used. The objective used for these images was an Olympus PlanC N 10X objective with a numerical aperture of 0.25.

Filipin Staining

Equal numbers of cells of both mating partners were mixed and cocultured on V8 pH = 5 plates and incubated at 21 °C in the dark for two weeks. Spores and basidia were scraped from the agar and inoculated into dH2O. Then, 1 μ L of 50 mg/mL filipin dissolved in DMSO was added to 99 μ L of cell suspension. After 15 min of incubation in the dark, the cells were visualized. Fluorescence intensity was quantified in Zen Pro software (Carl Zeiss Microscopy).

Results

Ergosterol Is Enriched in Basidia and Spores Based on Filipin Staining

Cryptococcal spores contain fewer ergosterol biosynthesis pathway proteins (EBPs) than yeast cells [18]. In *Fusarium* spp., EBP proteins increase only after 7–11 h post germination [38]. Therefore, spores must utilize the already present ergosterol, either stored in lipid bodies or the membrane that is derived from basidial cell membrane, for renewed growth before sufficient new ergosterol can be synthesized. We hypothesized that ergosterol would be enriched in basidia (also known as stem cells for sporulation) and spores. To test our hypothesis, we used the filipin stain to quantify relative ergosterol levels in different cryptococcal cell types. Filipin specifically binds to cholesterol in animals and ergosterol in fungi [39]. We found that the median filipin signal was 40-fold higher in spores than that in yeast cells or hyphae per surface area (Figure 2.1B,C). The median filipin signal for basidia was five times higher than yeast cells (Figure 2.1B,C). We noticed that ergosterol was not even distributed in the cell membrane. Rather, it was

accumulated at the leading edge of the basidial heads and at the septa of hyphae. The distribution of filipin stain was more even along the periphery of spores and yeast cells.

Crosses Involving $sre1\Delta$ Produce Abundant Hyphae but Are Defective at Sporulation

Ergosterol is synthesized from acetyl-CoA through 19 reactions carried out by 23 EBP enzymes. Sre1 is a transcription factor that governs the transcription of EBP genes in response to conditions that require enhanced ergosterol biosynthetic activities such as hypoxia or in the presence of antifungals that inhibit EBP enzymes [23,40]. Although deletion of the SRE1 gene reduces the total amount of ergosterol in the cell [23] based on filipin staining (Figure 2.2A), vegetative yeast growth of the $SRE1\Delta$ mutant is comparable to the wild type (Figure 2.2B).

During bisexual reproduction, two yeast cells of opposite mating types fuse and form dikaryotic hyphae. Given that H99 background strains do not self-filament on V8 media, filamentation is only produced after successful bisexual mating, which is visually observable as a fluffy white edge from the original yeast colonies with mixed $\bf a$ and α cells (Figure 2.2C). Here, we found that in unilateral bisexual crosses where the $srel\Delta$ mutant mated with a compatible wild-type partner ($srel\Delta$ $\bf a$ xH99 α or $srel\Delta$ α x KN99 $\bf a$), more abundant filamentation was produced compared to the WT cross (Figure 2.2C). This is in agreement with previous observations that describe this mutant as being enhanced for mating [30]. Interestingly, a bilateral cross between two $srel\Delta$ mutants had reduced filamentation (Figure 2.2C). This suggests that one copy of SREl is necessary during bisexual mating to cause the enhanced filamentation phenotype.

Basidia and basidiospores form after two weeks in a wild-type cross on V8 media. More than 80% of basidial heads carried four spore chains by this time point, resulting from repeated mitosis after one meiotic event (Figures 2.1A and 2.2C). However, in unilateral crosses where

one of the mating partners was a $sre1\Delta$ mutant (e.g., α x $sre1\Delta$ a or a x $sre1\Delta$ α), 92% of the basidia were deficient at producing spores after two weeks (Figure 2.2C). The sporulation defect persisted even after three and four weeks. There were rare occurrences of spore chains forming in $sre1\Delta$ unilateral crosses (8% of basidia); however, the vast majority of the basidia observed were barren (no spores) or had abnormal numbers of single spores (Figure 2.2D). Only ~10% of basidia were observed producing spore chains in unilateral crosses involving a $sre1\Delta$ mutant, compared to ~80% of basidia in the wild-type cross.

The fact that this sporulation defect was observed when the SRE1 gene was deleted in either the \mathbf{a} or the α mating partner indicates that this is not a mating type-specific phenomenon, and there is a haploinsufficiency for Sre1 during sporulation. Thus, functional Sre1 from both mating partners is required for normal sporulation. The bilateral cross of two $srel\Delta$ partners $(sre1\Delta \mathbf{a} \times sre1\Delta \alpha)$ showed an even more severe defect in sporulation where 95% of basidia were barren, 5% showed single spores, and none carried spore chains (Figure 2.2D). To test if the role of Srel in sporulation is specific to the serotype A reference strain H99, we deleted the SRE1 gene in the serotype D congenic pair strains JEC21α/JEC20a. The serotype D reference pair strains mate more robustly than the serotype A reference strain pair H99α/KN99a. Interestingly, a unilateral cross between wildtype JEC20a and the $sre1\Delta$ JEC21a did not filament as well as the wild type JEC21\alpha/JEC20a cross (Supplementary Figure S2.1). Nonetheless, the unilateral cross involving a sre $I\Delta$ mutant showed a sporulation defect, with 92% of basidia being barren or having produced only a single spore (Supplementary Figure S2.1). Therefore, the impact of haploid insufficiency of SRE1 on sporulation is conserved among the C. neoformans species.

It is known that maturation of basidia plays an important role in the ability of the basidial head to produce spores [29]. Thus, we hypothesized that the defect in sporulation could be caused by a defect in the basidial head maturation process. The basidial maturation score (BMS), an index derived from the division of the diameter of the widest part of the basidium by the diameter of the hypha at the base of the basidium (Figure 2.2E), was recently developed to determine the maturity of the basidia [29]. Basidia with maturation scores greater than 1.6 are considered mature basidia [29]. We measured the diameter of basidia generated from a wild-type cross, a $sre1\Delta$ unilateral cross, and a $sre1\Delta$ bilateral cross after 2 weeks. We found that all H99 BMS scores were greater than 1.6, indicating all of them were mature by this time point. Although the $sre1\Delta$ unilateral cross had some basidia of low BMS, 75% of the basidia examined were mature basidia that should be capable of sporulation (Figure 2.2E). Likewise, 71% of basidia from $sre1\Delta$ bilateral cross were also mature (Figure 2.2E). Basidia from both $sre1\Delta$ unilateral and bilateral crosses had single spores protruding with BMS scores at or over 1.6, similar to the wild-type basidia. Therefore, the minor population of immature basidia in crosses involving the $srel\Delta$ mutant does not account for the sporulation defect observed in the vast majority of the basidia.

sre 1 A Sporulation Defect Is Not Due to a Defect in Meiosis Gene Activation

The basidial head is the site of karyogamy, meiosis, and sporogenesis during bisexual reproduction [10] (Figure 2.1A). Mature basidia from the $sre1\Delta$ mutant that were incapable of producing spores could be deficient in completing meiosis or sporogenesis. Because cholesterol intermediates have been identified as activators of meiosis in oocytes in vitro [33], we hypothesized that meiosis may be blocked in the $sre1\Delta$ mutant due to reduced sterol content. Dmc1 is a recombinase known to mediate homologous recombination during double-stranded

break repair caused by crossing-over events in meiosis. In *C. neoformans*, Dmc1 is required for meiosis and sporulation [14]. Dmc1 is exclusively expressed in aerial hypha tips as the basidium develops and it disappears once sporulation starts [41]. The expression of this gene has also been used to determine if genes of interest are up or downstream of the meiotic event during mating [29].

To examine meiotic process, we decided to monitor the activation of Dmc1 using a fluorescently labeled Dmc1 with its expression driven by its own promoter. We found that Dmc1 was expressed in basidia generated from a $sre1\Delta$ unilateral bisexual cross, similar to its expression in basidia produced by a wild-type cross (Figure 2.3A). Thus, meiosis was initiated in the basidia from the $sre1\Delta$ involved crosses. The fluorescence intensity of the basidia had no significant difference, suggesting that the amount of Dmc1 was comparable between both crosses (Figure 2.3B). As four meiotic nuclei are generated as the end product of meiosis, we decided to determine if meiosis can be completed in the $sre1\Delta$ involved crosses by examining the presence of nuclei in mature basidia. To visualize the nuclei, we used a strain constitutively expressing mNeonGreen with a nuclear localization signal (NLS-mNG) as the mating partner of the $sre1\Delta$ mutant [42]. We found basidia with more than two nuclei, suggesting that meiosis was completed in these crosses (Figure .23C). Taken together, our results suggest that basidial maturation and meiosis can be completed in the $sre1\Delta$ involved crosses, and the defect of sporulation is most likely due to a defect in the late sporogenesis process itself.

Defective EBP Pathway Leads to Sporulation Defect

The EBP consists of 23 proteins that execute a series of reactions to transform acetyl Co-A into ergosterol. Many of these genes are essential, but a few genes (*ERG*2, 3, 4, and 5) encoding enzymes that function in the late step reactions are not (45). To determine if mutants

defective in the EBP pathway enzymes are also defective in sporulation, we examined filamentation and sporulation of crosses involving $erg3\Delta$ and $erg4\Delta$ mutants (Figure 2.4). Filipin staining showed that the $erg4\Delta$ and the $erg3\Delta$ mutants were less ergosterol rich than the H99 wildtype (Figure 2.4A). Indeed, the filipin signal in wildtype cells was 1.8 and 2.1 times higher than $erg4\Delta$ and $erg3\Delta$, respectively (Figure 2.4B). This reduction in filipin signal is similar to the reduction caused by the $sre1\Delta$ (Figure 2.2A).

Unilateral crosses with these mutants generated abundant hyphae (mutant x wild type), but filamentation was severely impaired in bilateral crosses (mutant x mutant) (Figure 2.4C,D). This indicates that one copy of the penultimate EBP genes is sufficient for filamentation to occur but is not sufficient to support wildtype levels of sporulation. Indeed, filamentation did not occur in a cross where neither parent possesses these EBP genes. This shows that the final ergosterol product is necessary for successful filamentation as well as sporulation. For instance, 55% of basidia from an $erg4\Delta$ unilateral cross were barren, and 16% bore single spores. Only 29% carried four chains of spores (Figure 2.4E,F). The $erg3\Delta$ unilateral cross yielded similar sporulation frequencies with 45% of basidia being barren, 16% having single spores, and 28% of basidia producing four chains of spores. The results indicate that sporulation is sensitive to even a modest deficiency of sterols, mimicking the unilateral crosses of the $sre1\Delta$ mutant.

Overexpression of Multiple Individual EBP Genes Partially Restore sre1 Δ 's Sporulation

Defect

As Sre1 upregulates the expression of some EBP genes in response to stresses that require increased expression of the EBP pathway (Figure 2.5A), we wondered if overexpressing EBP genes could compensate for the lack of Sre1 and rescue the sporulation defect. Here, we selected *ERG2*, *ERG11*, *ERG25*, *ERG26*, and *ERG27* for overexpression. Erg25 was chosen because it is

a known direct target of Sre1 [24]. Erg26 and Erg27 are known to form complexes with Erg25 in Saccharomyces [45,46]. We chose Erg11 because it is the target of fluconazole and Erg2 because it is a target of the morpholine class of antifungal drugs and lies downstream of *ERG11* [47]. The overexpression constructs of these *ERG* genes driven by the *TEF1* promoter were all integrated into the "safe haven" region *SH2* of the H99 genome to avoid any position effect [34].

The overexpression of these ERG genes was confirmed via RT-PCR (Supplementary Figure S2.2). The overexpression of *ERG2*, *ERG11*, *ERG25*, *ERG26*, and *ERG27* genes in wild-type H99 background increased cryptococcal resistance to fluconazole (Figure 2.5B), indicating that these overexpressed enzymes are functional. Notably, all the *ERG* genes selected for overexpression encode enzymes that function downstream of Erg11, the target of fluconazole. Thus, it appears that increased expression of any of the single genes in the EBP downstream of Erg11 is sufficient to overcome Erg11 inhibition by fluconazole.

The $sre1\Delta$ mutant, as expected, was susceptible to fluconazole (Figure 2.5C). In the mutant background, of the five ERG genes tested, only overexpression of ERG11 increased its tolerance to fluconazole. Therefore, the drug's target, Erg11, can confer fluconazole tolerance to the $sre1\Delta$ mutant, but the effect of overexpression of any other individual EBP gene cannot overcome fluconazole sensitivity caused by SRE1 deletion.

With the confirmation of the functionality of the overexpressed ERG genes, we proceeded to examine if the overexpression of these genes could rescue $sre1\Delta$'s sporulation defect. The overexpression of any of the five ERG genes in the wild-type H99 background did not alter sporulation (Figure 2.5D,E). Interestingly, the overexpression of ERG2, ERG11, ERG25, and ERG26 partially rescued the sporulation defect of $sre1\Delta$ in unilateral crosses (Figure

2.5D, E). Whereas the $srel\Delta$ unilateral cross only produced spore chains ~10% of the time, the $ERG2^{OE}$ $srel\Delta$ unilateral cross produced spore chains ~50% of the time, and the $ERG11^{OE}$ $srel\Delta$ produced spore chains ~60% of the time. The $ERG25^{OE}$ $srel\Delta$ and $ERG26^{OE}$ $srel\Delta$ unilateral crosses produced spore chains ~70% of the time (Figure 2.5E). The additive effect of EBP gene overexpression plus one wild-type copy of SRE1 in these unilateral crosses ($srel\Delta$ x WT) may explain why the sporulation defect was partially rescued during unilateral bisexual mating, but the vegetative growth of these EBP gene overexpression in the haploid $srel\Delta$ mutant was not restored on YNB+fluconazole. Taken together, we concluded that ergosterol is a critical nutrient for sporogenesis, and sporogenesis demands heightened expression of EBP genes.

Discussion

Cholesterol is an important component of meiosis and oocyte development in mammals and the nematode *Caenorhabditis elegans* [48]. Fungi undergo a sexual cycle that results in the production of meiotic spores. Here, we found that ergosterol is enriched in basidia and spores of the fungus *C. neoformans*, and, thus, we sought to determine if this fungal sterol was critical for sexual reproduction in *C. neoformans*. Indeed, we found that genetic mutations in the EBP pathway, such as deletion of *ERG3* and *ERG4* gene, compromise sporulation even in unilateral crosses where only one mating partner is deficient in the EBP pathway (haploid insufficiency). The importance of EBP genes in cryptococcal sporulation is also in agreement with previous studies on *Aspergillus fumigatus* where *ERG4* and *ERG5* are required for conidiation [49,50]. *ERG3* mutants do not have a conidiation defect in *A. fumigatus* [51], but conidiation defects of this mutant have been reported in *Fusarium oxysporum* [52]. Thus, the *ERG4* and *ERG3* phenotypes are conserved across phyla.

Modulating ergosterol content via the overexpression or reducing expression of EBP genes in *Aspergillus oryzae* reduces sporulation rates. Specifically, *ERG19* overexpression and RNAi knockdown both caused the number of spores produced by *A. oryzae* to decrease dramatically [53]. Both gene manipulations also caused significant delays in sporulation. A separate study showed that the overexpression of another EBP gene, *ERG10*, caused reduction in sporulation rates [54]. Two of three *ERG11* isoform overexpression strains showed increased overall ergosterol content of the cell, as well as increased sporulation [55]. Thus, it appears that the right amount of ergosterol and activities of the EBP enzymes are critical in sporulation.

Here, we showed that deletion of SRE1, a gene that encodes a transcription factor responsible for increased EBP pathway gene expression under stress conditions such as hypoxia, nearly abolishes sporulation in unilateral crosses in C. neoformans. Furthermore, the overexpression of some EBP genes, such as ERG2, ERG11, and ERG25, can partially rescue the sporulation defect of the $sre1\Delta$ mutant. Thus, enhanced ergosterol biosynthesis is required for successful sporogenesis of the $sre1\Delta$ mutant. Surprisingly, the hypoxia and ergosterol regulator SrbA gene knockout in A. fumigatus does not have any notable defects in filamentation or conidiation compared to the wild type [56]. This could be attributed to the fact that A. fumigatus encodes an additional gene SrbB, which creates a protein similar to SrbA. SrbB influences the transcription of ergosterol biosynthesis but also has functions independent of SrbA [57].

One aspect that we found fascinating was that the overexpression of a single EBP gene was capable of conferring resistance to fluconazole in the wild-type background. This is surprising since the EBP pathway requires 23 enzymes in C. neoformans. The observation that even the overexpression of genes downstream of Erg11, the target of fluconazole, is capable of this effect is remarkable. Reducing the function of Erg11 via fluconazole should have a negative

impact on biosynthetic steps downstream of this enzyme. Perhaps lanosterol, the substrate of Erg11, could serve (maybe poorly) as the substrate of the other downstream EBP enzymes, which allows the cells to produce other sterols that are functional in the presence of fluconazole in these overexpression strains. A sterol analysis of these overexpression strains in the presence and the absence of fluconazole would be necessary to determine if this was true.

In summary, we demonstrated here that ergosterol is necessary for sporogenesis in *C*. *neoformans*. Similar to oogenesis in high eukaryotes, basidia must accumulate a higher level of sterols by increasing the EBP pathway before initiating the production of spores.

Author Contributions

Conceptualization, A.R.M. and X.L.; methodology, A.R.M., X.X., and X.L.; validation, A.R.M., X.X., and X.L.; formal analysis, A.R.M. and X.L.; investigation, A.R.M. and X.L.; resources, X.L.; data curation, A.R.M., X.X., and X.L.; writing-original draft preparation, A.R.M. and X.L.; writing-review and editing, A.R.M. and X.L.; visualization, A.R.M. and X.L.; supervision, X.L.; project administration, A.R.M. and X.L.; funding acquisition, X.L. All authors have read and agreed to the published version of the manuscript.

Funding

This work was supported by National Institutes of Allergy and Infectious Diseases (http://www.niaid.nih.gov) (R01AI140719 to X.L.). The funder had no role in the study design, data collection and interpretation, or the decision to submit the work for publication.

Acknowledgement

We thank all Lin lab members for their helpful suggestions.

References

- Errington, J. Regulation of endospore formation in *Bacillus subtilis*. *Nat. Rev. Microbiol*.
 2003, 1, 117–126.
- 2. Setlow, P. Spores of *Bacillus subtilis*: Their resistance to and killing by radiation, heat and chemicals. *J. Appl. Microbiol.* **2006**, 101, 514–525.
- 3. Busse, O. Uber parasitare Zelleinschlusse und ihre Zuchtung. Zentralbl Bakteriol. **1894**, 16, 175–180.
- 4. Zhao, Y.; Lin, J.; Fan, Y.; Lin, X. Life Cycle of *Cryptococcus neoformans*. *Annu. Rev. Microbiol.* **2019**, 73, 17–42.
- 5. Kwon-Chung, K. A new genus, *Filobasidiella*, the perfect state of *Cryptococcus neoformans*. *Mycologia* **1975**, 67, 1197–1200.
- 6. Lin, J.; Idnurm, A.; Lin, X. Morphology and its underlying genetic regulation impact the interaction between *Cryptococcus neoformans* and its hosts. *Med. Mycol.* **2015**, 53, 493–504.
- 7. Fu, M.S.; Liporagi-Lopes, L.C.; dos Santos, S.R.; Tenor, J.L.; Perfect, J.R.; Cuomo, C.A.; Casadevall, A. Amoeba predation of *Cryptococcus neoformans* results in pleiotropic changes to traits associated with virulence. *MBio* **2021**, 12, 10–1128.
- 8. Velagapudi, R.; Hsueh, Y.-P.; Geunes-Boyer, S.; Wright, J.R.; Heitman, J. Spores as infectious propagules of *Cryptococcus neoformans*. *Infect. Immun.* **2009**, 77, 4345–4355.
- 9. Giles, S.S.; Dagenais, T.R.; Botts, M.R.; Keller, N.P.; Hull, C.M. Elucidating the pathogenesis of spores from the human fungal pathogen *Cryptococcus neoformans*. *Infect. Immun.* **2009**, 77, 3491–3500.

- 10. Zhao, Y.; Lin, X. *Cryptococcus neoformans*: Sex, morphogenesis, and virulence. *Infect. Genet. Evol.* **2021**, 89, 104731.
- 11. Kwon-Chung, K. Morphogenesis of *Filobasidiella neoformans*, the sexual state of *Cryptococcus neoformans*. *Mycologia* **1976**, 68, 821–833.
- 12. Hull, C.M.; Davidson, R.C.; Heitman, J. Cell identity and sexual development in *Cryptococcus neoformans* are controlled by the mating-type-specific homeodomain protein Sxi1α. *Genes. Dev.* **2002**, 16, 3046–3060.
- 13. McClelland, C.M.; Chang, Y.C.; Varma, A.; Kwon-Chung, K. Uniqueness of the mating system in *Cryptococcus neoformans*. *Trends Microbiol*. **2004**, 12, 208–212.
- 14. Lin, X.; Hull, C.M.; Heitman, J. Sexual reproduction between partners of the same mating type in *Cryptococcus neoformans*. *Nature*. **2005**, 434, 1017–1021.
- 15. Lin, X.; Jackson, J.C.; Feretzaki, M.; Xue, C.; Heitman, J. Transcription factors Mat2 and Znf2 operate cellular circuits orchestrating opposite-and same-sex mating in *Cryptococcus neoformans. PLoS Genet.* **2010**, 6, e1000953.
- 16. Sun, S.; Priest, S.J.; Heitman, J. *Cryptococcus neoformans* mating and genetic crosses. *Curr. Protoc. Microbiol.* **2019**, 53, e75.
- 17. Matha, A.R.; Lin, X. Current perspectives on uniparental mitochondrial inheritance in *Cryptococcus neoformans. Pathogens* **2020**, 9, 743.
- Huang, M.; Hebert, A.S.; Coon, J.J.; Hull, C.M. Protein composition of infectious spores reveals novel sexual development and germination factors in *Cryptococcus. PLoS Genet.* 2015, 11, e1005490.
- 19. Wyatt, T.T.; Wosten, H.A.; Dijksterhuis, J. Fungal spores for dispersion in space and time. Adv. Appl. Microbiol. **2013**, 85, 43–91.

- 20. Mukhopadhyay, K.; Prasad, T.; Saini, P.; Pucadyil, T.J.; Chattopadhyay, A.; Prasad, R. Membrane sphingolipid-ergosterol interactions are important determinants of multidrug resistance in *Candida albicans*. *Antimicrob*. *Agents Chemother*. 2004, 48, 1778–1787.
- 21. Abe, F.; Hiraki, T. Mechanistic role of ergosterol in membrane rigidity and cycloheximide resistance in *Saccharomyces cerevisiae*. *Biochim. Biophys. Acta (BBA)-Biomembr.* **2009**, 1788, 743–752.
- 22. Ortiz, S.C.; Huang, M.; Hull, C.M. Spore germination as a target for antifungal therapeutics. *Antimicrob. Agents Chemother.* **2019**, 63, 10–1128.
- 23. Chang, Y.C.; Bien, C.M.; Lee, H.; Espenshade, P.J.; Kwon-Chung, K.J. Sre1p, a regulator of oxygen sensing and sterol homeostasis, is required for virulence in *Cryptococcus neoformans. Mol. Microbiol.* **2007**, 64, 614–629.
- 24. Lee, H.; Bien, C.M.; Hughes, A.L.; Espenshade, P.J.; Kwon-Chung, K.J.; Chang, Y.C. Cobalt chloride, a hypoxia-mimicking agent, targets sterol synthesis in the pathogenic fungus *Cryptococcus neoformans*. *Mol. Microbiol.* 2007, 65, 1018–1033.
- Byskov, A.G.; Andersen, C.Y.; Nordholm, L.; Thogersen, H.; Guoliang, X.; Wassmann,
 O.; Andersen, J.V.; Guddal, E.; Roed, T. Chemical structure of sterols that activate
 oocyte meiosis. Nature 1995, 374, 559–562.
- Byskov, A.G.; Andersen, C.Y.; Leonardsen, L. Role of meiosis activating sterols, MAS, in induced oocyte maturation. *Mol. Cell. Endocrinol.* 2002, 187, 189–196.
- 27. Grondahl, C.; Breinholt, J.; Wahl, P.; Murray, A.; Hansen, T.H.; Faerge, I.; Stidsen, C.E.; Raun, K.; Hegele-Hartung, C. Physiology of meiosis-activating sterol: Endogenous formation and mode of action. *Hum. Reprod.* **2003**, 18, 122–129.

- 28. Tian, X.; He, G.-J.; Hu, P.; Chen, L.; Tao, C.; Cui, Y.-L.; Shen, L.; Ke, W.; Xu, H.; Zhao, Y.; et al. *Cryptococcus neoformans* sexual reproduction is controlled by a quorum sensing peptide. *Nat. Microbiol.* **2018**, 3, 698–707.
- 29. Liu, L.; He, G.-J.; Chen, L.; Zheng, J.; Chen, Y.; Shen, L.; Tian, X.; Li, E.; Yang, E.; Liao, G.; et al. Genetic basis for coordination of meiosis and sexual structure maturation in *Cryptococcus neoformans. eLife* **2018**, 7, e38683.
- 30. Jung, K.-W.; Yang, D.-H.; Maeng, S.; Lee, K.-T.; So, Y.-S.; Hong, J.; Choi, J.; Byun, H.-J.; Kim, H.; Bang, S.; et al. Systematic functional profiling of transcription factor networks in *Cryptococcus neoformans*. *Nat. Commun.* **2015**, 6, 6757.
- 31. Fan, Y.; Lin, X. Multiple applications of a transient CRISPR-Cas9 coupled with electroporation (TRACE) system in the *Cryptococcus neoformans* species complex. *Genetics* **2018**, 208, 1357–1372.
- 32. Lin, J.; Fan, Y.; Lin, X. Transformation of *Cryptococcus neoformans* by electroporation using a transient CRISPR-Cas9 expression (TRACE) system. *Fungal Genet. Biol.* **2020**, 138, 103364.
- 33. Edwards, P.A.; Ericsson, J. Sterols and isoprenoids: Signaling molecules derived from the cholesterol biosynthetic pathway. *Annu. Rev. Biochem.* **1999**, 68, 157–185.
- 34. Upadhya, R.; Lam, W.C.; Maybruck, B.T.; Donlin, M.J.; Chang, A.L.; Kayode, S.; Ormerod, K.L.; Fraser, J.A.; Doering, T.L.; Lodge, J.K. A fluorogenic *C. neoformans* reporter strain with a robust expression of m-cherry expressed from a safe haven site in the genome. *Fungal Genet. Biol.* **2017**, 108, 13–25.
- 35. Wang, L.; Zhai, B.; Lin, X. The link between morphotype transition and virulence in *Cryptococcus neoformans. PLoS Pathog.* **2012**, 8, e1002765.

- 36. Sephton-Clark, P.C.; Voelz, K. Spore germination of pathogenic filamentous fungi. In *Advances in Applied Microbiology*; Elsevier: Amsterdam, The Netherlands, 2018; pp. 117–157.
- 37. Van Leeuwen, M.; Smant, W.; De Boer, W.; Dijksterhuis, J. Filipin is a reliable in situ marker of ergosterol in the plasma membrane of germinating conidia (spores) of *Penicillium discolor* and stains intensively at the site of germ tube formation. *J. Microbiol. Methods* **2008**, 74, 64–73.
- 38. Eberlé, D.; Hegarty, B.; Bossard, P.; Ferré, P.; Foufelle, F. SREBP transcription factors: Master regulators of lipid homeostasis. *Biochimie* **2004**, 86, 839–848.
- 39. Wang, L.; Tian, X.; Gyawali, R.; Upadhyay, S.; Foyle, D.; Wang, G.; Cai, J.J.; Lin, X. Morphotype transition and sexual reproduction are genetically associated in a ubiquitous environmental pathogen. *PLoS Pathog.* **2014**, 10, e1004185.
- 40. Shi, R.; Lin, X. Illuminating *Cryptococcus neoformans*: Unveiling Intracellular Structures with Fluorescent-Protein-Based Markers. *Genetics* 2024, submitted.
- 41. Basante-Bedoya, M.A.; Bogliolo, S.; Garcia-Rodas, R.; Zaragoza, O.; Arkowitz, R.A.; Bassilana, M. Two distinct lipid transporters together regulate invasive filamentous growth in the human fungal pathogen *Candida albicans. PLoS Genet.* **2022**, 18, e1010549.
- 42. Goebels, C.; Thonn, A.; Gonzalez-Hilarion, S.; Rolland, O.; Moyrand, F.; Beilharz, T.H.; Janbon, G. Introns regulate gene expression in *Cryptococcus neoformans* in a Pab2p dependent pathway. *PLoS Genet.* **2013**, 9, e1003686.

- 43. Bhattacharya, S.; Esquivel, B.D.; White, T.C. Overexpression or deletion of ergosterol biosynthesis genes alters doubling time, response to stress agents, and drug susceptibility in *Saccharomyces cerevisiae*. *MBio* **2018**, 9, e01291-18.
- 44. Mo, C.; Valachovic, M.; Randall, S.; Nickels, J.; Bard, M. Protein–protein interactions among C-4 demethylation enzymes involved in yeast sterol biosynthesis. *Proc. Natl. Acad. Sci.* USA 2002, 99, 9739–9744.
- 45. Jordá, T.; Puig, S. Regulation of ergosterol biosynthesis in *Saccharomyces cerevisiae*. *Genes* **2020**, 11, 795.
- 46. Shim, Y.H.; Chun, J.H.; Lee, E.Y.; Paik, Y.K. Role of cholesterol in germ-line development of *Caenorhabditis elegans*. *Mol. Reprod. Dev.* **2002**, 61, 358–366.
- 47. Long, N.; Xu, X.; Zeng, Q.; Sang, H.; Lu, L. Erg4A and Erg4B are required for conidiation and azole resistance via regulation of ergosterol biosynthesis in *Aspergillus fumigatus*. *Appl. Environ. Microbiol.* **2017**, 83, e02924-16.
- 48. Long, N.; Zhong, G. The C-22 sterol desaturase Erg5 is responsible for ergosterol biosynthesis and conidiation in *Aspergillus fumigatus*. *J. Microbiol.* **2022**, 60, 620–626.
- 49. Alcazar-Fuoli, L.; Mellado, E.; Garcia-Effron, G.; Buitrago, M.J.; Lopez, J.F.; Grimalt, J.O.; Cuenca-Estrella, J.M.; Rodriguez-Tudela, J.L. *Aspergillus fumigatus* C-5 sterol desaturases Erg3A and Erg3B: Role in sterol biosynthesis and antifungal drug susceptibility. *Antimicrob. Agents Chemother.* **2006**, 50, 453–460.
- 50. Han, S.; Sheng, B.; Zhu, D.; Chen, J.; Cai, H.; Zhang, S.; Guo, C. Role of FoERG3 in Ergosterol Biosynthesis by *Fusarium oxysporum* and the Associated Regulation by *Bacillus subtilis* HSY21. *Plant Dis.* **2023**, 107, 1565–1575.

- 51. Sun, Y.; Niu, Y.; Huang, H.; He, B.; Ma, L.; Tu, Y.; Tran, V.-T.; Zeng, B.; Hu, Z. Mevalonate diphosphate decarboxylase MVD/Erg19 is required for ergosterol biosynthesis, growth, sporulation and stress tolerance in *Aspergillus oryzae*. *Front. Microbiol.* **2019**, 10, 1074.
- 52. Huang, H.; Niu, Y.; Jin, Q.; Qin, K.; Wang, L.; Shang, Y.; Zeng, B.; Hu, Z. Identification of six thiolases and their effects on fatty acid and ergosterol biosynthesis in *Aspergillus oryzae*. *Appl. Environ. Microbiol.* **2022**, 88, e02372-21.
- 53. Jin, Q.; Li, G.; Qin, K.; Shang, Y.; Yan, H.; Liu, H.; Zeng, B.; Hu, Z. The expression pattern, subcellular localization and function of three sterol 14α-demethylases in *Aspergillus oryzae. Front. Genet.* **2023**, 14, 1009746.
- 54. Willger, S.D.; Puttikamonkul, S.; Kim, K.-H.; Burritt, J.B.; Grahl, N.; Metzler, L.J.; Barbuch, R.; Bard, M.; Lawrence, C.B.; Cramer, R.A. A sterol-regulatory element binding protein is required for cell polarity, hypoxia adaptation, azole drug resistance, and virulence in *Aspergillus fumigatus*. *PLoS Pathog*. **2008**, 4, e1000200.
- 55. Chung, D.; Barker, B.M.; Carey, C.C.; Merriman, B.; Werner, E.R.; Lechner, B.E.; Dhingra, S.; Cheng, C.; Xu, W.; Blosser, S.J.; et al. ChIP-seq and in vivo transcriptome analyses of the *Aspergillus fumigatus* SREBP SrbA reveals a new regulator of the fungal hypoxia response and virulence. *PLoS Pathog.* **2014**, 10, e1004487.

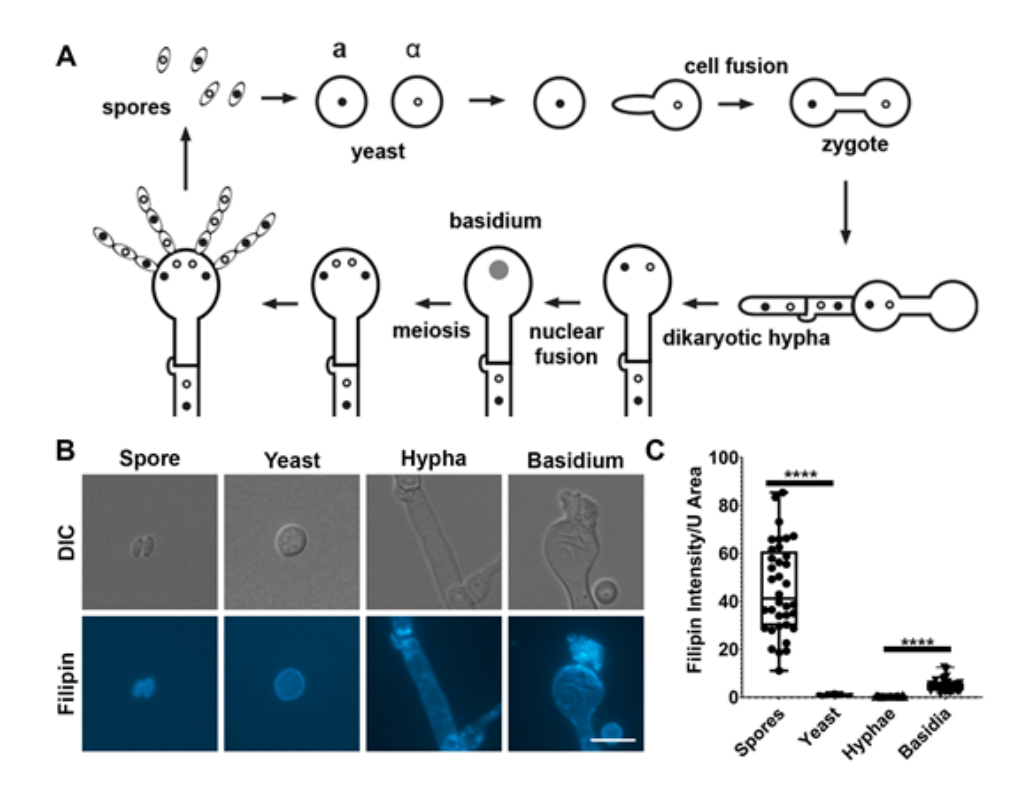


Figure 2.1 Ergosterol is enriched in spores and basidia based on filipin staining. (A)

Diagram of bisexual reproduction of C. neoformans. **(B)** Mating mixtures were spotted onto V8 pH = 5 agar plates and incubated at 21 °C in the dark for two weeks. Spores and basidia were scooped and suspended into dH2O. Then, 0.5 mg/mL of filipin was used to stain the cells for 10 min before visualization. Scale bar = 10 μ m. **(C)** Filipin fluorescence signal was quantified in Zen Pro software and standardized using approximate cell surface area (SA). The approximate SA of yeasts and basidia was calculated via the SA of a sphere, and the SA of hyphae and spores was calculated via the SA of a cylinder (see Materials and Methods for equations). Cell diameters and lengths were also measured in Zen Pro. Kruskal-Wallace test was used to assess statistical significance. **** p < 0.0001.

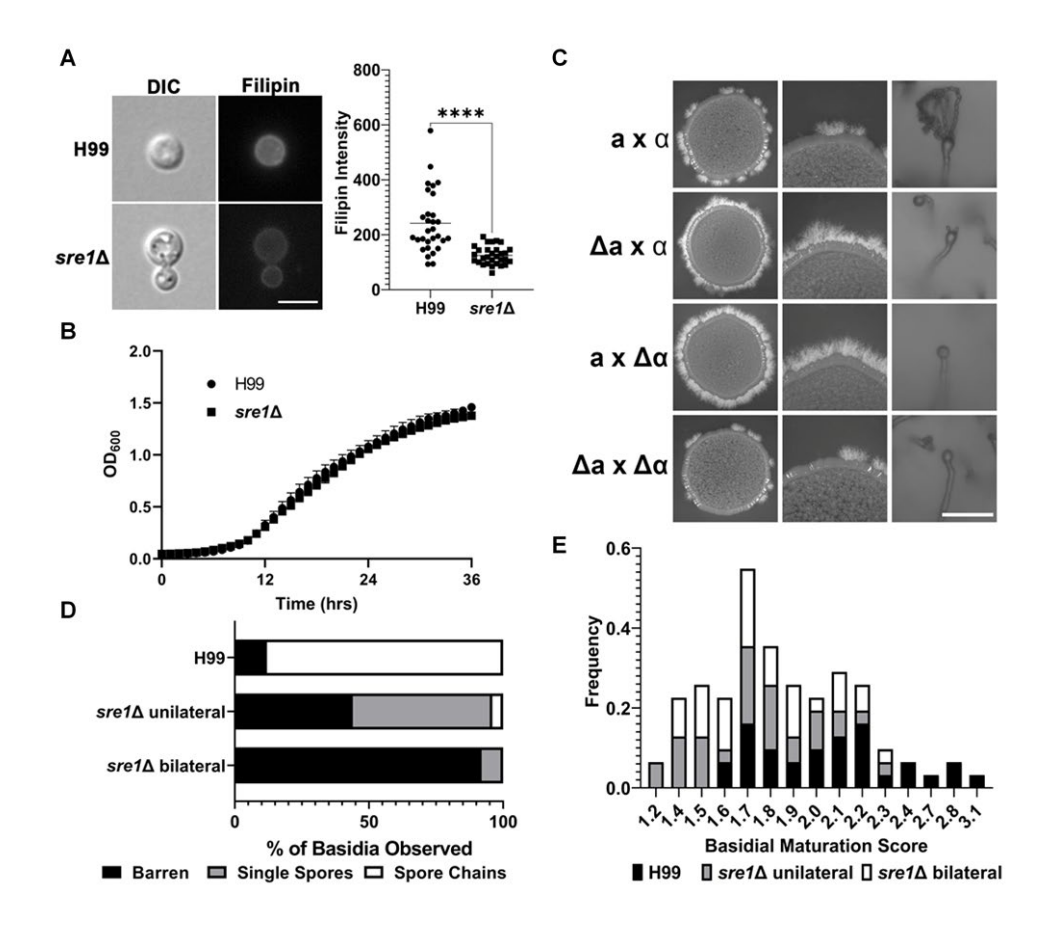


Figure 2.2 $sre1\Delta$ has a sporulation defect in both unilateral and bilateral crosses. (A) H99 and $sre1\Delta$ cells were grown to exponential growth in YPD media and stained with filipin for 10 min as in Figure 1 before visualization. Quantification of filipin fluorescent intensity was performed in Zen Pro. Scale bar = 10 μ m. Mann-Whitney was used to assess statistical significance. **** p < 0.0001. (B) Cells were inoculated into a 96 well plate with a starting OD₆₀₀ = 0.1 and shaken at 30 °C for 36 h. OD₆₀₀ was read every hour. (C) Wild type (H99 α x KN99a), $sre1\Delta$ unilateral, and $sre1\Delta$ bilateral crosses were made by mixing equal numbers of cells and spotting the mixed cells onto V8 pH = 5 agar plates. Plates were incubated at 21 °C in the dark for 20 days. The basidia and associated spore chains were imaged from the plate under microscope with a 20x objective. Scale bar = 100 μ m. (D) 100 basidia from colonies in Panel C were visualized via light microscopy and imaged. Basidia were classified based on if they lacked

spores (barren), had single/abnormal spore numbers, or had four spores/chains. **(E)** Basidia and hyphal diameters from the crosses in Panel C were measured in the Zen Pro software. The basidial maturation score was calculated per the inset figure.

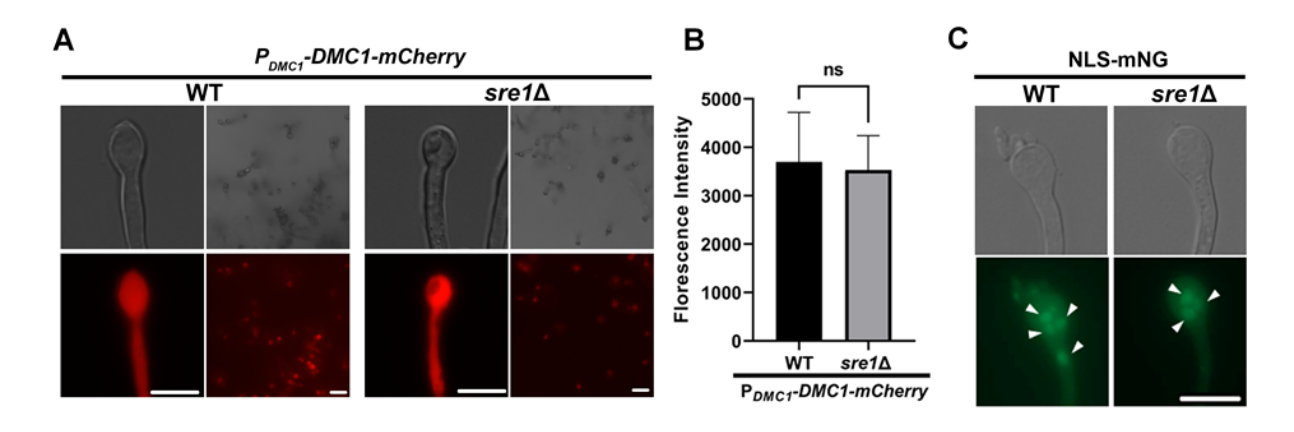


Figure 2.3: Meiosis is occurring in the basidia generated by $sre1\Delta$ crosses. (A) A strain with Dmc1-mCherry fusion protein with its expression driven by the native DMC1 promoter was mated with wild-type KN99a cells. A $sre1\Delta$ strain harboring the Dmc1-mCherry fusion protein was also mated with KN99a. Mating crosses on V8 pH = 5 agar plates were incubated at 21 °C in the dark for two weeks. The plates were examined directly for basidia and Dmc1 expression, and basidia were scraped from the plate and placed onto agarose slides for microscopic examination. Scale bar = 10 μ m. (B) Fluorescence intensity of the basidia from panel A was quantified using Zen Pro. Error bars reflect standard deviation. Student's t-test was used to assess statistical significance. ns = nots ignificant. (C) A strain constitutively expressing mNeonGreen fused with a nuclear localization signal (NLS-mNG) was mated with KN99a or the $sre1\Delta$ a mutant. After mating on V8 agar in the dark for two weeks, basidia were scraped as in panel A and visualized for nuclei, indicated by white arrows. Scale bar = 10 μ m.

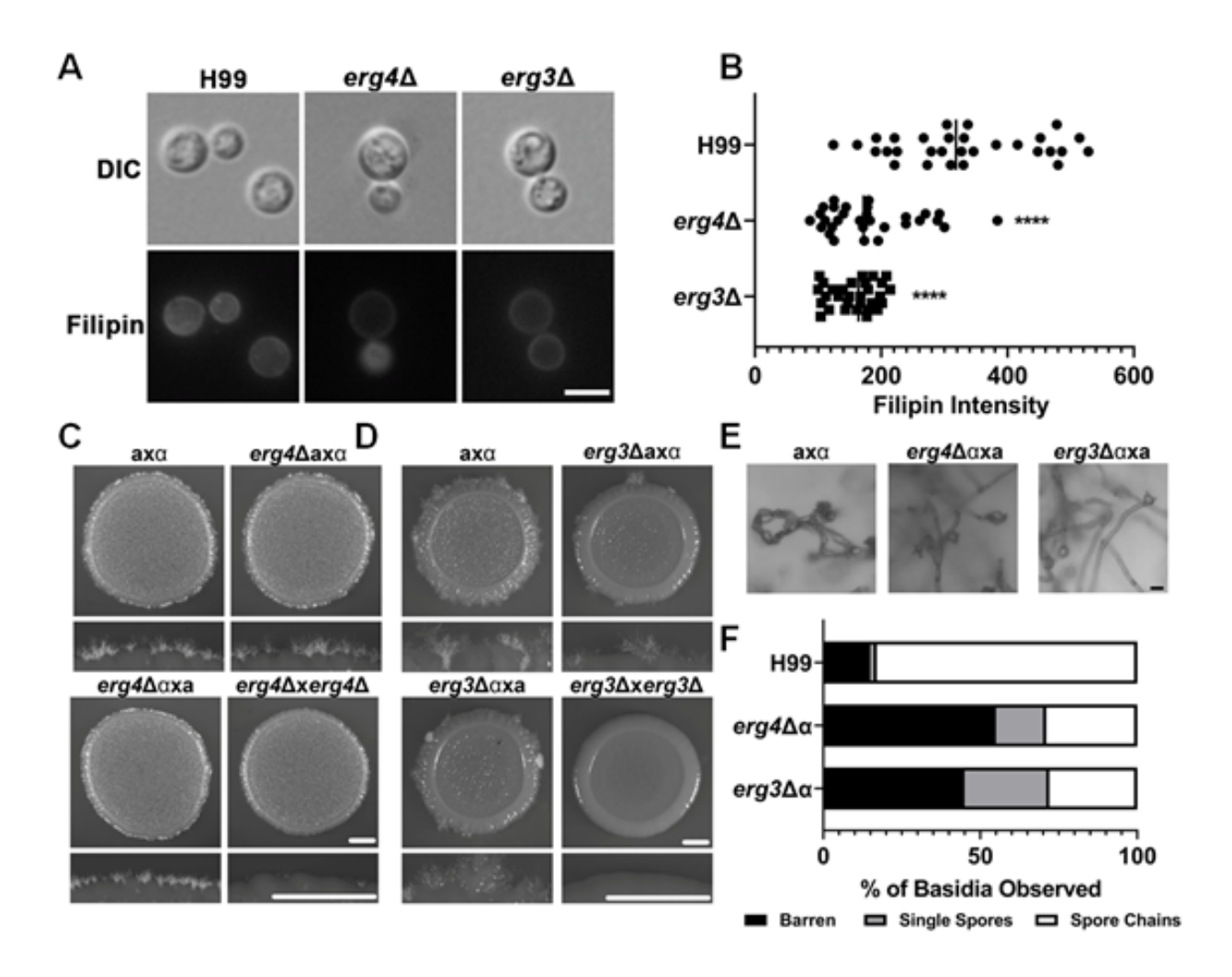


Figure 2.4 Deletion of EBP genes negatively impacts mating. (A) H99, $erg3\Delta$, and $erg4\Delta$ cells were grown to exponential growth in YPD media and stained with filipin for 10 min as in Figure 1 before visualization. (B) Quantification of filipin fluorescent intensity was performed in Zen Pro. Scale bar = 5 μm. Mann-Whitney was used to assess statistical significance **** = <0.0001. (C) Serotype A crosses (wild type, $erg4\Delta$ unilateral, and $erg4\Delta$ bilateral) were spotted onto V8 pH = 5 agar and incubated at 21 °C in the dark for 10 days. The whole colonies and colony edges were visualized via a stereoscope. Scale bar = 100 μm. (D) $erg3\Delta$ crosses were set up in the same way as in panel A. The whole colonies and colony edges were visualized. (E) Representative images of basidia from the $erg4\Delta$ and $erg3\Delta$ unilateral crosses. Basidia from the $erg4\Delta$ unilateral

cross were visualized at 10x objective via a light microscope. Scale bar = $5 \mu m$. (F) Quantification of the types of basidia for the unilateral and wild-type crosses as in Figure 2D.

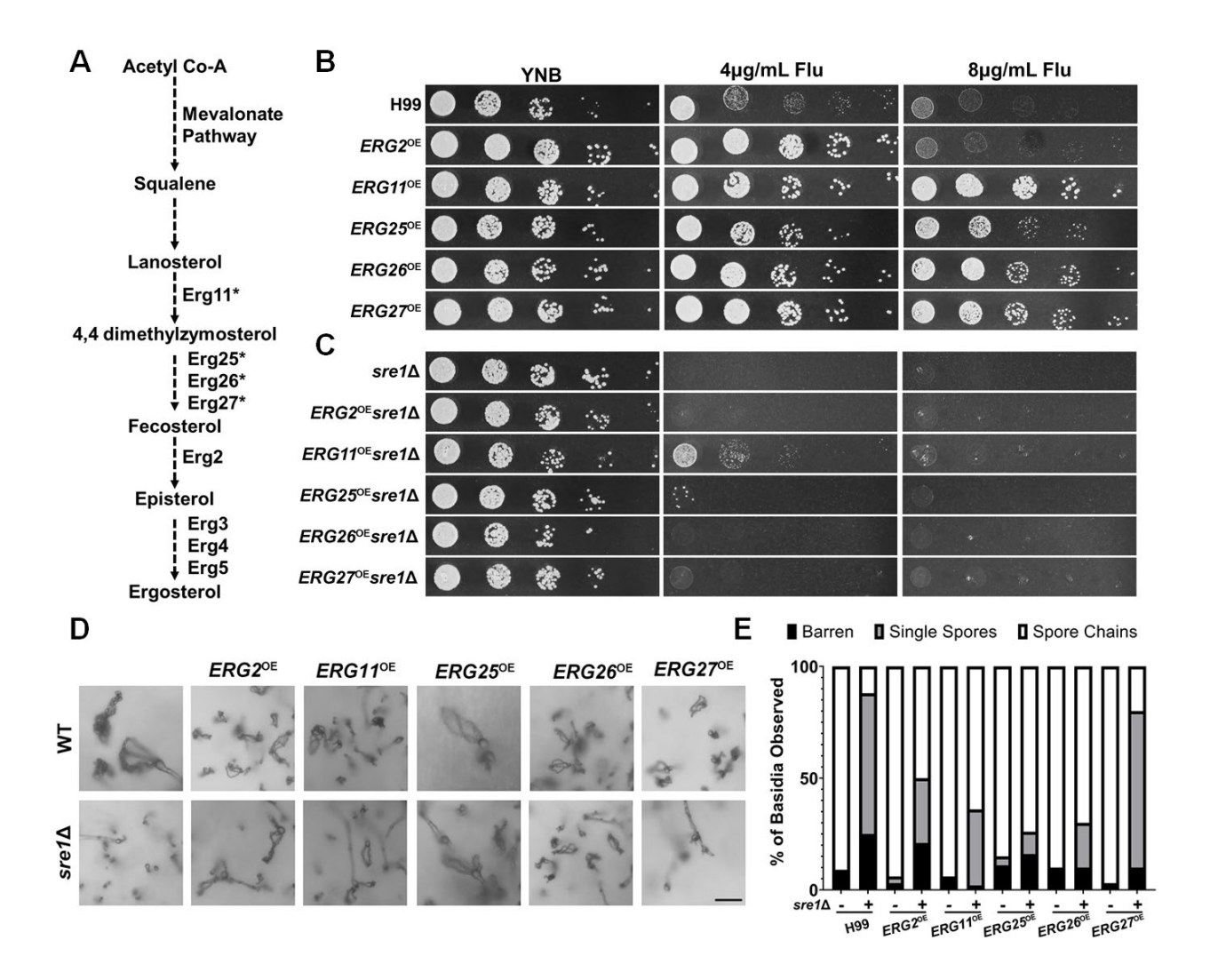


Figure 2.5 Overexpressed ergosterol biosynthetic genes are functional and can restore successful sporulation in the $sre1\Delta$ mutant. (A) Abbreviated ergosterol biosynthesis pathway highlighting ergosterol genes of relevance for this report. Essential Erg enzymes are marked with an asterisk. (B) The indicated EBP gene overexpression strains in the H99 were serially diluted and spotted onto YNB and YNB+fluconazole agar media. (C) EBP overexpression strains in the $sre1\Delta$ mutant background were spotted as in panel B. Plates were incubated at 30 °C for two days before imaging. (D) The indicated EBP gene overexpression strains with or without the SRE1 gene were crossed unilaterally with the wild-type strain of the opposite mating type. After two weeks, basidia were visualized to determine sporulation frequencies (n = 100). Scale bar =

 $10~\mu m.$ (E) Frequency of basidia with abnormal spores and spore chains for the crosses tested in Panel A.

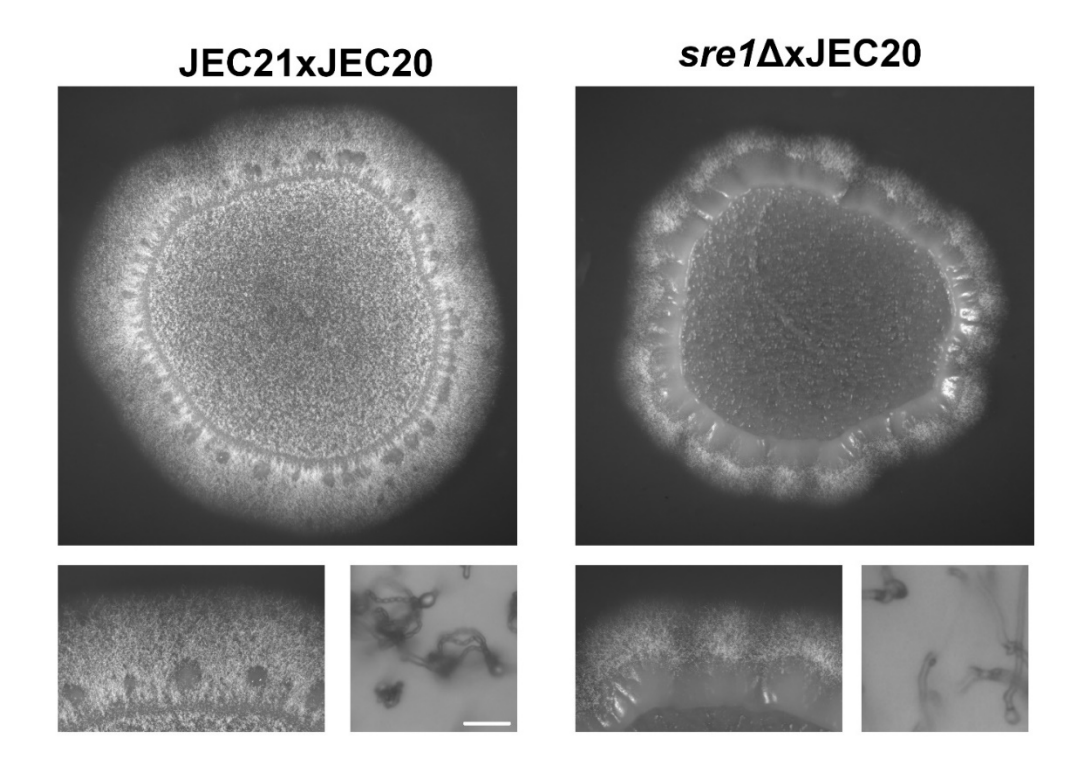


Figure S2.1 A wildtype serotype D cross (JEC21 α x JEC20a) and a *sre1* Δ unilateral cross (*sre1* $\Delta\alpha$ x JEC20a) were spotted onto V8 pH=7 agar and incubated at 21°C in the dark for two weeks. The whole colony and colony edge were visualized by a stereoscope and basidia were visualized by light microscopy with a 10x objective. Scale bar = 10 μ m.

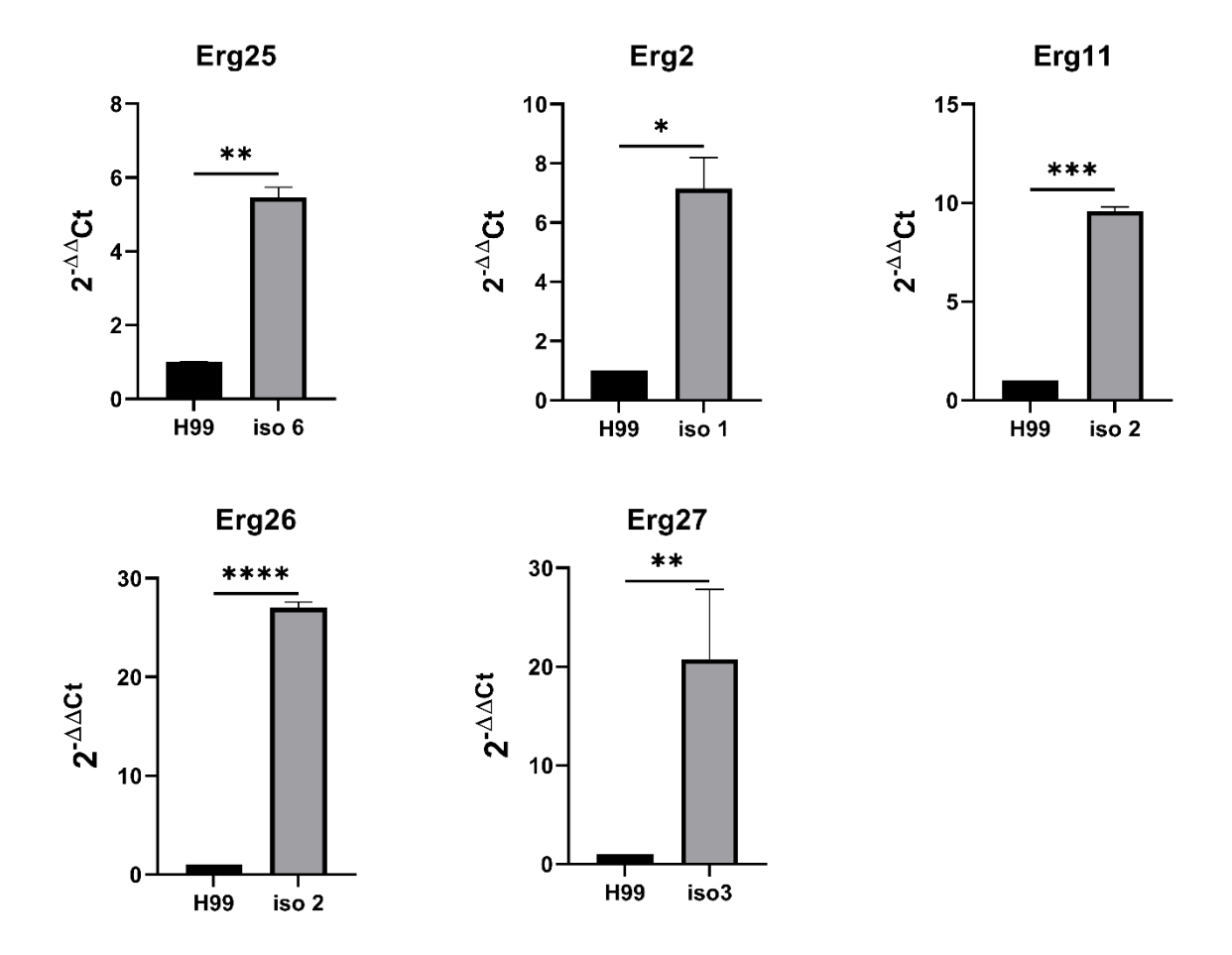


Figure S2.2 RT-PCR data was generated by harvesting cells from overnight YPD cultures. Housekeeping gene TEF1 was used as an internal control to ensure the quality of the original RNA sample used for cDNA amplification and for normalization. Error bars reflect the standard deviation. Student's t-test was used to assess statistical significance. *: $P = \le 0.05$, **: $P = \le 0.01$, ***: P = < 0.001, ***: P = < 0.0001.

Table S2.1 Fungal strains used in this study

Reagent				
Name	Source	Identifier		
Fungal Strains				
H99		C. neoformans serotype A, wild type, MATalpha		
KN99a		C. neoformans serotype A, wild type, MATa		
JEC21		C. neoformans serotype D, wild type, MATalpha		
JEC20		C. neoformans serotype D, wild type, MATa		
Linlab3062	(22)	MATalpha serotype A, SRE1::NAT		
Linlab5382	YZ611	MATa serotype A, SRE1::NAT		
Linlab7999	This manuscript	MATalpha serotype A, <i>P</i> _{GPDI} -ERG2-HYG		
		MATalpha serotype A, <i>P</i> _{GPDI} -ERG2-HYG,		
Linlab8000	This manuscript	SRE1::NAT		
Linlab7996	This manuscript	MATalpha serotype A, <i>P</i> _{GPDI} -ERG11-HYG		
		MATalpha serotype A, <i>P</i> _{GPD1} -ERG11-HYG,		
Linlab8002	This manuscript	SRE1::NAT		
Linlab7724	This manuscript	MATa serotype A, <i>P</i> _{TEF1} -ERG25-NEO		
Linlab8507	This manuscript	MATa serotype A, <i>P</i> _{TEF1} -ERG25-NEO, SRE1::NAT		
Linlab8428	This manuscript	MATalpha serotype A, <i>P</i> _{TEF1} -ERG26-NEO		
		MATalpha serotype A, <i>P</i> _{TEF1} -ERG26-NEO,		
Linlab8433	This manuscript	SRE1::NAT		
Linlab8431	This manuscript	MATalpha serotype A, <i>P</i> _{TEF1} -ERG27-NEO		
		MATalpha serotype A, <i>P</i> _{TEF1} -ERG27-NEO,		
Linlab8435	This manuscript	SRE1::NAT		
Linlab7834	This manuscript	MATalpha serotype A, P _{DMC1} -DMC1-mcherry-HYG		
		MATalpha serotype A, P_{DMCI} -DMC1-mcherry-HYG,		
Linlab7994	This manuscript	SRE1::NAT		
	FGSC deletion			
Linlab8504	set 6A3	MATalpha serotype A, <i>ERG3</i> ::NAT		
	FGSC deletion			
Linlab8505	set 5F6	MATalpha serotype A, <i>ERG4</i> ::NAT		
Linlab8506	This manuscript	MATalpha serotype A, ERG5::NAT		
Linlab8585	This manuscript	MATa serotype A, <i>ERG4</i> ::NAT		
Linlab9608	This manuscript	MATa serotype A, <i>ERG3</i> ::NAT		
Linlab9607	This manuscript	MATalpha serotype D, SRE1::NAT		

Table S2.2 Plasmids and primers used in this study

Plasmids		
pLinlab995		P _{TEF1} -CNE02650-TdTomato- NEO
pLinlab1059	[39,40]	P _{GPDI} -cas9-HYG
pLinlab1996	This manuscript	P _{GPD1} -ERG11-HYG
pLinlab1918	This manuscript	P _{TEF1} -ERG25-NEO
pLinlab2148	This manuscript	P _{TEF1} -ERG26-NEO
pLinlab2149	This manuscript	P _{TEF1} -ERG27-NEO
pLinlab756		P _{DMC1} -DMC1-mcherry-HYG
pLinlab1292		P _{CTR4-2} -mNeonGreen-Fse1/Pac1- T _{GPD1} -NEO
Oligonucleotides		
M13F	GTAAAACGACGCCAG	Amplify drug marker
M13R	CAGGAAACAGCTATGAC	Amplify drug marker
Linlab7894/AM	TACTTGCATAAATACAGGC	erg2 T5 integration F GPD1
Emilia (6) I/I I/I	CGGCCcaCATCACCCACCAT	promoter overhang
Linlab7895/AM	GCCCG	2 T5 :
Liniab/895/AM	ACTGCTACTGTAACGCTTA ATTAATTAGATCTTGCCTCT	erg2 T5 integration R GPD1 terminator overhang
	CAA	terminator overnang
Linlab7869/AM	TACTTGCATAAATACAGGC	erg11 T5 integration F GPD1
<u> </u>	CGGCCcATGTCTGCTATCAT	promoter overhang
	CCCCC	
Linlab7870/AM	ACTGCTACTGTAACGCTTA	erg11 T5 integration R GPD1
	ATTAACTATTTGACCTCGG CATTTC	terminator overhang
Linlab7933/AM	GCTTTGGAGTATGCTAGAG	Erg2 RTPCR F
Linlab7934/AM	TTAGATCTTGCCTCTCAACA	Erg2 RTPCR R
Linlab7935/AM	AATACAGCAAGGCCGAGCA A	Erg11 RTPCR F
Linlab7936/AM	AACATAGGTGAAGATGGTT GA	Erg11 RTPCR R
Linlab7308/AM	ACAGGCCGGCCcgcaccccaccc aacATG	Erg25-F-FseI
Linlab7309/AM	GTATTAATTAACTACTCGTT CTTTCCCCG	Erg25-R-PacI
Linlab7791/AM	CTTGCGCAAGGAACGATCT C	Erg25 RTPCR F
Linlab7792/AM	GAAGTGAAAGTGGCATGGT GGA	Erg25 RTPCR R
Linlab8086/AM	aaacttcaaaggccggcctaacatgtccaac tcgcc	Erg26-F-FseI

Linlab8087/AM	actgtaacccttaattaattactttgtcttctccg	Erg26-R-PacI
Linlab8088/AM	aaacttcaaaggccggcctatgctcgacaca cccagc	Erg27-F-FseI
Linlab8089/AM	actgtaaccettaattaatatacaatactetact cc	Erg27-R-PacI
Linlab8557/AM	ctgtctatgctgaccaag	Erg27 RTPCR F
Linlab8558/AM	ccagtctctccgaacagc	Erg27 RTPCR R
Linlab8559/AM	gettetettgeegagate	Erg26 RTPCR F
Linlab8560/AM	ctcattctgtctctccaac	Erg26 RTPCR R
Linlab8532/AM	CTCAGAACCCGAACACTC	Forward primer to amplify deletion cassette from $sre1\Delta$
Linlab8533/AM	ATTGATGCCGAGAGCTGAG	Reverse primer to amplify
		deletion cassette from $sre1\Delta$
Linlab7751/AM	CTACCATTGGCAAGCACAA	Reverse primer to amplify
	CAACAGTATACCCTGCCGG TG	gRNA for SRE1 deletion
Linlab7752/AM	GTTGTGCTTGCCAATGGTA	Forward primer to amplify
	GGTTTTAGAGCTAGAAATA	gRNA for SRE1 deletion
	GCAAGTT	
Linlab4627/YF	ggctcaaagagcagatcaatg	Forward primer to amplify U6
		promoter
Linlab4628/YF	cctctgacacatgcagctcc	Reverse primer to amplify
		sgRNA scaffold
Linlab4594/YF	CCATCGATTTGCATTAGAA	Forward primer to amplify final
	CTAAAAACAAAGCA	gRNA cassette
Linlab4595/YF	CCGCTCGAGTAAAACAAAA	Reverse primer to amplify final
	AAGCACCGAC	gRNA cassette
Linlab4722/YF	agactccacagcctaagatcAACAGT	Reverse primer to amplify U6
	ATACCCTGCCGGTG	promoter with SH2 gRNA
Linlab4723/YF	gatcttaggctgtggagtctGTTTAG	Reverse primer to amplify
	AGCTAGAAATAGCAAGTT	gRNA scaffold with SH2 gRNA
Linlab4895/YZ	AAGGAAAAAGCGGCCGC	SRE1 native promoter forward
	AAATCGGCTGATCTTGTG	primer
Linlab3792/YF	GCCACTCGAATCCTGCATG	For screening of <i>SRE1</i> deletion,
T : 1 1 500 (NIZ	C	inside of NAT reverse
Linlab5936/YZ	GGGTTACAGTAGCAGTAGT	GPD1 terminator R primer for
Lim1ah 401 4/X/E	attatttaaagastsssssts	SH2 screening
Linlab4814/YF	gttgtttcaggcctgcggatg	SH2 sequencing primer F
Linlab4815/YF	GACTCATTCCTATGCCGTTC	SH2 sequencing primer R
Linlab8488/AM	CAACGCGGTAAGCATTAT	SRE1 inside ORF forward
Linlab4897/YZ	ATAGCGATCGCGATTTTGG TCTTGGCTGTTG	SRE1 inside ORF reverse

CHAPTER 3

NICKEL TOLERANCE IS CHALLENED THROUGH C-4 METHYL STEROL OXIDASE ERG25 IN THE STEROL BIOSYNTHESIS PATHWAY

² Amber R. Matha, Xiaofeng Xie, Robert J. Maier and Xiaorong Lin*. Submitted to *PLoS Genetics*, March 27, 2024.

Abstract

Nickel (Ni) is an abundant element on Earth and it can be toxic to all forms of life. Unlike our knowledge of other metals, little is known about the biochemical response to Ni overload. Previous studies in mammals have shown that Ni induces various physiological changes including redox stress, hypoxic responses, as well as cancer progression pathways. However, the primary cellular targets of nickel toxicity are unknown. Here, we used the environmental fungus Cryptococcus neoformans as a model organism to elucidate the cellular response to exogenous Ni. We discovered that Ni causes alterations in ergosterol (the fungal equivalent of mammalian cholesterol) and lipid biosynthesis, and that the Sterol Regulatory Element-Binding transcription factor Sre1 is required for Ni tolerance. Interestingly, overexpression of the C-4 methyl sterol oxidase gene ERG25, but not other genes in the ergosterol biosynthesis pathway tested, increases Ni tolerance in both the wild type and the $sre1\Delta$ mutant. Overexpression of ERG25 with mutations in the predicted binding pocket to a metal cation cofactor sensitizes Cryptococcus to nickel and abolishes its ability to rescue the Ni-induced growth defect of $srel\Delta$. As overexpression of a known nickel-binding protein Ure7 or Erg3 with a metal binding pocket similar to Erg7 does not impact on nickel tolerance, Erg25 does not appear to simply act as a nickel sink. Furthermore, nickel induces more profound and specific transcriptome changes in ergosterol biosynthetic genes compared to hypoxia. We conclude that Ni targets the sterol biosynthesis pathway primarily through Erg25 in fungi. Similar to the observation in C. neoformans, Ni exposure reduces sterols in human A549 lung epithelial cells, indicating that nickel toxicity on sterol biosynthesis is conserved.

Author Summary

Nickel is commonly known as an allergen and toxin for humans, but the way in which nickel causes adverse effects is unknown. We sought to use C. neoformans as a model to investigate the primary targets of nickel and how cells tolerate this commonly occurring metal. We found that in both mammalian cells and fungal cells, exposure to nickel causes sterol deficiency. We discovered that Erg25, an essential enzyme key to the production of ergosterol (fungal equivalent of cholesterol), was critical for cryptococcal cells to tolerate nickel. Cells unable to increase production of this enzyme in response to nickel exposure, such as the $sre1\Delta$ mutant with the Sterol Regulatory Element-Binding regulator disrupted, were incapable of growing in the presence of nickel. Therefore, it appears that both cells react to nickel through upregulating a conserved biochemical pathway and particularly the Erg25 enzyme. This work could guide future investigations into novel approaches to manage nickel toxicity.

Introduction

Ni is an abundant natural element ubiquitously found in soil and through industrial pollution (1, 2). The concentrations of this metal vary widely in different environments and organisms cope in various ways (2). Unlike metals such as copper (Cu) or iron (Fe), no mammalian enzymes require Ni as a cofactor (3). Indeed, Ni is generally characterized as a toxic heavy metal for humans. Exposure to Ni primarily occurs by inhalation or ingestion but also through interaction with everyday items that contain Ni, such as jewelry, zippers, paper clips, and stainless steel dining flatware (4). Additionally, corrosion of Ni-containing implants used in joint and hip prostheses may lead to elevated Ni levels in the body (5). Occupational exposure to nickel is the highest for those involved in producing, processing, and using nickel (6). A National

Occupational Exposure Survey conducted by the NIOSH agency from 1981 to 1983 estimated that 727,240 workers in the US were exposed to toxic levels of Ni (NIOSH 1990).

It is hypothesized that Ni is toxic to mammalian cells due to its ability to catalyze Fenton chemistry, which culminates in oxidative stress to the cells (7, 8), including lipid peroxidation (9-11). Ni is also capable of inducing calcium signaling pathways and activating HIF1-α (12, 13), which plays a central role in the progression of some cancers (14). HIF1-α is typically activated when cells experience hypoxia in the tumor microenvironment. This activation causes transcriptional increases in genes associated with angiogenesis, growth factors, pH regulation, and apoptosis (15). Thus, Ni has been characterized as a carcinogen in mammalian systems. Additionally, Ni has been shown to induce a disturbance in testosterone synthesis (16). The main therapy to mitigate Ni toxicity is administration of antioxidants, such as glutathione, which reduces lipid peroxidation in human lymphocytes (17). Because of the pleiotropic effects of Ni on cell structures and metabolism, it is difficult to define the primary mechanism of nickel toxicity.

Despite the fact that Ni is abundant in the environment, little research has been done to identify how environmental microbes tolerate this metal. *Cryptococcus neoformans*, a ubiquitous environmental fungus, is a model organism for studying fungal cellular biology due to the abundance of tools available to study and manipulate the fungus (18-21). *C. neoformans* has been used as a model to better understand cellular mechanisms conserved in mammals such as uniparental mitochondrial inheritance (22, 23), meiosis (24-27), epigenetic regulation (28, 29), and intercellular communication (30, 31). Here, we chose this fungus to investigate the molecular mechanism for Ni tolerance. In *C. neoformans*, urease is the only known protein that requires Ni for its function, although there are nine known Ni-dependent enzymes in other

microbes (32). Despite the fact that the role of urease in cryptococcal pathogenesis is well defined (33-36), its role in nickel tolerance is unknown.

Given that animals and fungi are closely related in the eukaryotic domain, understanding the effect of nickel on fungi and how fungi tolerate Ni could be informative. This study aims to identify pathways and factors critical for cryptococcal tolerance to Ni. We found that Ni exposure reduces ergosterol levels and altered lipid profiles in C. neoformans. We screened the transcription factor deletion set and identified Sre1 as an essential factor for cryptococcal growth on Ni-supplemented medium. Sre1 is highly conserved across Eukarya, and it is known to regulate the ergosterol biosynthesis pathway (EBP) in response to hypoxia and hypoxiamimicking conditions (37-41). We found that nickel, in contrast to hypoxia that exerts a broad impact on cryptococcal transcriptome, more narrowly but profoundly alters expression of EBP genes. Erg25, a conserved C-4 methyl sterol oxidase, but not other Erg enzymes in the sterol biosynthetic pathway or the known nickel-binding protein Ure7, is specifically required for cryptococcal tolerance to Ni. Increasing the levels of the C-4 methyl sterol oxidase effectively mitigates Ni toxicity, suggesting that Erg25 is a primary target of Ni toxicity. We further demonstrated that exposure to Ni in mammalian cells also reduced the sterol levels, mimicking what we observed in the fungus. Thus, nickel might exert its toxicity effects by primarily targeting the conserved sterol biosynthetic pathway in both fungi and animals.

Results

Screening transcription factor and kinase gene deletion libraries identified transcription factor Sre1 as required for cryptococcal tolerance of Ni.

As a ubiquitous environmental fungus often found in soils, *C. neoformans* is subjected to exogenous Ni. Here we first determined the Ni tolerance level of the wild-type H99 cells and

found that Ni concentrations beyond 250 μ M impaired growth of H99 (Figure S3.1A). As the only known *C. neoformans* enzyme that requires Ni is urease, we tested if urease plays a role in nickel tolerance. Nic1 imports Ni from the environment and Ure7 likely binds and delivers Ni to the apourease, Ure1 (35). As expected, all three mutants, $ure1\Delta$, $ure7\Delta$, and $nic1\Delta$, had abolished urease activity as indicated on Christensen Urea Agar (CUA) (Supplemental Fig 3.1B). As urease activity was dependent on Ni, addition of Ni chelator dimethylglyoxime (DMG) (42) abolished urease activity in H99 cells (Supplemental Fig 3.1C-D). However, we found neither $ure1\Delta$ nor $ure7\Delta$ were hypersensitive to exogenously added Ni (Supplemental Fig 3.1E), indicating that urease is not involved in Ni tolerance in *C. neoformans*.

To identify factors that contribute to Ni tolerance, we screened *C. neoformans* kinase (43) and transcription factor (44) deletion library collections (representing 155 and 129 genes, respectively) to identify mutants sensitive to Ni at 250 μ M. We found the $sre1\Delta$ mutant was the only strain hypersensitive to Ni (Figure 3.1A).

Sre1, or Sterol Regulatory Element Binding Protein (SREBP) as it is known in animals, is a transcription factor well known to control the regulation of the sterol biosynthetic pathway in response to several stimuli including hypoxia (37, 45). Sre1 exists in an inactive state as a full-length protein on the endoplasmic reticulum in coordination with the anchor protein Scp1. Upon various stimuli (hypoxia or low levels of ergosterol), this complex is trafficked to the Golgi where the protease Stp1 cleaves the N-terminus of Sre1. Once cleaved, the Sre1 N-terminus (N-Sre1) translocates to the nucleus to induce transcription of downstream target genes (Figure 3.1B, (38)). Indeed, all the deletion mutants of Sre1 pathway components, namely $scp1\Delta$ and $stp1\Delta$, were also hypersensitive to Ni (Figure 3.1A). Expression of the N-terminus portion of Sre1 in the $stp1\Delta$ background partially restored its growth on Ni (Figure 3.1A), consistent with

the idea that activation of Sre1 is required for nickel tolerance. To confirm that Ni activates Sre1, we constructed a Sre1 allele with a FLAG tag at its N-terminus and expressed this construct in the wild type. When cultured on RPMI, only the full length Sre1 protein was detected (Fig. 1C). However, when the strain was grown on RPMI media containing 250µM Ni (N) or 4µg/mL Fluconazole (F), a lower band at 75kDa consistent with the cleaved N-Sre1 became visible in addition to the full length band (39) (Figure 3.1C). Thus, nickel, like fluconazole, activates the cleavage of Sre1. Collectively, these results demonstrate that activated Sre1 is critical for *C. neoformans* to tolerate Ni.

We hypothesized that Ni may outcompete other important metal cofactors (e.g., copper, iron, or zinc) in the $sre1\Delta$ mutant, rendering the strain unable to grow in the presence of Ni. Typically, enzymes utilize specific metal cofactors for their activity and strict homeostasis mechanisms ensure correct metalation of proteins. When metal homeostasis becomes imbalanced, mis-metalation can occur, inhibiting protein function (46). However, the addition of iron (Fe), copper (Cu), or zinc (Zn) to the Ni medium failed to rescue the growth defect of the $sre1\Delta$ mutant (Figure 3.1D). Mutants defective in iron and copper-specific regulators Cir1 (47) and Mac1 (also known as Cuf1) (48) did not show any growth defect in Ni-supplemented medium (Figure S3.2A), indicating that Sre1 plays a specific role in regulating cryptococcal tolerance to Ni.

We considered the possibility that poor growth of $sre1\Delta$ on Ni could indicate toxicity caused by accumulation of excessive intracellular Ni. To test this possibility, we analyzed the cellular Ni concentrations in wild-type (WT) H99, the $sre1\Delta$, the $cir1\Delta$, and the $mac1\Delta$ strains grown on RPMI, RPMI+Ni, or RPMI+DMG (Ni chelator) by Inductively Coupled Plasma Mass Spectrometry (ICP-MS) using a previously established method (49). We also included a known

Ni transporter mutant, $nic1\Delta$ (35). The level of Ni associated with $sre1\Delta$ cells was comparable to WT when cells were cultured in Ni-supplemented medium (Figure 3.1E). By contrast, $nic1\Delta$, $cir1\Delta$ and $mac1\Delta$ showed altered cellular accumulation of Ni (Figure 3.1E), with $nic1\Delta$ and $mac1\Delta$ accumulating 1.7 and 2.4 times more Ni than wild type, respectively. Surprisingly, the $sre1\Delta$ mutant accumulated significantly more Cu and Zn than wild type when cultured on Ni-supplemented medium (Figure S3.2B). However, the $sre1\Delta$ mutant was not hypersensitive to either copper or zinc (Figure 3.1D). The increased amount of Ni in $nic1\Delta$ cells is consistent with previous findings suggesting that Nic1 is not the only transporter of Ni (35). Given that increased accumulation of Ni in $nic1\Delta$ and $mac1\Delta$ did not cause growth defect on media with Ni and that the $sre1\Delta$ mutant did not accumulate more Ni than wild type, these results indicate that the growth defect of the $sre1\Delta$ mutant is not due to the over-accumulation of intracellular Ni.

Ni causes up-regulation of ergosterol biosynthesis pathway (EBP) genes.

Addition of copper and iron cause dramatic changes to cryptococcal transcriptome (50, 51). To investigate the transcriptomic response to Ni exposure and the role of Sre1, we conducted a comparative transcriptome analysis by RNA deep sequencing (RNA-seq). Wildtype and $sre1\Delta$ cells were grown on RPMI plates with or without supplementation of Ni (0.25mM) or DMG (4mM) at 37°C. RPMI was chosen as growth medium since it is a defined medium and commonly used for testing antifungal or stress susceptibility. The cells were cultured for eight hours prior to RNA extraction and sequencing.

We found 87 genes in H99 were upregulated and 71 genes downregulated on Ni versus the RPMI control (Table S3.1). Here we consider genes showing at least a 2-fold change ($|\log 2(\text{Fold Change})| \ge 1$) in transcript level differentially expressed genes (DEGs). Six of the 87 upregulated genes were EBP genes (namely *ERG10*, *ERG8*, *ERG25*, *ERG6*, *ERG2*, *ERG4*:

red spots outside of the shaded area in Figure 3.2A) and SRE1 was also significantly upregulated on Ni (log2(Fold Change) = 1.05). Ten additional EBP genes were considered modestly upregulated, with log2(Fold Change) values between 0.3 and 0.99 (red spots within the shaded area in Figure 3.2A, Figure. 3.2B). The six highly upregulated EBP DEGs were spread throughout the pathway, with two occurring in the mevalonate pathway and four in the late pathway (Figure 3.2C). Interestingly, although Ni was able to upregulate ergosterol biosynthesis genes, DMG did not cause any significant downregulation of these genes (Table S3.2). We also noted that addition of Ni did not change the transcript levels of *URE1* and *URE7*.

Given that Sre1 is known to impact transcription of EBP genes, the impact of Ni on transcription of these genes might be largely due to the response of Sre1 to this metal. To assess this, we looked at the transcriptome of $sre1\Delta$ grown on Ni and in hypoxia conditions. When compared to the wildtype grown on Ni, there were 12 negative DEGs that belonged to the EBP pathway (Table S3.4, Supplemental Fig 3.3A). 20 EBP genes showed altered expression. In comparison, hypoxia had a more limited impact on EBP gene expression in the $sre1\Delta$ mutant compared to the wildtype (Table S3.5, Supplemental Fig 3.3B). Only four EBP genes (ERG2, ERG5, ERG25, and ERG3) were differentially expressed. Seven EBP genes showed altered gene expression. Thus, Ni exacerbates the reduced transcription of EBP genes in the $sre1\Delta$.

Sre1 is also known to regulate the expression of Fe homeostasis genes (37). Interestingly, Fe-starvation-related genes were overrepresented in the downregulated DEGs on Ni in wildtype cells. This is in contrast to EBP genes, which were upregulated in response to Ni. The most downregulated gene is an iron-starvation-responsive mannoprotein, *CIG1* (52). Two oxidoreductases, *FRE7* and CNAG_02839, and two siderophore transporters, *STR1* and *SIT2*, were among the 20 most downregulated genes (Table S3.1). All of these genes were significantly

upregulated in cells grown on DMG-supplemented medium (Table S3.2). Interestingly, addition of Ni to the RPMI medium decreased intracellular iron content in wild type but increased iron level in $sre1\Delta$ cells based on our ICP-MS data (Supplemental Fig. 3.4A). We speculated that Ni supplementation might have caused the cells to mistakenly sense that they were in an iron excess environment and that downregulation of iron-limitation responsive genes might contribute to the hyper-sensitivity of $sre1\Delta$ to Ni. However, the observation that adding iron to the Ni supplemented medium did not restore growth of the $sre1\Delta$ mutant (Figure 3.1D) and that neither deletion nor overexpression of CIG1 had any effect on the susceptibility of $sre1\Delta$ to Ni (Figure S3.4B) suggest that the ability to respond to intracellular Fe may not be the driving force behind the Ni sensitivity of $sre1\Delta$.

As Sre1 is critical for hypoxia growth (53), and other divalent cations such as cobalt chloride (CoCl₂) have been characterized as hypoxia-mimicking agents (39, 54), it is possible that Ni has a similar hypoxia-mimicking effect on *C. neoformans*. We found that CoCl₂ is highly toxic to *Cryptococcus* as both the wildtype and the $sre1\Delta$ cells were unable to tolerate 250 μ M CoCl₂ in RPMI media (Figure S3.5A). Another transcription factor, Pas2, is important for remodeling cellular metabolism in response to hypoxia (53). Deletion of this gene renders cells sensitive to hypoxia and CoCl₂ stress (53). We hypothesized that if Ni mimics hypoxia, then $pas2\Delta$ would be sensitive to Ni as well. Indeed, $pas2\Delta$ was slightly more sensitive to Ni than WT, but much tolerant than the $sre1\Delta$ mutant (Figure S3.5B). This is consistent with previous findings in which $pas2\Delta$ is less sensitive to hypoxia than is $sre1\Delta$. In all, this data suggests that Ni and hypoxia have some shared effects on cryptococcal cells.

To further compare cryptococcal response to hypoxia and Ni, we performed comparative analyses of RNA-seq data between cells exposed to hypoxia and cells exposed to Ni. Under

hypoxia conditions (0.1% O2, 5% CO2, 37°C), we found 167 upregulated DEGs and 434 downregulated DEGs (Table S3.3), showing that hypoxia has a broader effect on gene expression than Ni. Despite the larger number of DEGs, hypoxia resulted in only one EBP gene, *ERG25*, being an DEG with more than a 2-fold change in transcript level (Figure 3.3D-E). The data indicates that Ni, relative to hypoxia, has a more narrow, but profound impact specifically on the EBP. We also examined genes that were shared between wildtype cells grown exposed to Ni and wildtype cells exposed to hypoxia (Table S3.6). We discovered that only 8 genes were upregulated and 28 genes were downregulated DEGs in both conditions (Supplemental Fig. 3.3C). Thus, Ni and hypoxia have distinct effects on cryptococcal transcriptome.

Overexpression of ERG25, but not other four ERG genes tested, confers Ni tolerance.

Sre1 is known to regulate ergosterol biosynthesis, and our RNA-seq data showed that Ni causes an upregulation of multiple EBP genes. We postulated that ergosterol deficiency due to the SRE1 deletion may contribute to $sre1\Delta$ Ni hypersensitivity. If this is true, then perturbations of the EBP pathway may also alter cryptococcal tolerance to Ni. So, we tested the deletion mutants of the non-essential ERG3 and ERG4 genes. Previous studies have shown that mutation of these genes perturbs ergosterol biosynthesis. For example, deletion of ERG3 causes increased resistance to azoles (target Erg11) and Amphotericin B (bind to ergosterol directly) in C. neoformans and in Candida species (55-57). Deletion of ERG4 causes an increased sensitivity to caspofungin that targets $\beta1$ -3 glucan synthase in the membrane (58). To our surprise, $erg3\Delta$ and $erg4\Delta$ mutants grew like the wild type on RPMI+Ni (Supplemental Fig 3.6). Thus, it appears that perturbation of the EBP pathway, in general, does not alter cryptococcal tolerance to Ni.

To further interrogate our hypothesis, we decided to examine the impact of overexpression of ERG genes on Ni tolerance. We chose to overexpress ERG genes because

most ERG genes are essential and cannot be deleted. Overexpression of ERG genes has been adopted as an effective approach to study the EBP pathway in S. cerevisiae (59). To that end, we selected and overexpressed five EBP genes – ERG2, ERG11, ERG25, ERG26, and ERG27– in the wildtype and the $sre1\Delta$ backgrounds. To determine if these overexpressed ERG genes are functional, we first tested the susceptibility of these ERG gene overexpression strains in H99 background to fluconazole (60). Fluconazole is an antifungal drug that inhibits Erg11, causing a reduction of ergosterol and a buildup of methylated sterols, collectively disrupting membrane stability (61). We found that overexpression of any of the five EBP genes enhanced resistance to fluconazole, albeit at varied degrees (Figure 3.3A). As expected, overexpression of *ERG11*, the direct target of azole drugs, offered the highest level of resistance to fluconazole relative to the other ERG genes (Figure 3.3A). This result indicates that the overexpressed ERG genes are functional. However, when introduced to the $sre1\Delta$ mutant, none of the ERG overexpression was able to restore tolerance to fluconazole, with *ERG11* being the only exception (Figure 3.3B). This result reaffirms that Erg11 is the direct target of fluconazole and that overexpression of ERG11 confers resistance to fluconazole regardless of the strain background.

After confirmation that these overexpressed EBP genes are functional, we sought to determine the effect of overexpression of these EBP genes on Ni tolerance. In contrast to what we observed in fluconazole resistance, the $ERG25^{OE}$ strain in H99 background was exceedingly tolerant of Ni. The $ERG25^{OE}$ strain grew much better than the wild type on RPMI+500 μ M Ni, a condition that all other strains, including wild-type H99, were unable to tolerate (Figure 3.3C). Overexpression of ERG25, a known direct target of Sre1 (39), conferred marked Ni tolerance to the $sre1\Delta$ mutant as well. The $ERG25^{OE}$ $sre1\Delta$ strain was much more tolerant to Ni than the wildtype strain (Figure 3.3D). Interestingly, overexpression of any of the other ergosterol

biosynthesis genes, including ERG11 and ERG2 that lie upstream and downstream of ERG25 respectively, did not confer Ni tolerance to either the wild type or the $sre1\Delta$ mutant. The overexpression of ERG26 and ERG27, which encode enzymes that complex with Erg25, did not impact Ni tolerance either. This suggests that Erg25 specifically, not the EBP in general, plays a major role in mediating cryptococcal tolerance to Ni.

As we noted previously, hypoxia and Ni elicit both shared and distinct transcriptome changes in Cryptococcus, with Ni eliciting more profound and specific changes in the EBP pathway. ERG25 is the shared gene upregulated by both stressors. A previous study identified ERG25 as a multicopy suppressor of $scp1\Delta$ and $sre1\Delta$ sensitivity on CoCl₂, a known hypoxiamimicking agent (39). We found that overexpression of ERG25 conferred tolerance to CoCl₂ in both wild-type and $sre1\Delta$ backgrounds (Figure S3.7A-B), in agreement with the previous study. Overexpression of other ERG genes tested failed to confer significant tolerance to CoCl₂ in either the wild-type or the $sre1\Delta$ background. When the strains were grown in hypoxia conditions, we found that all overexpression strains in the wildtype background grew similarly to the H99 control (Figure S3.7C). However, the overexpression of ERG25, ERG2, ERG11, and ERG26 all rescued the $sre1\Delta$ hypoxia growth defect albeit in varying degrees in that order (Figure S3.6D). The ERG25 overexpression best rescued sre1 Δ growth in hypoxia, which could be attributable to the upregulation of ERG25 in the hypoxia condition that was indicated by our RNA-seq data (Figure 3.2D). The results support that upregulation of the EBP pathway genes generally enhances growth in hypoxia and confers resistance to fluconazole, but ERG25 is specifically required for cryptococcal tolerance to cobalt and Ni.

Ni alters the cellular lipid profile.

Our results above demonstrate that Ni increases transcription of ergosterol genes and overexpression of ERG25 in particular increases cryptococcal tolerance of Ni. To examine if Ni indeed impacts ergosterol levels, we extracted cellular ergosterol from wild-type and $sre1\Delta$ cells cultured on RPMI medium with or without the addition of Ni, and quantified ergosterol levels by measuring the absorbance at 282nm (62). We found that the ergosterol content in WT was reduced by 10% when exposed to Ni (Figure 3.4A). As expected, the ergosterol level in $sre1\Delta$ cells was lower under the normal growth condition with 80% of that in wildtype H99 cells, and exposure to Ni caused a further reduction to 65% of that in untreated H99 cells. When exposed to Ni, the resulting amount of ergosterol in $sre1\Delta$ cells was similar to that in H99 cells exposed to fluconazole (Figure 3.4A). Filipin staining of ergosterol present in the outer leaflet of plasma membrane (60, 63, 64) showed that Ni exposure caused a 50% reduction in plasma membrane ergosterol in H99 (Fig 3.4B-C), consistent with the lower ergosterol levels in the presence of nickel measured spectrophotometrically (Figure 3.4B-C). The fluorescence intensity of $sre1\Delta$ cells was 50% of the wild-type level. Ni exposure reduced the fluorescence intensity even further to about 16% of that in H99 cells grown on RPMI (Figure 3.4C). Although both measurements revealed the same trend, the stronger reduction caused by the SRE1 deletion or by Ni treatment measured by fluorescence intensity of filipin staining compared to spectrometry may be due to the fact that the extracts contain other lipids in addition to ergosterol or its intermediates.

Thin layer chromatography (TLC) analysis also revealed altered lipid profiles when cells were treated with Ni (Figure 3.4D). Based on previous literature using the same procedures for extraction and TLC (65), Ni causes an increase in the intensity of two of these bands, likely the methyl sterol (white arrow) and free fatty acid band (yellow arrow), and there is a slight decrease

in the ergosterol band at the bottom (Figure 3.4D). Previous studies in yeast have shown that mutations that reduce the activity of ERG25 caused a similar increase in the intensity of the methyl sterol and free fatty acid bands (65). This result corroborates our hypothesis that Ni primarily targets Erg25 in the EBP pathway. In agreement with other measurements, the TLC analysis also revealed that ergosterol level was reduced in the $sre1\Delta$ mutant. The thick ergosterol band was reduced compared to the wildtype H99 strain when grown on RPMI medium, and this band was almost undetectable when the mutant was grown on RPMI with Ni (Figure 3.4E). The ERG25 overexpression strain still showed a decrease in ergosterol content when plated on Ni media (Figure 3.4D). However, when ERG25 was overexpressed in the $sre1\Delta$ background, an ergosterol band is still observable in contrast to the $sre1\Delta$ strain on Ni.

Two histidine residues in Erg25 metal binding motifs are important for Ni tolerance.

The results presented earlier indicate that Erg25 is critical for Ni tolerance in C. neoformans. Erg25 contains four conserved metal binding motifs enriched in histidine (Figure S3.8). According to AlphaFold, several histidine residues are predicted to associate in a histidine-rich pocket present in Erg25 (66, 67). These histidine residues are from three of the four metal binding motifs and are not simply histidine residues proximal to each other in the primary sequence. In these regions, pairs of His residues (H187 and H272) are predicted to interact via cation-pi interactions (Figure 3.5A). I-TASSER, a protein structure prediction software (68-70), similarly predicts that these histidine residues are capable of interacting with a cation. We postulate that Ni binds to Erg25, and these His residues are critical for the function of Erg25.

To test our hypothesis, we mutated histidine residues 187 and 272, and overexpressed the $ERG25^{\rm H187A\,H272A}$ allele in both the wild-type and the sre1 Δ background. Although

overexpression of the $ERG25^{H187A\ H272A}$ allele in wild type did not have any effect on growth on RPMI medium, it slightly reduced cryptococcal tolerance to Ni, in contrast to the muchenhanced Ni tolerance by the overexpression of the ERG25 allele (Figure 3.5B). Accordingly, the overexpression of the $ERG25^{H187A\ H272A}$ allele failed to rescue the growth defect of $sre1\Delta$ on Ni supplemented medium (Figure 3.5C). We speculate that mutations of these histidine residues prevented the binding of $ERG25^{H187A\ H272A}$ to Ni, which might have allowed Ni to bind to the native Erg25, compromising ergosterol biosynthesis. Moreover, $ERG25^{H187A\ H272A}$ may compete with the native Erg25 to complex with Erg26 and Erg27, further impairing the EBP pathway, rendering cells hypersensitive to Ni. Indeed, TLC analysis revealed that the $ERG25^{H187A\ H272A}$ overexpression strain had a larger reduction in ergosterol when exposed to Ni compared to the wildtype (Figure 3.5D).

Overexpression of *ERG3* nor *URE7* are capable of rescuing $sre1\Delta$ growth on Ni.

We hypothesize that either Erg25 enzymatic function is required for nickel tolerance or Erg25 acts as a nickel sink because of its metal binding pocket can bind to nickel efficiently. Deletion of SRE1 reduces Erg25 abundance and thus renders the fungus sensitive to nickel. Conversely, over-production of Erg25 confers Cryptococcus nickel resistance. However, these observations do not distinguish the two aforementioned hypotheses. To that end, we decided to overexpress another protein with a similar metal binding pocket. We expect that if the "nickel sink" hypothesis is true then overexpression of this protein would also confer nickel tolerance. Erg3 possesses similar conserved metal binding motifs as Erg25 (Figure 3.5D) (66,67). ERG3 is not on our DEG list because its transcript level increase in response to Ni was below 2-fold (Figure 3.2B). However, we found that unlike ERG25, overexpression of ERG3 did not have any obvious impact on cryptococcal growth or Ni tolerance in either the wild type or the $Sre1\Delta$

mutant (Figure 3.5B). Consistent with ERG3 being non-consequential in conferring Ni tolerance, TLC analysis revealed a similar trend noted above regarding lipid changes in response to Ni in both wild type and in $sre1\Delta$ with or without ERG3 overexpression. Therefore, Erg3 simply possessing a similar binding pocket to Erg25 is not sufficient for $sre1\Delta$ growth rescue on Ni.

We decided to test our hypotheses further with a known nickel-binding protein. Ure7 binds Ni as a chaperone protein during the activation of Ure1 (35). Again, if the "nickel sink" hypothesis is true, we expect URE7 overexpression would allow for Ni tolerance of the $sre1\Delta$ mutant. We first confirmed that our overexpression construct indeed increased the URE7 transcript level in the wild type and we then deleted SRE1 in the $URE7^{OE}$ overexpression strain. We confirmed increased URE7 transcript level in both WT and $sre1\Delta$ background via RT-PCR (Supplemental Figure 3.9). The URE7 overexpression construct, once introduced into the $ure7\Delta$ mutant, was able to restore its urease activity assay based on CUA assay (Figure 3.6A), thus confirming that the overexpressed Ure7 is functional. Upon spotting strains onto RPMI media $+/-250\mu$ M Ni, we found that the URE7 overexpression failed to restore growth of the $sre1\Delta$ mutant on Ni (Figure 3.6B). In all, the findings indicate that in contrast to ERG25, overexpression of ERG3 or URE7 does not confer nickel tolerance. Thus, Erg25 is likely not acting simply as a Ni sink.

Ni reduces cholesterol in mammalian cells.

Ni is known to affect lipid profiles in mammals. In humans and animals, exposure to Ni is associated with decreased serum cholesterol levels (71, 72). Given our finding about the impact of Ni on the sterol biosynthetic pathway in *C. neoformans* and the fact that the sterol biosynthetic pathway is highly conserved between fungi and humans/animals (73), we hypothesized that exposure of Ni will reduce cholesterol at the cellular level in mammals as well.

Here, we cultured human epithelial A549 cells with or without addition of Ni at 10, 50 or 100 μM. We then stained the cells at 72 hours with filipin. The epithelial cells were able to grow desmosomes in all Ni concentrations tested (Figure 3.7A). We found that after passaging epithelial cells for 72 hours with 10, 50, or 100μM Ni, cells showed a 2.1, 4, or 5-fold reduction in filipin fluorescence intensity compared to unexposed cells (Figure 3.7A-B). This result suggests that Ni also reduces the amount of cholesterol in mammalian cells, similar to its ergosterol reduction effect in fungal cells. Whether Erg25 homolog Fet6 is also involved in nickel tolerance in mammals is yet to be tested.

Discussion

Ni at high concentrations is toxic to cells, prokaryotic or eukaryotic (2, 74, 75). However, some bacteria species utilize Ni for essential protein functions (76-78). Only one protein in *C. neoformans* (and in some other fungi), urease, is known to bind Ni. We have shown here that urease activity cannot occur when Ni is unavailable but urease is not required for the fungus to tolerate Ni. What mechanisms cryptococcal cells employ to regulate Ni homeostasis, particularly tolerance to Ni, remained unknown.

Ni has been shown to decrease plasma lipids; including total cholesterol, high-density lipoprotein-cholesterol, low-density lipoprotein-cholesterol (LDL) in a general population captured by NHANES study (72). Ni is also capable of causing lipid peroxidation (11). In rats, Ni depletion has been shown to increase the amount of cholesterol and LDLs (79). However, in chickens, Ni supplementation did not alter cholesterol content (80). We found that Ni supplementation decreases ergosterol content in *C. neoformans* and cholesterol in A549 human lung epithelial cells. Via RNA-sequencing we have also characterized the role of Ni as a stimulant of the EBP pathway.

Strikingly, Erg25 is the most upregulated EBP in response to Ni from these experiments and the only ERG gene that confers remarkably tolerance to nickel when overexpressed. This is in contrast to tolerance of fluconazole, where overexpression of multiple ERG genes conferred resistance even though the direct target Erg11 was the most effective. Erg25 is known to complex with Erg26 and Erg27 (59, 81), but the overexpression of ERG26 or ERG27 does not have any significant impact on Ni tolerance. The stoichiometry of Erg25, Erg26 and Erg27 protein levels in the cell is not 1:1:1. In the fission yeast Schizosaccharomyces pombe, cells contain approximately 41 ERG25, 6 ERG26, and 3 ERG27 RNA molecules per cell (82). Erg25 in S. pombe was 2.5 times more abundant at the protein level than other complex members (83). A similar phenomenon was observed in S. cerevisiae (84). If Erg25 formed dimers or trimers, that may explain why the cell would produce Erg25 in such excess compared to other complex members. However, this has not been shown to be the case (81). It is possible that Erg25 may perform a function outside of the studied complex that has not yet been revealed. Alternatively, Erg25 may control the rate limiting step and more Erg25 proteins are needed to produce the precursors used by the downstream enzymes. This is possible as the complex formation is likely more important for metabolic channeling rather than for specific enzymatic reactions carried out by these proteins per se, similar to subcellular compartmentalization of fungal secondary metabolism (85). We suspect that overexpression of Erg25 is able to serve as a chelator of Ni, and due to its abundance, still has sufficient level of the proteins to serve its function in the Erg25/Erg26/Erg27 complex in the sterol biosynthetic pathway in the presence of Ni. This ultimately allows the $sre1\Delta$ mutant to grow on Ni supplemented medium. Production of abundant ERG25^{H187A H272A} could compete and thus compromise the activity of the native Erg25

protein, becoming a poisonous subunit in the complex. Its ill effect becomes apparent in the presence of Ni.

We argue that Erg25 does not simply act as a sink for intracellular Ni. The adverse effect of Ni on growth in $sre1\Delta$ is more likely attributable to its impact on Erg25's specific function, which cannot be recapitulated by overexpression of another enzyme with the same or similar metal binding pocket. Consistent with this idea, overexpression of ERG3 is incapable of rescuing the growth of $sre1\Delta$ on Ni or conferring Ni tolerance to the wildtype cells despite the conserved histidine enriched region present in Erg3. That said, it is also possible that this could be due to differences in protein structures that allow different levels of access to Ni ion. Ni-binding proteins are difficult to predict. Our screening of gene deletion mutants of genes that encode histidine enriched proteins did not identify any additional genes that are essential for Ni tolerance. We also used Ni-beads to try to identify proteins in C. neoformans that can bind Ni, and the only reliable nickel-binding protein pulled down in these assays was Ure7. The finding that overexpression of this known nickel-binding protein Ure7 does not rescue nickel sensitivity in the $sre1\Delta$ mutant further bolstered the conclusion that Erg25 is not acting simply as a nickel sink, but rather its function integrity is required for nickel tolerance.

In all, we have described that Ni impacts sterol profiles in *C. neoformans* and cells respond by upregulating the sterol biosynthesis pathway in order to tolerate this metal. Multiple lines of evidence support the idea that Ni specifically targets Erg25 analogous to how fluconazole targets Erg11. Furthermore, the reduction of sterols in the presence of Ni is conserved in both fungi and mammals. Whether Ni acts on the same targets in fungi and mammals for such an effect is unknown. The current findings could stimulate research and development of effective ways to mitigate or prevent Ni toxicity.

Materials and Methods

Strains and Growth Conditions

C. neoformans strains used in this study are listed in Table S3.7. Strains were stored at -80°C in 15% glycerol stocks and freshly streaked onto yeast peptone dextrose (YPD) media prior to experimentation. Cells were maintained on YPD medium at 30°C unless stated otherwise. RPMI 1640 medium (catalog number. SH30011.04, Cytiva)+ 165mM MOPS was prepared and adjusted to pH=7 for all experiments in which cells were grown on RPMI medium.

Gene Deletion Mutant Library Screen for Sensitivity to Ni or DMG

To identify genes deletion mutants sensitive to the Ni chelator DMG or Ni, the transcription factor and kinase deletion libraries generated by Dr. Yong-Sun Bahn's group (43, 44), and the partial genome deletion library generated by Dr. Hiten Madhani's group were replicated into RPMI liquid media at 37°C and incubated for 1-2 days to allow them to reach the stationary phase. The libraries were replicated in RPMI medium to ensure that any phenotype we observed on our RPMI+Ni or RPMI+DMG plates was not due to the mutant's growth impairment in RPMI media. These cultures were spotted onto solid RPMI supplemented with 4 mM DMG or 250 µM Ni and grown at 37°C for three days to assess sensitivity visually.

To examine sensitivity to various metals, strains were grown in YPD liquid medium overnight with shaking at 220 rpm at 30°C. Cells were collected, washed once with sterile water, and adjusted to a cell density of OD600=1. The cells were then serially diluted in 10-fold and spotted onto RPMI plates with the indicated metals: CuSO₄ (Cu), ZnCl₂ (Zn), and FeSO₄ (Fe) at 250 μM. Unless otherwise indicated, RPMI+Ni plates contained 250 μM NiSO₄. The plates were incubated at 37°C for two days before imaging.

Urease Activity

Urea Agar (Becton Dickinson 211795) was prepared following the manufacturer's protocol. Plates were supplemented with indicated concentrations of DMG. Cryptococcal cells of the indicated strains (OD600=3) were spotted onto agar plates and incubated at 30°C for 2 days before imaging.

Fluconazole Sensitivity Assay

To examine fluconazole sensitivity, similarly prepared cells with serial dilutions were spotted onto yeast nitrogen base (YNB) agar as well as YNB with fluconazole at the indicated concentrations.

Western Blot

Strain Linlab7787 expressing 3xFlag-Sre1 were cultured on RPMI, RPMI+ 250μM Ni, and RPMI+4μg/mL fluconazole plates. The cells were collected by centrifugation and the supernatant was discarded. The cell pellet was frozen in liquid nitrogen. 1mL pre-chilled 0.2 M NaOH (0.2% β-ME) and 0.5mm glass beads were added to the cell pellet. The cells were disrupted at 4°C with a bead beater (Next Advance) 5 times at 1 min working and 1 min rest. The supernatant was transferred to a new Eppendorf tube and 75μL of 100% trichloroacetic acid (TCA) was added. After 10-minute incubation on ice, the extraction was centrifuged at 12,000rpm for 5 minutes at 4°C and the supernatant was discarded. The pellet was resuspended in 100μL 1M Tris and was denatured with an SDS-containing loading buffer prior to electrophoresis on an SDS-12% PAGE gel. Samples separated on the SDS-PAGE gel were transferred to polyvinylidene difluoride (PVDF) membrane (Millipore), using the eBlot L1 Fast Wet Protein Transfer System (GenScript) using preset protocols. The blots were incubated with Mouse anti-Flag antibody diluted 1:2,000 (Sigma; Lot #: SLCJ3741), washed, and then

incubated with Rabbit anti-mouse secondary antibody diluted 1:20,000 (Clontech Inc.). Signals were detected using enhanced chemiluminescence (ECL) according to manufacturer instructions (Pierce). Protein loading was confirmed via Coomassie staining.

Gene Manipulation

All primers and plasmids used in this study are listed in Table S3.8. For gene overexpression, open reading frames (ORFs) of the indicated genes were amplified by PCR from *C. neoformans* H99 genomic DNA and cloned into vectors containing *TEF1* (pLinlab995) or *GPD1* (pLinlab1059) promoters. Plasmids were confirmed via two rounds of restriction enzyme digestion. M13F and M13R primers were used to PCR amplify the donor DNA, which was introduced into the indicated recipient strains using the Transient CRISPR-Cas9 coupled with Electroporation (TRACE) protocol as we described previously (86). Constructs were integrated into the safe haven SH2 region (87).

For gene deletion of *SRE1*, the deletion cassette was amplified from genomic DNA (gDNA) of a sre1Δ mutant, which is part of the *C. neoformans* transcription factor deletion library generated by Dr. Yong-Sun Bahn and colleagues (44). To generate the sgRNA for the *SRE1* deletion, the U6 promoter was amplified from JEC21 gDNA and the sgRNA scaffold was amplified from plasmid pDD162, using primer pairs Linlab4627/Linlab7751 and Linlab4628/Linlab7752, respectively. The *U6* promoter and sgRNA scaffold pieces were fused together by overlap PCR with primers Linlab4594/Linlab4595 to generate the final sgRNA construct as described previously (88, 90).

Overexpression and deletion constructs were transformed into the indicated *C*.

neoformans strains via TRACE (88, 90). Transformants were selected on YPD medium with

100 μg/ml of nourseothricin (NAT), 100 μg/ml of neomycin (NEO), or 200 μg/ml of hygromycin (HYG) depending on the drug marker used.

The successful deletion of *SRE1* was screened via diagnostic PCR. Primer pair Linlab4895 (a *SRE1* promoter forward) and Linlab3792 (a reverse primer inside the NAT cassette) were used to ensure that the drug marker was inserted into the *SRE1* locus. Primers Linlab8488 and Linlab4897, which both lie on the *SRE1* open reading frame, were used to ensure that the ORF was missing. The successful integration of EBP gene overexpression constructs into the *SH2* region was screened via 3-primer PCR (89). Since the construct can insert into the *SH2* region in either the forward or the reverse direction, primer Linlab5936, a reverse primer on the overexpression construct was paired with *SH2* sequencing primers Linlab4814 and 4815. A band indicative of the direction the construct was inserted into the genome, or if it was not inserted would be amplified with three primer PCRs.

The *ERG25*^{H187A H272A} overexpression strain was constructed by amplifying the gene with primers with nucleotide changes that would mutate the indicated histidine codons to alanine. The successfully amplified ORF was cloned into pLinlab995 to be under the control of the constitutively active *TEF1* promoter. All overexpression constructs were PCR amplified with M13F and M13R, and transformed into the *SH2* region in the indicated recipient strains using TRACE.

RNA Extraction and Real-Time PCR

Real-Time PCR (RT-PCR) was used to confirm the EBP gene and *URE7* overexpression strains. Cells were grown in YPD liquid cultures with shaking at 30°C overnight. Cells were collected, flash-frozen with liquid nitrogen, and lyophilized overnight. Desiccated cells were disrupted with glass beads, and total RNA was extracted using the PureLink RNA Mini Kit

(Invitrogen) according to the manufacturer's instructions. To remove any potential DNA contamination, samples were treated with DNase using the TURBO DNA-free Kit (Invitrogen) following the manufacturer's protocol. First-strand cDNA was synthesized using the GoScript Reverse Transcription System (Promega) following the manufacturer's instructions. Power SYBR Green (Invitrogen) was used for all RT-PCR reactions. TEF1 was used as an internal control for all RNA samples. All RT-PCR primers used are listed in Table S3.2. Relative transcript level was determined using the $\Delta\Delta$ Ct method as we described previously (90) and statistical significance was determined using Student's t-test.

RNA Deep Sequencing

For transcriptome analysis in response to DMG, Ni, or hypoxia, overnight cultures in liquid YPD of the indicated strains were collected and washed twice with sterile dH₂O. Approximately 3x10⁸ cells were plated onto RPMI plates with or without supplementation with 250µM Ni or 4mM DMG. Cells were then incubated for eight hours at 37°C. Under the hypoxia condition, cells were cultured on RPMI plates for eight hours in the hypoxia chamber set to 0.1% O₂, 5% CO₂. The hypoxic environment was maintained using a Biospherix C chamber with O₂ levels controlled by a Pro-Ox controller and CO₂ levels controlled by a Pro-CO₂ controller (Biospherix, Lacona, NY, USA). At the designated time, cells were scrapped from the plates quickly, snap-frozen with liquid nitrogen, and then lyophilized. Total RNA from these cell samples was extracted using the PureLink RNA mini kit (Life Technologies) as described earlier. RNA samples were sent to GENEWIZ, Inc. for sequencing (polyadenylated RNA enrichment, non-strand-specific, paired end 150 bp on Illumina HiSeq platform). The raw reads were trimmed using Trim_Galore (0.6.5) and aligned to Cryptococcus neoformans var. grubii H99 reference genome using STAR (2.7.1a). The alignment files (Bam) were used to generate read

counts and Fragments Per Kilobase of transcript per Million mapped reads (FPKM) with Cufflinks (2.2.1). Differential gene expression analysis was performed using DESeq2 with false discovery rate (FDR) adjusted p-value ≤ 0.05 as threshold.

RNA-Seq Data Availability

The raw sequencing reads from this study have been submitted to the NCBI Sequence Read Archive (BioProject PRJNA1082343).

Microscopy

For fluorescence observation of filipin staining samples were examined under a Zeiss Imager M2 microscope equipped with an AxioCam 506 mono camera. Filipin was visualized with the FL Filter Set 49 DAPI (Carl Zeiss Microscopy). The fluorescence intensity was quantified via Zen Pro software (Carl Zeiss Microscopy).

Inductively Coupled Plasma Mass Spectrometry (ICP-MS)

For metal accumulation analysis, 50 mL cultures of *C. neoformans* strains were grown on YPD for 16 hours at 30°C. Cells were collected by centrifugation and washed twice with sterile dH₂O. 3x10⁸ cells suspended in water were plated onto RPMI, RPMI+ 250 μM Ni, and RPMI+ 4 mM DMG. The plates were incubated at 37°C overnight. Cells were harvested from the plates and washed twice with sterile dH₂O. Approximately 200mg of cell pellets were aliquoted into pre-weighed tubes. Most of the dH₂O was removed and the cell pellet was heat-killed at 95°C for 20 minutes. Heat-killed cell samples were submitted to the Center for Applied Isotope Studies Plasma Chemistry Laboratory at the University of Georgia for ICP-MS.

Metals analysis was performed by Dr. Sarah Jantzi at the Plasma Chemistry Laboratory, Center for Applied Isotope Studies, University of Georgia. Samples, reference material, and method blanks were digested in PTFE vessels (Savillex, USA) using 0.5 mL trace metal grade

concentrated nitric acid (Fisher Scientific, USA) for 1 hour 95 °C, followed by 0.5 mL trace metal grade hydrogen peroxide (Fisher Scientific) for 1 hour at 95 °C. Digestates were diluted with deionized water to 2 % w/w nitric acid and the concentrations of Fe, Co, Ni, Cu, and Zn were determined by inductively-coupled plasma mass spectrometry (ICP-MS) using an indium internal standard. A Thermo X-Series 2 ICP-MS with collision cell technology and chilled spray chamber (Thermo, Germany) was used in kinetic energy discrimination (KED) mode with 8 % hydrogen in helium to reduce interferences.

Ergosterol Extraction

The same number of cells $(5x10^7)$ for the indicated strains were plated onto RPMI, RPMI+ 250 μ M Ni and incubated at 37°C for 2 days. The cells were collected with sterile water and were snap-frozen in liquid nitrogen. The cells were then lyophilized overnight. Samples were normalized to the same dry weight and desiccated cells were disrupted manually with glass beads. Ergosterol was extracted using a previously established protocol (62). Briefly, 3mL 25% alcoholic KOH was added to the cells and transferred to a borosilicate glass tube with screw cap, vortexed for 1 minute, and incubated at 85°C for 1 hour. After cooling to room temperature, 1 mL of sterile water and 2 mL of n-heptane were added to each tube. Each tube was vortexed for 3 minutes and the solution was allowed to separate for \sim 5 minutes without centrifugation. The n-heptane layer was transferred to a microcentrifuge tube and concentrated via speedvac. 30 μ L of n-heptane was added to the concentrated pellet for TLC analysis.

Thin Layer Chromatography (TLC)

A standard curve to quantify amounts of ergosterol was done by creating a 2 mg/mL stock of ergosterol in chloroform. This stock was serially diluted in 2-fold increments. 5 μ L of each sample was spotted onto 10x20cm HPTLC Silica gel coated glass plates (EMD Chemicals)

with 1µL drop at a time. The spots were placed 0.5 cm apart and 1 cm from the bottom of the plate. A mobile phase of petroleum ether, diethyl ether, and acetic acid (vol 85:15:1) was used to run the TLC plate in a covered TLC chamber. The TLC plate was then allowed to air dry in the chemical hood, and was developed for 45 minutes with iodine crystals in the covered TLC chamber and imaged. The density of the spots was quantified via the standard curve data. *Mammalian Cell Culture with or without Ni*

A549 cells are human type II lung epithelial cells. A549 cells were maintained in Dulbecco's modified Eagle's medium (DMEM) supplemented with 10% fetal bovine serum (FBS) and incubated at 37°C with 5% CO₂ in 250mL CellStar culture flasks (Greiner Bio-One). To test the effect of Ni on membrane lipids, A549 cells were seeded into 24-well glass bottom cell culture plates (Southern LabWare) at a concentration of 5x10⁴ cells per well in DMEM+FBS media with or without Ni. Concentrations of Ni used were 0, 10, 50, and 100μM. After 72 hours of growth, cells were washed with warm sterile PBS, and then incubated in 25 μg/mL filipin III (Cayman Chemical) stain for 45 minutes at 22°C in the dark before imaging. The cells were viewed using a Zeiss Axio Observer 7 inverted microscope using a Plan-APOCHROME 20x objective lens (Carl Zeiss Microscopy).

Data Availability

All data supporting this study are presented herein, and the reported fungal strains generated for this study are available on request.

Completing Interest

We declare no competing interests.

Funding

This work was supported by National Institutes of Allergy and Infectious Diseases (http://www.niaid.nih.gov) (R01AI140719 to X.L.) and University of Georgia Gene E. Michaels endowment fund (to X.L.). The funders had no role in study design, data collection and interpretation, or the decision to submit the work for publication.

Acknowledgements

We thank all Lin lab members for their helpful suggestions. We also thank Dr. Sarah Jantzi at the Plasma Chemistry Laboratory, Center for Applied Isotope Studies, University of Georgia for her assistance and expertise with ICP-MS. We also thank the Yong-Sun Bahn laboratory for generating the transcription factor and kinase deletion collections, and the Madhani laboratory for generating the deletion collection (funded by NIH R01AI100272).

References

- 1. Iyaka YA. Nickel in soils: A review of its distribution and impacts. Scientific Research and Essays. 2011;6(33):6774-7.
- 2. Macomber L, Hausinger RP. Mechanisms of nickel toxicity in microorganisms. *Metallomics*. 2011;3(11):1153-62.
- 3. Denkhaus E, Salnikow K. Nickel essentiality, toxicity, and carcinogenicity. Critical reviews in oncology/hematology. 2002;42(1):35-56.
- 4. Genchi G, Carocci A, Lauria G, Sinicropi MS, Catalano A. Nickel: Human health and environmental toxicology. International journal of environmental research and public health. 2020;17(3):679.
- 5. Reclaru L, Unger R, Kirkpatrick C, Susz C, Eschler P-Y, Zuercher M-H, et al. Ni–Cr based dental alloys; Ni release, corrosion and biological evaluation. Materials Science and Engineering: C. 2012;32(6):1452-60.
- 6. Zhao J, Shi X, Castranova V, Ding M. Occupational toxicology of nickel and nickel compounds. Journal of Environmental Pathology, Toxicology and Oncology. 2009;28(3).
- 7. Strlic M, Kolar J, Selih V-S, Kocar D, Pihlar B. A comparative study of several transition metals in Fenton-like reaction systems at circum-neutral pH. Acta Chimica Slovenica. 2003;50(4):619-32.
- 8. Sule K, Umbsaar J, Prenner EJ. Mechanisms of Co, Ni, and Mn toxicity: From exposure and homeostasis to their interactions with and impact on lipids and biomembranes. Biochimica et Biophysica Acta (BBA)-Biomembranes. 2020;1862(8):183250.
- 9. Repetto MG, Ferrarotti NF, Boveris A. The involvement of transition metal ions on iron-dependent lipid peroxidation. Archives of toxicology. 2010;84:255-62.

- 10. Athar M, Hasan SK, Srivastava RC. Evidence for the involvement of hydroxyl radicals in nickel mediated enhancement of lipid peroxidation: implications for nickel carcinogenesis.

 Biochemical and biophysical research communications. 1987;147(3):1276-81.
- 11. Chen C-Y, Su Y-J, Wu P-F, Shyu M-M. Nickel-induced plasma lipid peroxidation and effect of antioxidants in human blood: involvement hydroxyl radical formation and depletion of α-tocopherol. Journal of Toxicology and Environmental Health, Part A. 2002;65(12):843-52.
- 12. Salnikow K, Kluz T, Costa M. Role of Ca2+ in the regulation of nickel-inducible Cap43 gene expression. Toxicology and applied pharmacology. 1999;160(2):127-32.
- 13. Salnikow K, An WG, Melillo G, Blagosklonny MV, Costa M. Nickel-induced transformation shifts the balance between HIF-1 and p53 transcription factors. Carcinogenesis. 1999;20(9):1819-23.
- 14. Pezzuto A, Carico E. Role of HIF-1 in cancer progression: novel insights. A review. Current molecular medicine. 2018;18(6):343-51.
- 15. Harris AL. Hypoxia—a key regulatory factor in tumour growth. Nature reviews cancer. 2002;2(1):38-47.
- 16. Han A, Zou L, Gan X, Li Y, Liu F, Chang X, et al. ROS generation and MAPKs activation contribute to the Ni-induced testosterone synthesis disturbance in rat Leydig cells. Toxicology Letters. 2018;290:36-45.
- 17. Chen C-Y, Wang Y-F, Lin Y-H, Yen S-F. Nickel-induced oxidative stress and effect of antioxidants in human lymphocytes. Archives of toxicology. 2003;77:123-30.
- 18. Wang P. Genetic transformation in *Cryptococcus* species. Journal of Fungi. 2021;7(1):56.
- 19. Knowles CM, McIntyre KM, Panepinto JC. Tools for assessing translation in *Cryptococcus neoformans*. Journal of Fungi. 2021;7(3):159.

- 20. Frerichs AB, Huang M, Ortiz SC, Hull CM. Methods for manipulating *Cryptococcus* spores. Journal of Fungi. 2021;8(1):4.
- 21. Shi R, Lin X. Illuminating the *Cryptococcus neoformans* species complex: unveiling intracellular structures with fluorescent-protein-based markers. Genetics. 2024:iyae059.
- 22. Gyawali R, Lin X. Prezygotic and postzygotic control of uniparental mitochondrial DNA inheritance in *Cryptococcus neoformans. mBio.* 2013;4(2):e00112-13.
- 23. Matha AR, Lin X. Current perspectives on uniparental mitochondrial inheritance in *Cryptococcus neoformans*. Pathogens. 2020;9(9):743.
- 24. Zhao Y, Wang Y, Upadhyay S, Xue C, Lin X. Activation of meiotic genes mediates ploidy reduction during cryptococcal infection. Current biology. 2020;30(8):1387-96. e5.
- 25. Sun S, Hsueh Y-P, Heitman J. Gene conversion occurs within the mating-type locus of *Cryptococcus neoformans* during sexual reproduction. PLoS Genetics. 2012;8(7):e1002810.
- 26. Priest SJ, Coelho MA, Mixão V, Clancey SA, Xu Y, Sun S, et al. Factors enforcing the species boundary between the human pathogens *Cryptococcus neoformans* and *Cryptococcus deneoformans*. PLoS genetics. 2021;17(1):e1008871.
- 27. Roth C, Sun S, Billmyre RB, Heitman J, Magwene PM. A high-resolution map of meiotic recombination in *Cryptococcus deneoformans* demonstrates decreased recombination in unisexual reproduction. Genetics. 2018;209(2):567-78.
- 28. Catania S, Dumesic PA, Pimentel H, Nasif A, Stoddard CI, Burke JE, et al. Evolutionary persistence of DNA methylation for millions of years after ancient loss of a de novo methyltransferase. Cell. 2020;180(2):263-77. e20.

- 29. Yadav V, Mohan R, Sun S, Heitman J. Calcineurin contributes to RNAi-mediated transgene silencing and small interfering RNA production in the human fungal pathogen *Cryptococcus neoformans*. Genetics. 2024;226(3):iyae010.
- 30. Tian X, He G-J, Hu P, Chen L, Tao C, Cui Y-L, et al. *Cryptococcus neoformans* sexual reproduction is controlled by a quorum sensing peptide. Nature Microbiology. 2018;3(6):698-707.
- 31. Homer CM, Summers DK, Goranov AI, Clarke SC, Wiesner DL, Diedrich JK, et al. Intracellular action of a secreted peptide required for fungal virulence. Cell host & microbe. 2016;19(6):849-64.
- 32. Alfano M, Cavazza C. Structure, function, and biosynthesis of nickel-dependent enzymes. *Protein Science*. 2020;29(5):1071-89.
- 33. Cox GM, Mukherjee J, Cole GT, Casadevall A, Perfect JR. Urease as a virulence factor in experimental cryptococcosis. Infect Immun. 2000;68(2):443-8.
- 34. Olszewski MA, Noverr MC, Chen G-H, Toews GB, Cox GM, Perfect JR, et al. Urease expression by *Cryptococcus neoformans* promotes microvascular sequestration, thereby enhancing central nervous system invasion. *The American journal of pathology*. 2004;164(5):1761-71.
- 35. Singh A, Panting RJ, Varma A, Saijo T, Waldron KJ, Jong A, et al. Factors required for activation of urease as a virulence determinant in *Cryptococcus neoformans*. MBio. 2013;4(3):e00220-13.
- 36. Feder V, Kmetzsch L, Staats CC, Vidal-Figueiredo N, Ligabue-Braun R, Carlini CR, et al. *Cryptococcus gattii* urease as a virulence factor and the relevance of enzymatic activity in cryptococcosis pathogenesis. FEBS J. 2015;282(8):1406-18.

- 37. Chang YC, Bien CM, Lee H, Espenshade PJ, Kwon-Chung KJ. Sre1p, a regulator of oxygen sensing and sterol homeostasis, is required for virulence in *Cryptococcus neoformans*. *Molecular Microbiology*. 2007;64(3):614-29.
- 38. Bien CM, Espenshade PJ. Sterol regulatory element binding proteins in fungi: hypoxic transcription factors linked to pathogenesis. *Eukaryotic cell*. 2010;9(3):352-9.
- 39. Lee H, Bien CM, Hughes AL, Espenshade PJ, Kwon-Chung KJ, Chang YC. Cobalt chloride, a hypoxia-mimicking agent, targets sterol synthesis in the pathogenic fungus *Cryptococcus neoformans*. *Molecular microbiology*. 2007;65(4):1018-33.
- 40. Lewis C, Brault C, Peck B, Bensaad K, Griffiths B, Mitter R, et al. SREBP maintains lipid biosynthesis and viability of cancer cells under lipid-and oxygen-deprived conditions and defines a gene signature associated with poor survival in glioblastoma multiforme. Oncogene. 2015;34(40):5128-40.
- 41. Horton JD, Goldstein JL, Brown MS. SREBPs: activators of the complete program of cholesterol and fatty acid synthesis in the liver. The Journal of clinical investigation. 2002;109(9):1125-31.
- 42. Godycki LE, Rundle R. The structure of nickel dimethylglyoxime. Acta Crystallographica. 1953;6(6):487-95.
- 43. Lee KT, So YS, Yang DH, Jung KW, Choi J, Lee DG, et al. Systematic functional analysis of kinases in the fungal pathogen *Cryptococcus neoformans*. Nat Commun. 2016;7:12766.
- 44. Jung K-W, Yang D-H, Maeng S, Lee K-T, So Y-S, Hong J, et al. Systematic functional profiling of transcription factor networks in *Cryptococcus neoformans*. *Nature communications*. 2015;6(1):1-14.

- 45. Eberlé D, Hegarty B, Bossard P, Ferré P, Foufelle F. SREBP transcription factors: master regulators of lipid homeostasis. Biochimie. 2004;86(11):839-48.
- 46. Foster AW, Osman D, Robinson NJ. Metal preferences and metallation. Journal of biological chemistry. 2014;289(41):28095-103.
- 47. Jung WH, Kronstad JW. Iron and fungal pathogenesis: a case study with *Cryptococcus neoformans*. Cellular microbiology. 2008;10(2):277-84.
- 48. Jiang N, Liu X, Yang J, Li Z, Pan J, Zhu X. Regulation of copper homeostasis by Cufl associates with its subcellular localization in the pathogenic yeast *Cryptococcus neoformans* H99. FEMS yeast research. 2011;11(5):440-8.
- 49. Singh A, Panting RJ, Varma A, Saijo T, Waldron KJ, Jong A, et al. Factors required for activation of urease as a virulence determinant in *Cryptococcus neoformans*. MBio. 2013;4(3).
- 50. Garcia-Santamarina S, Festa RA, Smith AD, Yu CH, Probst C, Ding C, et al. Genomewide analysis of the regulation of Cu metabolism in *Cryptococcus neoformans*. Molecular microbiology. 2018;108(5):473-94.
- 51. Lian T, Simmer MI, D'Souza CA, Steen BR, Zuyderduyn SD, Jones SJ, et al. Iron-regulated transcription and capsule formation in the fungal pathogen *Cryptococcus neoformans*. Molecular microbiology. 2005;55(5):1452-72.
- 52. Cadieux B, Lian T, Hu G, Wang J, Biondo C, Teti G, et al. The mannoprotein Cig1 supports iron acquisition from heme and virulence in the pathogenic fungus *Cryptococcus neoformans*. The Journal of infectious diseases. 2013;207(8):1339-47.
- 53. Zhao Y, Lin X. A PAS Protein Directs Metabolic Reprogramming during Cryptococcal Adaptation to Hypoxia. Mbio. 2021;12(2):e03602-20.

- 54. Muñoz-Sánchez J, Chánez-Cárdenas ME. The use of cobalt chloride as a chemical hypoxia model. *Journal of Applied Toxicology*. 2019;39(4):556-70.
- 55. Geber A, Hitchcock CA, Swartz JE, Pullen FS, Marsden KE, Kwon-Chung KJ, et al. Deletion of the *Candida glabrata* ERG3 and ERG11 genes: effect on cell viability, cell growth, sterol composition, and antifungal susceptibility. Antimicrobial agents and chemotherapy. 1995;39(12):2708-17.
- 56. Kelly SL, Lamb DC, Taylor M, Corran AJ, Baldwin BC, Powderly WG. Resistance to amphotericin B associated with defective sterol Δ 8→ 7 isomerase in a *Cryptococcus* neoformans strain from an AIDS patient. FEMS microbiology letters. 1994;122(1-2):39-42.
- 57. Young LY, Hull CM, Heitman J. Disruption of ergosterol biosynthesis confers resistance to amphotericin B in *Candida lusitaniae*. Antimicrobial agents and chemotherapy. 2003;47(9):2717-24.
- 58. Moreira-Walsh B, Ragsdale A, Lam W, Upadhya R, Xu E, Lodge JK, et al. Membrane integrity contributes to resistance of *Cryptococcus neoformans* to the cell wall inhibitor caspofungin. Msphere. 2022;7(4):e00134-22.
- 59. Bhattacharya S, Esquivel BD, White TC. Overexpression or deletion of ergosterol biosynthesis genes alters doubling time, response to stress agents, and drug susceptibility in *Saccharomyces cerevisiae*. MBio. 2018;9(4):10.1128/mbio. 01291-18.
- 60. Matha AR, Xie X, Lin X. Ergosterol Is Critical for Sporogenesis in *Cryptococcus neoformans*. Journal of Fungi. 2024;10(2):106.
- 61. Ghannoum MA, Rice LB. Antifungal agents: mode of action, mechanisms of resistance, and correlation of these mechanisms with bacterial resistance. Clinical microbiology reviews. 1999;12(4):501-17.

- 62. Arthington-Skaggs BA, Jradi H, Desai T, Morrison CJ. Quantitation of ergosterol content: novel method for determination of fluconazole susceptibility of *Candida albicans*. Journal of Clinical Microbiology. 1999;37(10):3332-7.
- 63. Van Leeuwen M, Smant W, De Boer W, Dijksterhuis J. Filipin is a reliable in situ marker of ergosterol in the plasma membrane of germinating conidia (spores) of *Penicillium discolor* and stains intensively at the site of germ tube formation. Journal of microbiological methods. 2008;74(2-3):64-73.
- 64. Altamirano S, Simmons C, Kozubowski L. Colony and single cell level analysis of the heterogeneous response of *Cryptococcus neoformans* to fluconazole. Frontiers in Cellular and Infection Microbiology. 2018;8:203.
- 65. Li L, Kaplan J. Characterization of yeast methyl sterol oxidase (ERG25) and identification of a human homologue. Journal of Biological Chemistry. 1996;271(28):16927-33.
- 66. Jumper J, Evans R, Pritzel A, Green T, Figurnov M, Ronneberger O, et al. Highly accurate protein structure prediction with AlphaFold. Nature. 2021;596(7873):583-9.
- 67. Varadi M, Anyango S, Deshpande M, Nair S, Natassia C, Yordanova G, et al. AlphaFold Protein Structure Database: massively expanding the structural coverage of protein-sequence space with high-accuracy models. Nucleic acids research. 2022;50(D1):D439-D44.
- 68. Yang J, Yan R, Roy A, Xu D, Poisson J, Zhang Y. The I-TASSER Suite: protein structure and function prediction. Nature methods. 2015;12(1):7-8.
- 69. Roy A, Kucukural A, Zhang Y. I-TASSER: a unified platform for automated protein structure and function prediction. Nature protocols. 2010;5(4):725-38.
- 70. Zhang Y. I-TASSER server for protein 3D structure prediction. BMC bioinformatics. 2008;9:1-8.

- 71. Schroeder HA. Serum cholesterol levels in rats fed thirteen trace elements. The Journal of Nutrition. 1968;94(4):475-80.
- 72. Chen Z, He J, Chen L, Wu X, Yu X. Association between the nickel exposure and lipid profiles in general population from NHANES. Environmental Science and Pollution Research. 2022;29(44):66383-8.
- 73. Espenshade PJ, Hughes AL. Regulation of sterol synthesis in eukaryotes. Annu Rev Genet. 2007;41:401-27.
- 74. Das KK, Reddy RC, Bagoji IB, Das S, Bagali S, Mullur L, et al. Primary concept of nickel toxicity—an overview. Journal of basic and clinical physiology and pharmacology. 2019;30(2):141-52.
- 75. Shahzad B, Tanveer M, Rehman A, Cheema SA, Fahad S, Rehman S, et al. Nickel; whether toxic or essential for plants and environment-A review. Plant physiology and biochemistry. 2018;132:641-51.
- 76. Benoit SL, Miller EF, Maier RJ. *Helicobacter pylori* stores nickel to aid its host colonization. Infection and immunity. 2013;81(2):580-4.
- 77. Benoit SL, Schmalstig AA, Glushka J, Maier SE, Edison AS, Maier RJ. Nickel chelation therapy as an approach to combat multi-drug resistant enteric pathogens. Scientific reports. 2019;9(1):1-10.
- 78. Maier RJ, Benoit SL. Role of Nickel in Microbial Pathogenesis. Inorganics. 2019;7(7).
- 79. Stangl GI, Kirchgessner M. Nickel deficiency alters liver lipid metabolism in rats. The Journal of nutrition. 1996;126(10):2466-73.

- 80. Kolesarova A, Capcarova M, Arpasova H, Kalafova A, Massanyi P, Lukac N, et al. Nickel-induced blood biochemistry alterations in hens after an experimental peroral administration. Journal of Environmental Science and Health, Part B. 2008;43(7):625-32.
- 81. Mo C, Valachovic M, Randall S, Nickels J, Bard M. Protein–protein interactions among C-4 demethylation enzymes involved in yeast sterol biosynthesis. Proceedings of the National Academy of Sciences. 2002;99(15):9739-44.
- 82. Marguerat S, Schmidt A, Codlin S, Chen W, Aebersold R, Bähler J. Quantitative analysis of fission yeast transcriptomes and proteomes in proliferating and quiescent cells. Cell. 2012;151(3):671-83.
- 83. Carpy A, Krug K, Graf S, Koch A, Popic S, Hauf S, et al. Absolute proteome and phosphoproteome dynamics during the cell cycle of *Schizosaccharomyces pombe* (Fission Yeast). Molecular & Cellular Proteomics. 2014;13(8):1925-36.
- 84. Kelliher CM, Leman AR, Sierra CS, Haase SB. Investigating conservation of the cell-cycle-regulated transcriptional program in the fungal pathogen, *Cryptococcus neoformans*. PLoS genetics. 2016;12(12):e1006453.
- 85. Upadhyay S, Xu X, Lowry D, Jackson JC, Roberson RW, Lin X. Subcellular compartmentalization and trafficking of the biosynthetic machinery for fungal melanin. Cell Reports. 2016;14(11):2511-8.
- 86. Lin J, Fan Y, Lin X. Transformation of *Cryptococcus neoformans* by electroporation using a transient CRISPR-Cas9 expression (TRACE) system. Fungal Genetics and Biology. 2020;138:103364.

- 87. Upadhya R, Lam WC, Maybruck BT, Donlin MJ, Chang AL, Kayode S, et al. A fluorogenic *C. neoformans* reporter strain with a robust expression of m-cherry expressed from a safe haven site in the genome. Fungal Genetics and Biology. 2017;108:13-25.
- 88. Fan Y, Lin X. Multiple applications of a transient CRISPR-Cas9 coupled with electroporation (TRACE) system in the *Cryptococcus neoformans* species complex. Genetics. 2018;208(4):1357-72.
- 89. Baek S, Utomo JC, Lee JY, Dalal K, Yoon YJ, Ro D-K. The yeast platform engineered for synthetic gRNA-landing pads enables multiple gene integrations by a single gRNA/Cas9 system. Metabolic Engineering. 2021;64:111-21.
- 90. Wang L, Zhai B, Lin X. The link between morphotype transition and virulence in *Cryptococcus neoformans*. PLoS pathogens. 2012;8(6):e1002765.

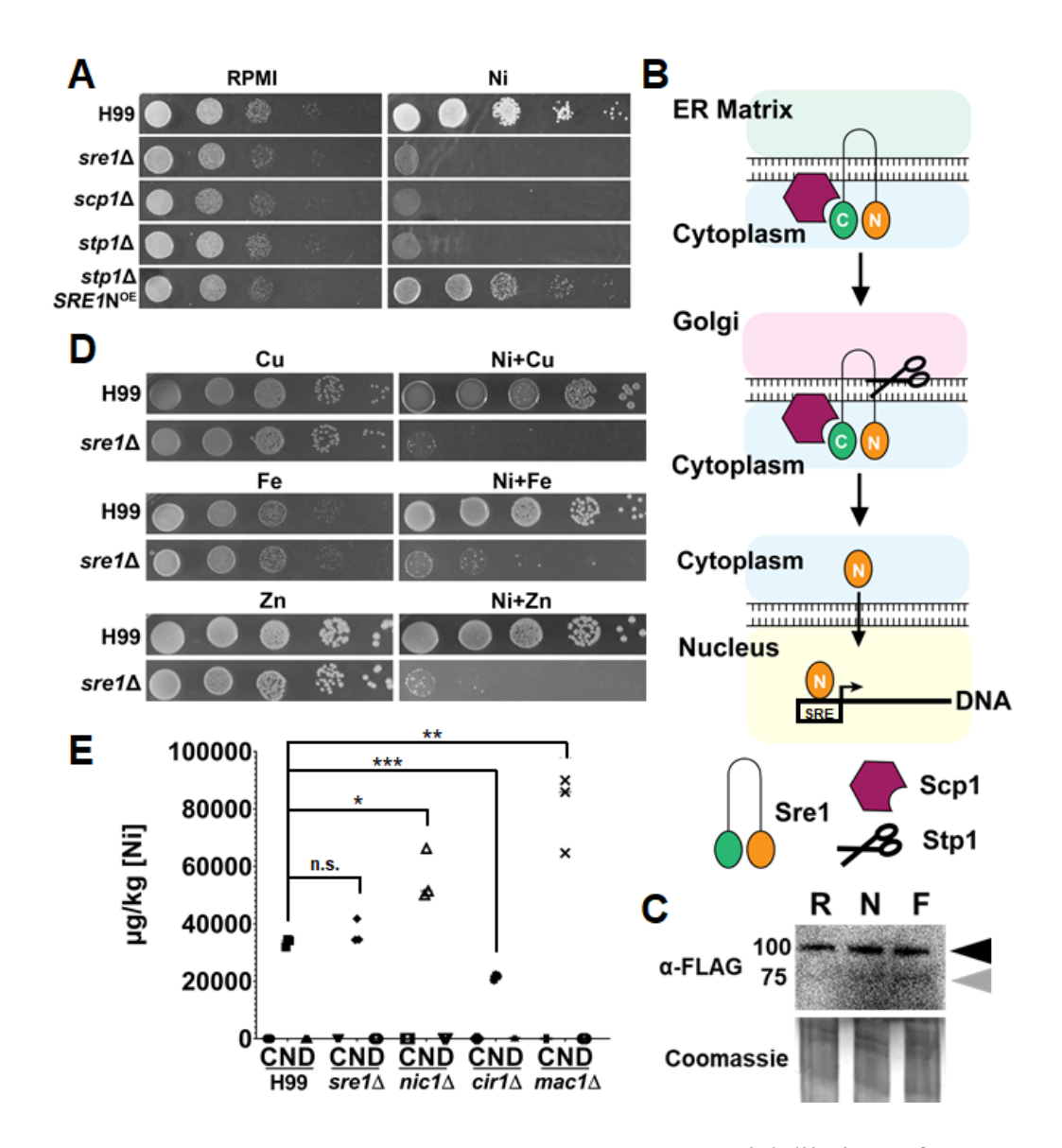


Figure 3.1: $sre1\Delta$ growth defect is specific to Ni. (A) Serial dilutions of H99, $sre1\Delta$, $stp1\Delta$, and $scp1\Delta$ cells were spotted onto RPMI agar ± 250 μM NiSO₄ (Ni). (B) Diagram of the activation process for Sre1. In response to a stimulus (e.g. drop of the ergosterol level in membrane in response to hypoxia), the full-length Sre1 residing in the ER membrane will be shuttled to the Golgi. Here, the protease Stp1 cleaves Sre1. The released N-Sre1 then translocates to the nucleus and binds the sterol regulatory element (SRE) in promoter regions of downstream targets to initiate transcription. (C) Cells constitutively expressing Flag-Sre1 were grown on RPMI (R), RPMI+ 250 μM Ni (N), and RPMI+ 4μg/mL Fluconazole (F). Whole-cell extracts were prepared

and immunoblot analysis was done using anti-Flag purified antibody. The black and grey arrowheads denote the full-length and cleaved forms of Sre1, respectively. Coomassie staining indicates the loading. **(D)** Growth of H99 and $sre1\Delta$ on RPMI with the indicated metals: CuSO₄ (Cu), ZnCl₂ (Zn), and FeSO₄ (Fe) at 250 μ M with or without addition of 250 μ M Ni. **(E)** ICP-MS quantification of Ni concentrations in H99, $sre1\Delta$, $nic1\Delta$, $cir1\Delta$, and $mac1\Delta$ cells grown on RPMI (C), RPMI+Ni (N), or RPMI+DMG (D). The same dry weight of cells was used for the analysis. Student's t-test was done to test for statistical significance. n.s. not significant *= \leq 0.05, **= \leq 0.01, ***= \leq 0.001

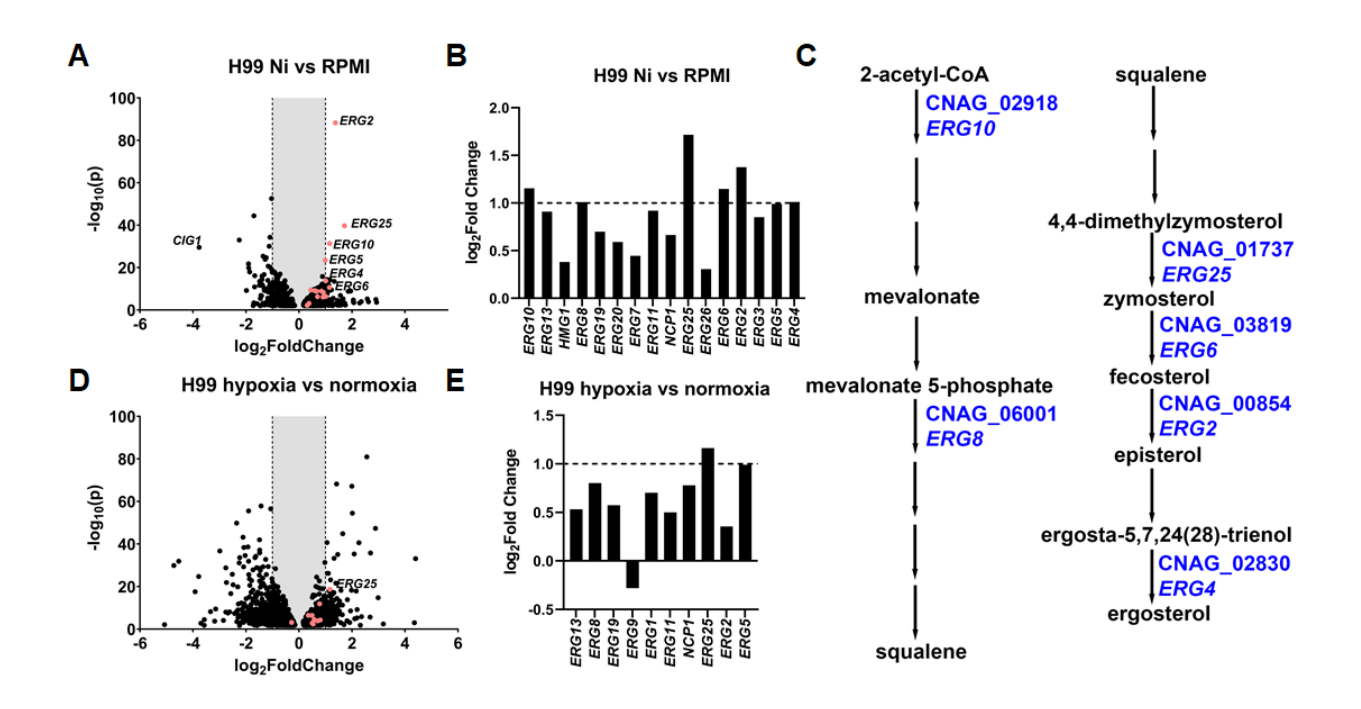


Figure 3.2: Ni causes increased expression of multiple genes in the ergosterol biosynthesis pathway. (A) Volcano plot of transcript changes of H99 growing on RPMI+Ni versus RPMI based on RNA-seq data. The red dots indicate EBP genes present in the data set. (B) Log₂(Fold Change) of EBP gene expression when grown on Ni. Differentially expressed genes are genes with a Log₂(Fold Change) value greater than 1, indicated by the dashed line. (C) Abbreviated ergosterol biosynthesis pathway. EBP genes differentially expressed on Ni were labeled in blue. (D) Volcano plot of transcript changes of H99 growing on RPMI+hypoxia versus RPMI+normoxia based on RNA-seq data. The red dots indicate EBP genes present in the data set. (E) Log₂(Fold Change) of EBP genes expression in hypoxia conditions.

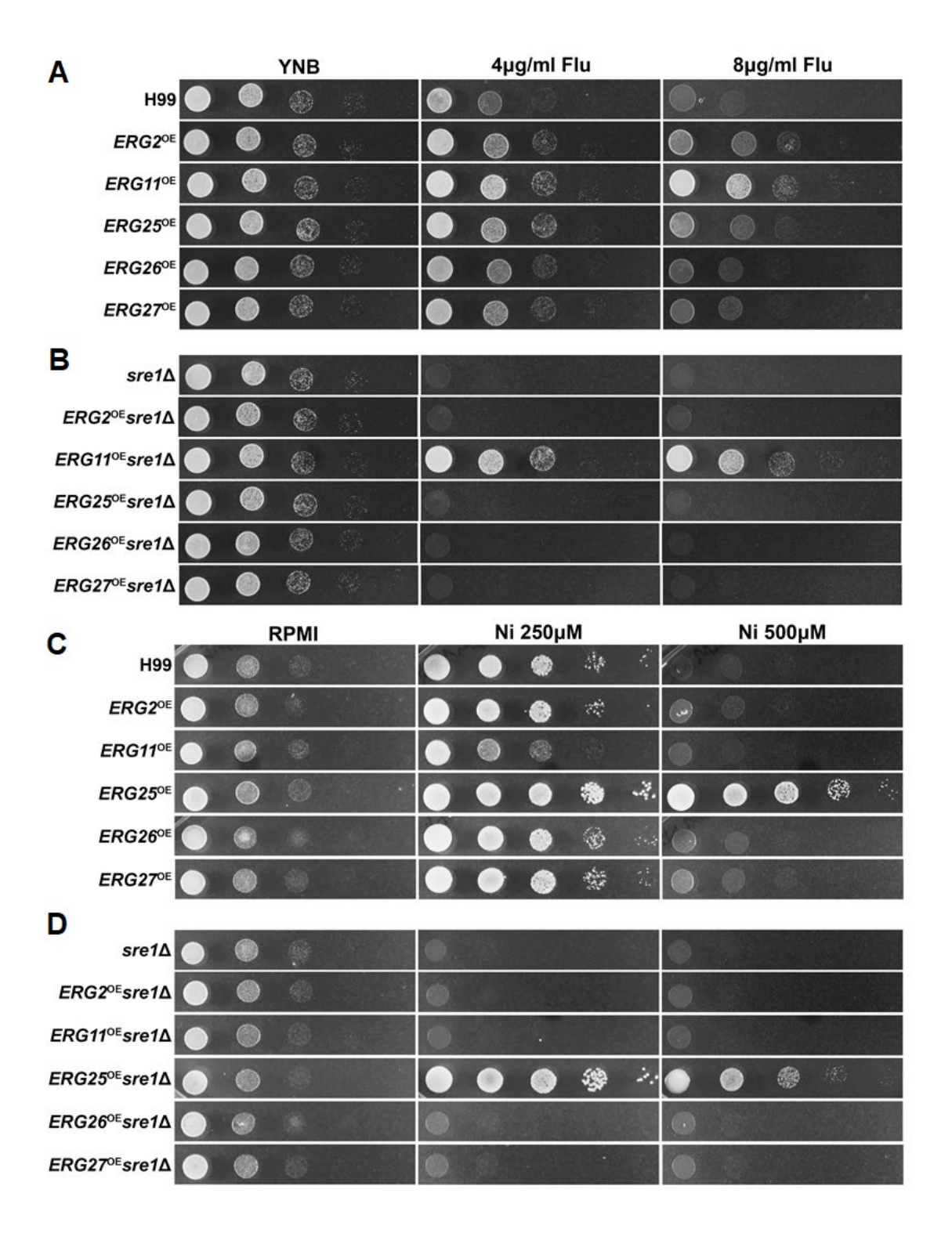


Figure 3.3: Overexpression of ERG25, but not other ERG genes tested, drastically increases Ni tolerance in both wild type and $sre1\Delta$. (A) H99 strains with overexpression of the indicated ERG genes (ERG2, 11, 25, 26, and 27) were serially diluted and plated on RPMI plates with

fluconazole (Flu) at 4 or 8 μg/ml. (B) The *sre1*Δ strains with overexpression of the indicated *ERG* genes (*ERG2*, 11, 25, 26, and 27) were serially diluted and plated on RPMI plates with Flu at the indicated concentrations. (C) The same strains as in Panel A were spotted onto RPMI media with the indicated concentrations of Ni. (D) The same strains as in Panel B were spotted onto RPMI media with the indicated concentrations of Ni. All plates were incubated for two days prior to imaging.

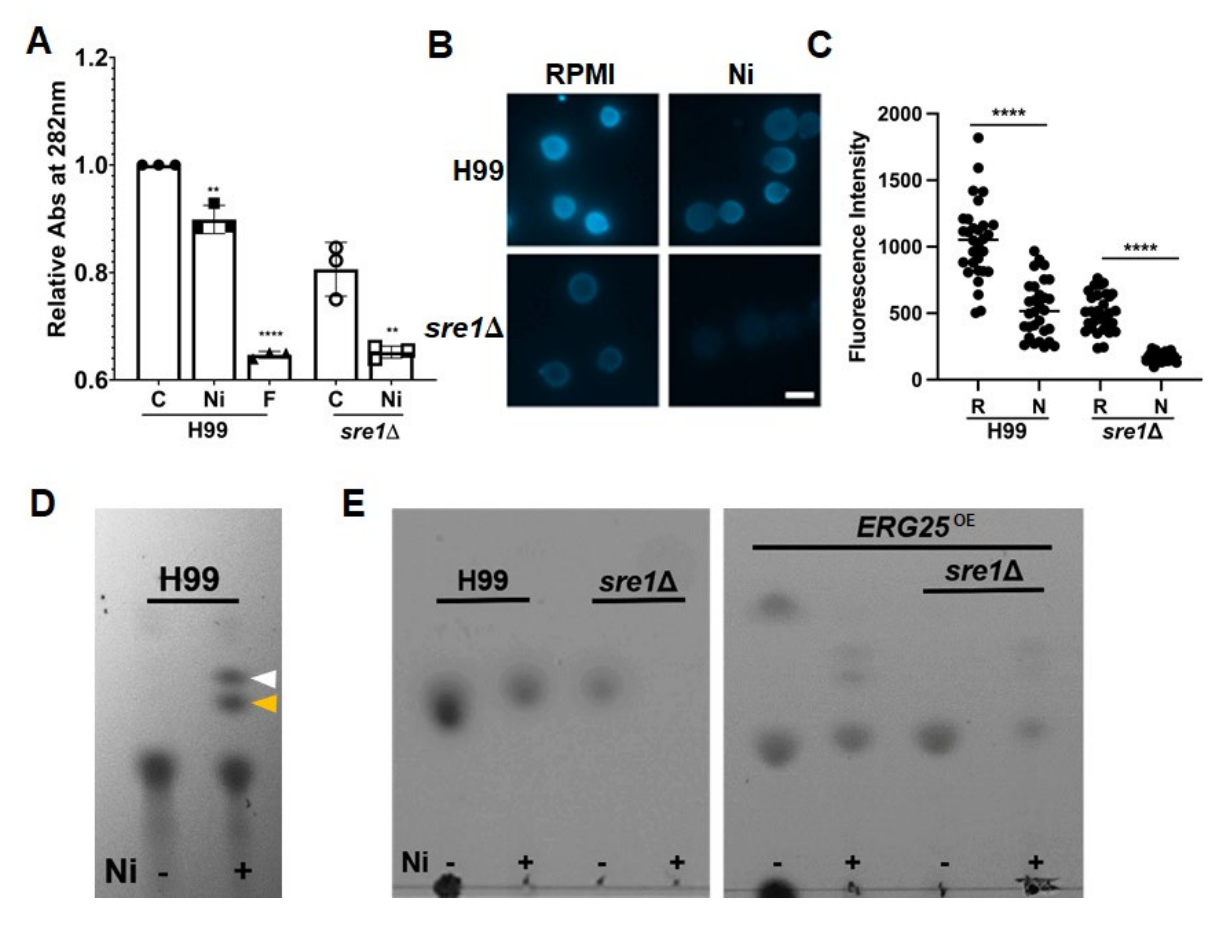


Figure 3.4: Ni causes alteration of sterol profiles. (A) Ergosterol was extracted from the indicated strains grown on RPMI (C), RPMI+250μM Ni (Ni), or RPMI+4μg/mL Flu (F). The extract was measured at 282nm. Student's t-test was used to assess statistical significance. **= ≤0.01, ****= ≤0.0001 (B) H99 and *sre1*Δ cells were grown overnight on RPMI or RPMI+250μM Ni plates. Cells were harvested and incubated for 45 minutes in 25μM filipin III at 21°C in the dark. Cells were imaged with a Zeiss Imager M2 microscope. Scale bar = 5μm. (C) Quantification of fluorescence intensities of cells prepared as in panel B. RPMI (R), RPMI+250μM Ni (N). Mann-Whitney test was used to assess statistical significance ****= ≤0.0001. (D) Equal dry weight of wildtype cells grown on RPMI media alone (-) or RPMI+Ni (+) media were used to extract membrane sterols from indicated strains. 5μL of ergosterol extract were spotted onto glass backed HPTLC Silica gel plates. The white arrow indicates free fatty acids

band. The yellow arrow indicates the methyl sterol band. The bottom band indicates ergosterol.

(E) Lipid extractions from the indicated strains were spotted onto a TLC plate. $5\mu L$ of ergosterol extract was spotted onto glass backed HPTLC Silica gel plates as in panel D.

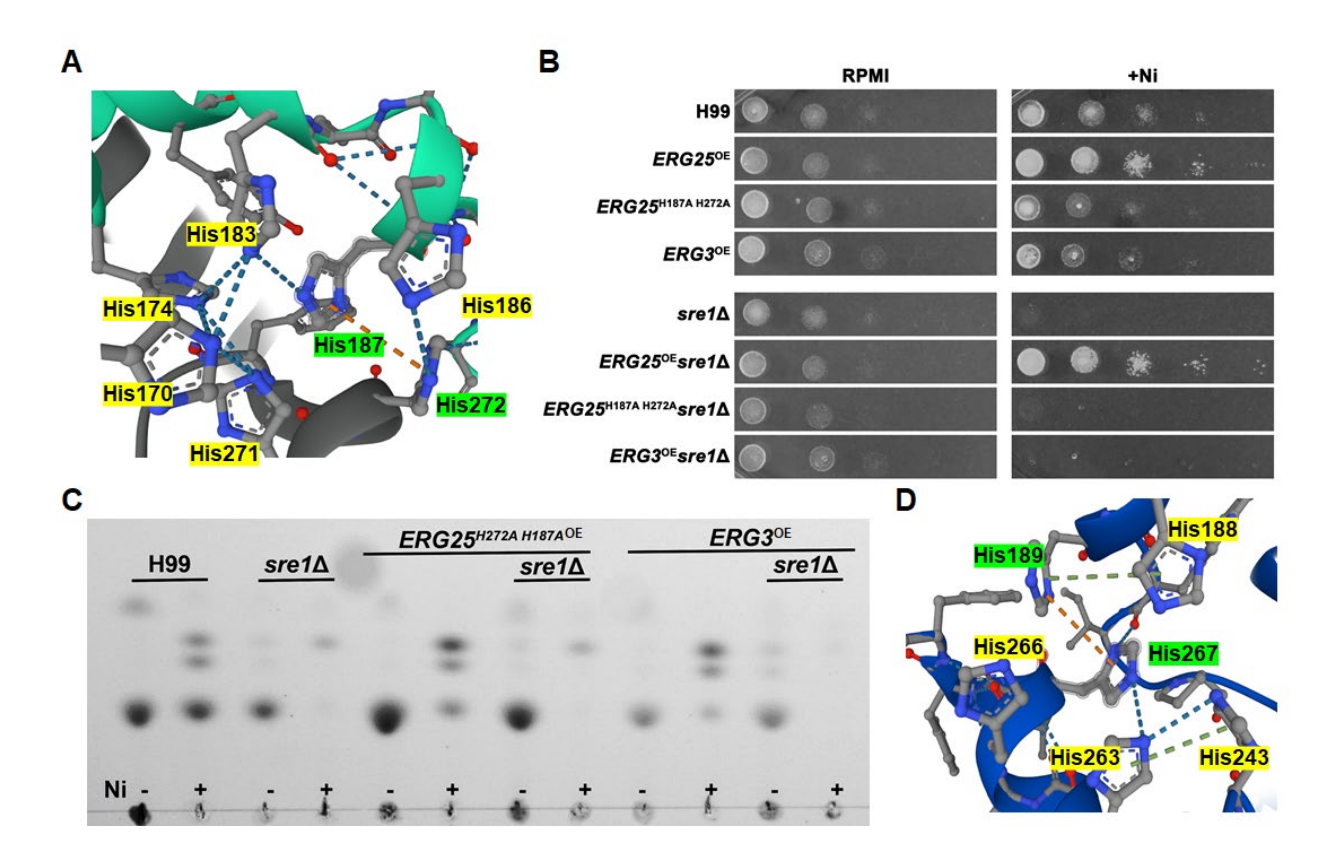


Figure 3.5: Mutating histidine enriched pocket abolishes the ability of Erg25 to confer Ni tolerance. (A) Alphafold generated images of histidine enriched pocket of Erg25. Predicted cation-pi interaction is indicated by an orange dashed line. (B) The indicated strains were serially diluted and spotted onto RPMI and RPMI+ 250μM Ni plates. The plates were incubated for 2 days before imaging. (C) Equal dry weight of cells was used to extract membrane sterols from indicated strains. 5μL of ergosterol extract were spotted onto glass backed HPTLC Silica gel plates. (D) Alphafold generated image of Erg3 histidine enriched pocket.

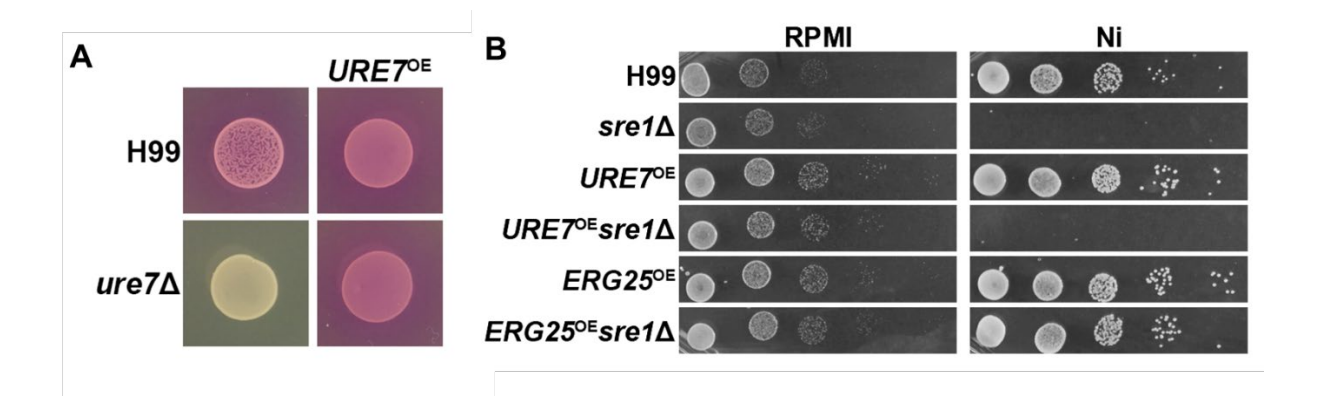


Figure 3.6: Overexpression of Ure7 does not confer Ni tolerance to $sre1\Delta$

(A) H99, $ure7\Delta$, and URE7 overexpression in both strain backgrounds with cell density OD₆₀₀=3 were spotted onto CUA plates. The plates were incubated for three days and imaged. Urease activity is indicated by the yellow to pink color change. (B) The indicated strains were serially diluted and spotted onto RPMI and RPMI+ 250 μ M Ni plates. The plates were incubated for 2 days before imaging.

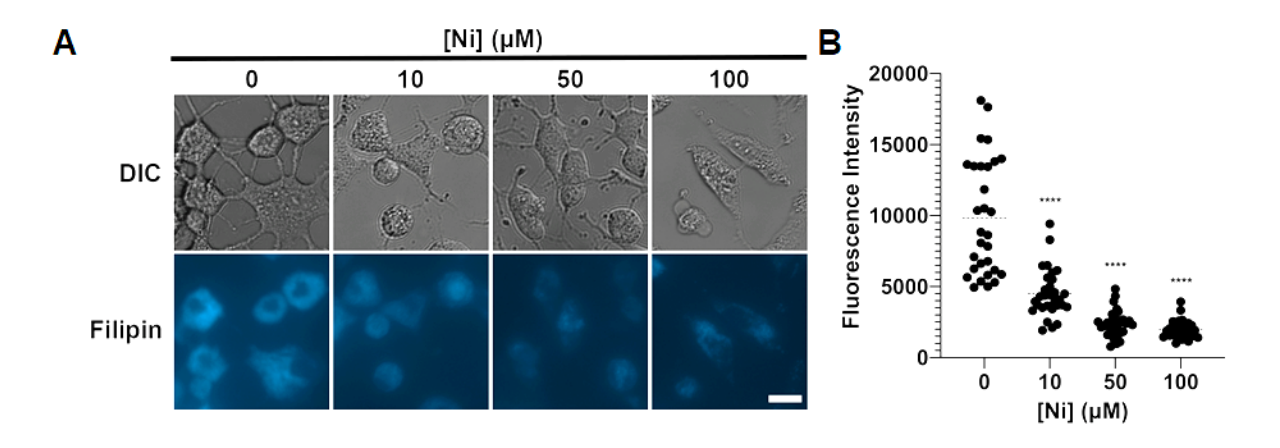


Figure 3.7: Ni causes a decrease in membrane sterols in A549 lung epithelial cells. (A) A549 lung epithelial cells were seeded into a 24-well glass bottom multi-well plate at $5x10^4$ cells per well. Ni was added to the DMEM+FBS media to achieve the indicated concentrations and the cells were incubated at 37°C with 5% CO₂ for 72 hours. After being washed with warm PBS, the cells were incubated with Filipin III for 45 minutes and imaged. Scale bar = 15μ m. (B) Fluorescence intensity was calculated via Zen Pro software. Mann-Whitney test was used to determine statistical significance. *= ≤ 0.05 .

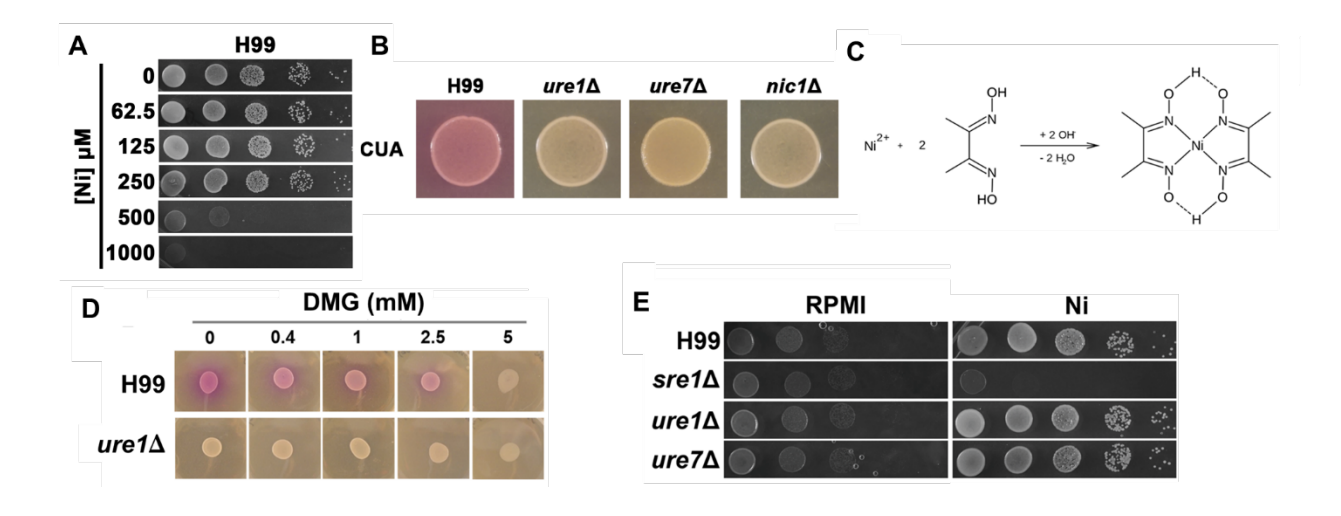


Figure S3.1: Urease is not required for Ni tolerance

(A) H99 cells were serially diluted and spotted onto RPMI and RPMI+Ni at the indicated concentrations. The plates were imaged after two days of incubation. (B) The indicated strains with cell density $OD_{600}=3$ were spotted onto Christensen Urea Agar (CUA) plates. The plates were incubated for three days and imaged. Urease activity is indicated by the yellow to pink color change of the media due to alkalization of the media by released ammonia. (C) Two molecules of DMG chelate one molecule of Ni. (D) H99 and $ure1\Delta$ with cell density $OD_{600}=3$ were spotted onto Christensen Urea Agar (CUA) plates with increasing concentrations of DMG. The plates were incubated for three days and imaged. (E) The indicated strains were serially diluted and spotted onto RPMI and RPMI+ 250 μ M Ni plates. The plates were imaged after two days of incubation.

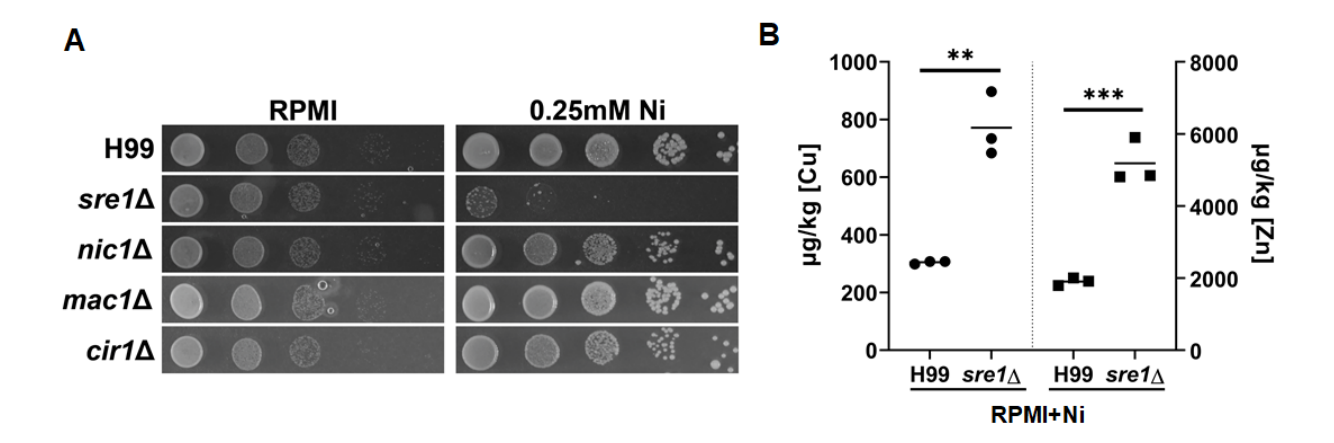


Figure S3.2: Metal accumulation does not dictate metal sensitivity. (A) The indicated strains were plated onto RPMI media with or without Ni, and incubated at 37°C for 2 days. (B) ICP-MS quantification of Cu (left) and Zn (right) concentrations in cells grown on RPMI+Ni. The same dry weight of cells was used for the analysis. Student's *t*-test was done to test for statistical significance. **= ≤ 0.01 , ***= ≤ 0.001

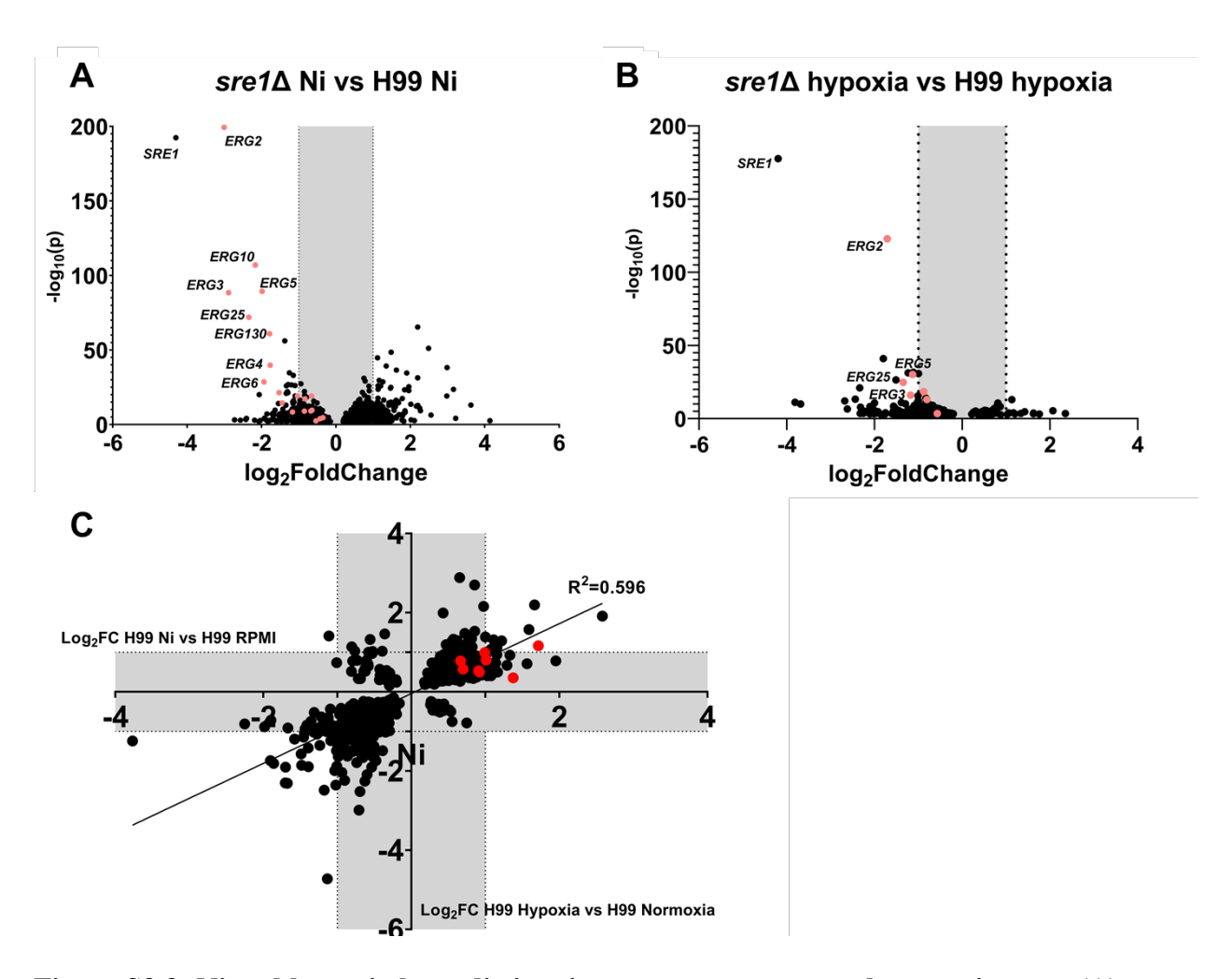


Figure S3.3: Ni and hypoxia have distinct impacts on cryptococcal transcriptome. (A)

Volcano plot of transcript changes of *sre1*Δ grown on RPMI+Ni versus H99 grown on RPMI+Ni based on RNA-seq data. (**B**) Volcano plot of transcript changes of *sre1*Δ grown on RPMI+hypoxia versus H99 grown on RPMI+hypoxia based on RNA-seq data. The red dots in both panels indicate EBP genes present in the data set. (**C**) Plot of transcript changes of genes shared between H99 Ni vs RPMI and H99 hypoxia vs normoxia data sets. Red highlighted genes are EBP genes. In all panels, dots that fall outside of the shaded grey areas are DEGs.

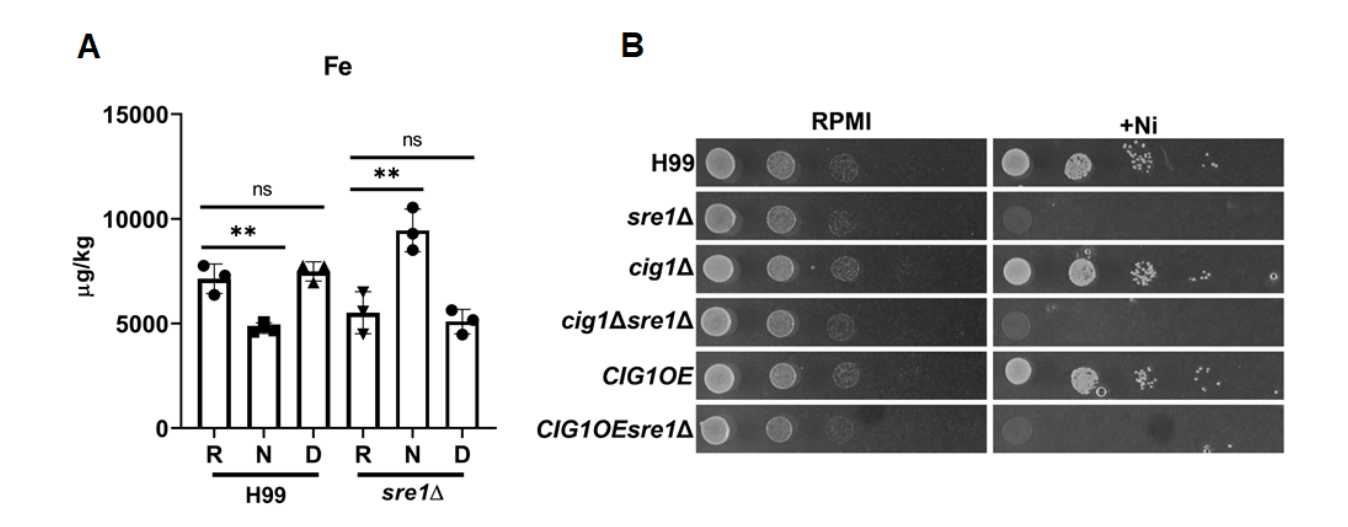


Figure S3.4: The $sre1\Delta$ sensitivity to Ni is not due to iron starvation

(A) ICP-MS data showing intracellular iron concentrations in H99 and $sre1\Delta$ on RPMI (C), RPMI+250 μ M Ni (N), and RPMI+DMG (D). Student's t-test was performed to assess statistical significance. **= \leq 0.01, ns = not significant. (B) The indicated strains were serially diluted and spotted onto RPMI and RPMI+250 μ M Ni media. Plates were incubated at 37°C for two days prior to imaging.

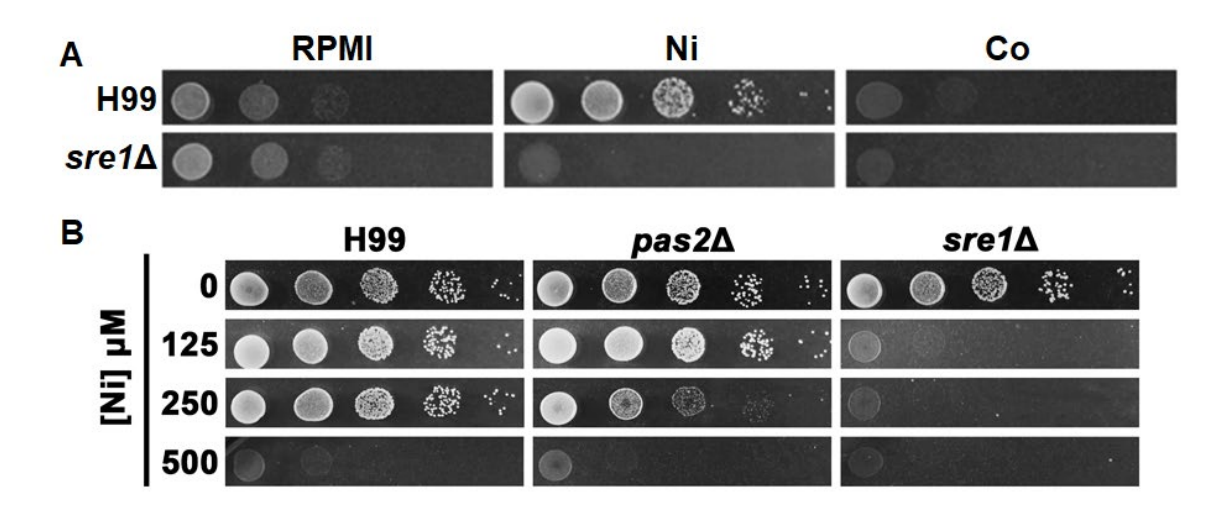


Figure S3.5: Ni and Cobalt (Co) elicit overlapping and different effects on growth.

(A) Wildtype H99 and $sre1\Delta$ cells were serially diluted and spotted onto RPMI, RPMI+250 μ M Ni, and RPMI+250 μ M Co. The plates were incubated at 37°C for two days prior to imaging. (B) H99, $pas2\Delta$ and $sre1\Delta$ cells were serially diluted and spotted onto RPMI, and RPMI with the indicated concentration of Ni. The plates were incubated at 37°C for two days prior to imaging.

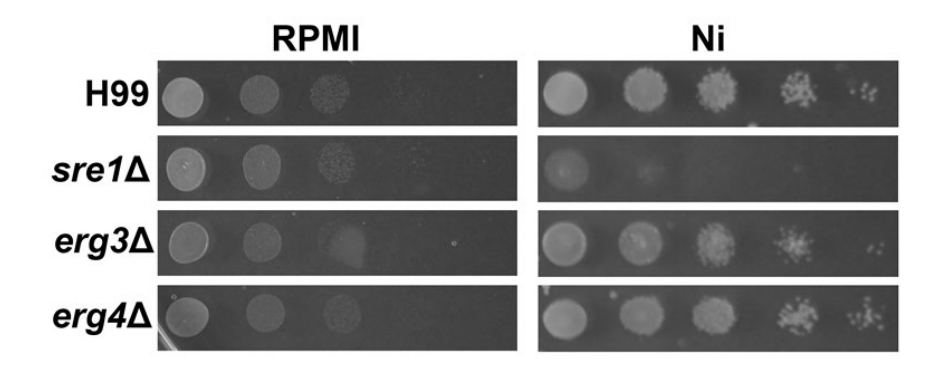


Figure S3.6: Neither ERG3 nor ERG4 is required for cryptococcal tolerance of Ni.

Cells of the indicated strains were serially diluted and spotted on RPMI and RPMI+250µM Ni.

Plates were incubated at 37°C for two days prior to imaging.

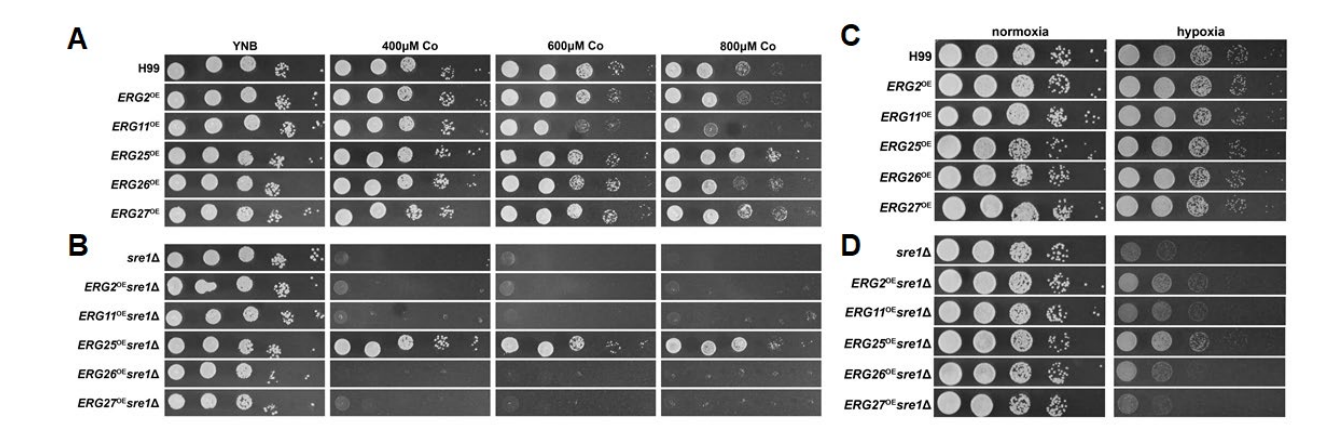


Figure S3.7: *ERG25* is required for tolerance of Co and *ERG* overexpression can partially restore the growth defect of $sre1\Delta$ in hypoxia

(A) Cells of H99 with overexpression of the indicated ERG genes were serially diluted and plated onto YNB plates with CoCl₂ at the indicated concentration. (B) Cells of the $sre1\Delta$ mutant with overexpression of the indicated ERG genes were serially diluted and plated on RPMI plates with the indicated concentrations of CoCl₂. (C) Cells of the same strains as in Panel A were spotted onto YPD media and incubated in ambient air (normoxia) or hypoxia (0.1% O₂, 5% CO₂) conditions. (D) Cells of the same strains as in Panel B were spotted onto RPMI media with the indicated concentrations of Ni. All plates were incubated for two days prior to imaging.

>Erg25

MAAAAAFDLLDKYIPGASDSLTIVNATTAQNTLYPGVDFAALNWLERLWA
SYYIWVGNPIIATGLMSFLLHEIVYFGRCIPWLIIDAMPYFQKWKLQPNK
HVSRAQILKCTKVVLLTHFTCEAPLILAFHPICCLFGMKTYEIPFSSIGL
MAAQIAFFFVFEDTFHYWAHRALHFGPLYKHIHKLHHIFSAPIGIAAEYA
HPLEVLILAQGTISGPFLYAVFRDDLHIFTVYVWITLRLWQAVIAHSGYI
FPWSLRHFIPFWAGADHHDFHHATFTSCFSTSFRWWDYYFGTDVKYHAYK
ARVAAASAKERAAVEKNEMERLEKEGILEERAAASHGKRGKNE

Figure S3.8: Erg25 protein sequence contains histidine residues in predicted metal binding regions.

C. neoformans Erg25 protein is 343 amino acids in length. Four histidine enriched putative metal binding motifs are boxed in various colors. The histidine residues predicted to interact with a cation are highlighted in yellow.

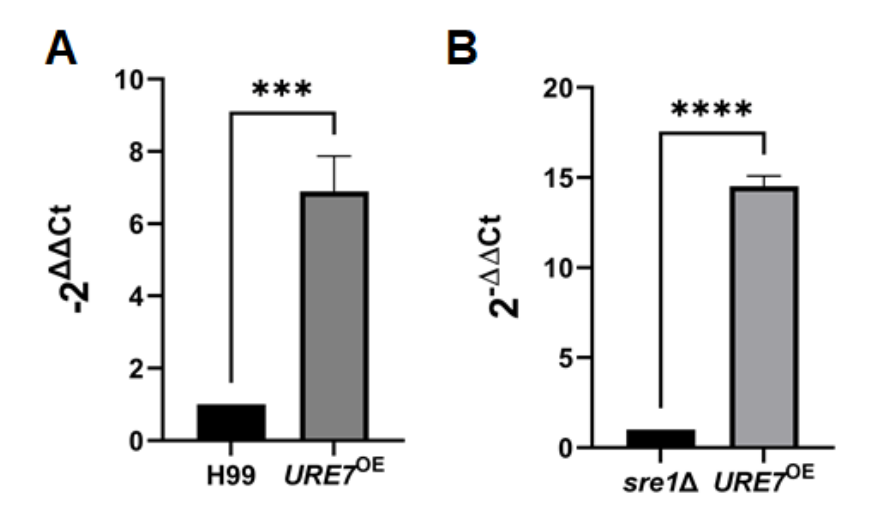


Figure S3.9: *URE7* is overexpressed in both wildtype and *sre1* Δ backgrounds. RT-PCR data was generated by harvesting cells from overnight YPD cultures of (A) wild type and *URE7*^{OE} in the wild type background as well as (B) $sre1\Delta$ and $sre1\Delta URE7^{OE}$. Housekeeping gene TEF1 was used as an internal control to ensure the quality of the original RNA sample used for cDNA amplification and for normalization. Student's *t*-test was done to test for statistical significance.

= ≤ 0.001 , *= < 0.0001.

- Table S3.1: Differentially expressed genes H99 Ni vs H99 RPMI
- Table S3.2: Differentially expressed genes H99 DMG vs H99 RPMI
- Table S3.3: Differentially expressed genes H99 Hypoxia vs H99 normoxia
- Table S3.4: Differentially expressed genes sre1Δ Ni vs H99 Ni
- Table S3.5: Differentially expressed genes sre1Δ Hypoxia vs H99 Hypoxia
- Table S3.6: Differentially expressed genes shared between H99 Ni vs H99 RPMI and H99

hypoxia vs H99 normoxia data sets

Data for these tables available at the NCBI Sequence Read Archive (BioProject PRJNA1082343)

Table S3.7: Fungal strains used in this study

Name	Source	Genotype
H99		C. neoformans serotype A, wild type,
		MATalpha
KN99		C. neoformans serotype A, wild type, MATa
Linlab3062		MATalpha, serotype A SRE1::NAT
Linlab5289		MATalpha, STP1::NAT
		MATalpha, NICI::NAT
Linlab7017		MATalpha, CIR1::NAT
Linlab7726		MATalpha, MAC1::NAT
Linlab7584	This manuscript	MATalpha, SCP1∆::NAT
Linlab7724	This manuscript	MATa, P_{TEFI} -ERG25-NEO
Linlab7741	This manuscript	MATa, PTEF1-ERG25-NEO SRE1::NAT
Linlab7996	This manuscript	MATalpha P _{GPDI} -ERG11-HYG
Linlab8002	This manuscript	MATalpha <i>P_{GPDI}-ERG11-HYG SRE1</i> ::NAT
Linlab7999	This manuscript	MATalpha P_{GPDI} -ERG2-HYG
Linlab8000	This manuscript	MATalpha <i>P_{GPDI}-ERG2-HYG SRE1</i> ::NAT
Linlab8428	This manuscript	MATalpha, <i>P</i> _{TEF1} -ERG26-NEO
Linlab8431	This manuscript	MATalpha, <i>P</i> _{TEF1} -ERG27-NEO
Linlab8433	This manuscript	MATalpha, PTEF1-ERG26-NEO SRE1::NAT
Linlab8435	This manuscript	MATalpha, PTEF1-ERG27-NEO SRE1::NAT
Linlab9422	This manuscript	MATalpha, <i>P</i> _{TEF1} -ERG3-NEO
	This manuscript	MATalpha, <i>P</i> _{TEF1} -ERG3-NEO SRE1::NAT
Linlab9430	This manuscript	MATalpha, P _{TEF1} -ERG25 ^{H187A} H272A-NEO
Linlab9432	This manuscript	MATalpha, P _{TEF1} -ERG25 ^{H187A} H272A-NEO
		SRE1::NAT
Linlab8504		MATalpha serotype A, ERG3::NAT
Linlab8505		MATalpha serotype A, ERG4::NAT
Linlab10215		MATalpha, URE7 (CNAG 00678)::NAT
Linlab10259	This manuscript	MATalpha P _{TEF1} -URE7-hyg
Linlab10264	This manuscript	MATalpha <i>URE7</i> ::NAT P _{TEF1} - <i>URE7</i> -NEO
Linlab10261	This manuscript	MATalpha P _{TEF1} - <i>URE7</i> -NEO <i>SRE1</i> ::NAT
Linlab7787	This manuscript	MATalpha P _{GPD1} -3XFlag-SRE1

Table S3.8: Primers and plasmids used in this study

Primer Name		Notes
Linlab7749/ AM	GCTGTGGACCTGAAAAGCATTC	Sre1 deletion construct F
Linlab7750/ AM	AATAGGATGCCCCGTCGTATTG	Sre1 Deletion construct R
Linlab7751/ AM	CTACCATTGGCAAGCACAACAACAGTATACCCTGCCGGTG	Sre1
Linlab7752/ AM	GTTGTGCCTAGCCAATGGTAGGTTTTAGAGCTAGAAATAGCAA GTT	Sre1
Linlab7791/ AM	CTTGCGCAAGGAACGATCTC	Erg25 RTPCR F
Linlab7792/ AM	GAAGTGAAAGTGGCATGGTGGA	Erg25 RTPCR R
Linlab7869/ AM	TACTTGCATAAATACAGGCCGGCCcATGTCTGCTATCATCCCCC	FseI- erg11 F GPD1 promoter overhang
Linlab7870/ AM	ACTGCTACTGTAACGCTTAATTAACTATTTGACCTCGGCATTT C	PacI- erg11 R GPD1 terminator overhang
LinLab7871/ AM	CTGGCCGTCGTTTTACTACTGGAGTGTGAAGGTACA	M13 F complement - sre1 LR
Linlab7872/ AM	GTCATAGCTGTTTCCTGAATGTCGTCCTTATTTTCCGTC	M13 R complement - sre1 RF
Linlab7894/ AM	TACTTGCATAAATACAGGCCGGCCcaCATCACCCACCATGCCCG	FseI-erg2 F GPD1 promoter overhang
Linlab7895/ AM	ACTGCTACTGTAACGCTTAATTAATTAGATCTTGCCTCTCAA	PacI- erg2 R GPD1 terminator overhang
Linlab7933/ AM	GCTTTGGAGTATGCTAGAG	Erg2 RTPCR F
Linlab7934/ AM	TTAGATCTTGCCTCTCAACA	Erg2 RTPCR R
Linlab7935/ AM	AATACAGCAAGGCCGAGCAA	Erg11 RTPCR F
Linlab7936/ AM	AACATAGGTGAAGATGGTTGA	Erg11 RTPCR R
Linlab8083/ AM	ACTGGAGTGTGAAGGTACACGTTTTAGAGCTAGAAATAGCAA GTT	sgrna1- gRNAScaff

		old-F sre1
		promoter
Linlab8085/	cTGGCCGTCGTTTTACAGAAAGTGGATACGAATC	sgrna1-
AM		GnU6-R
		sre1
		promoter
Linlab8086/ AM	aaacttcaaaggccggcctaacatgtccaactcgcc	Erg26 OE F
Linlab8087/ AM	actgtaacccttaattaattactttgtcttctccga	Erg26 OE R
Linlab8088/ AM	aaacttcaaaggccggcctatgctcgacacacccagc	Erg27 OE F
Linlab8089/ AM	actgtaaccettaattaatatacaatactetactee	Erg27 OE R
Linlab8092/	CTGGCCGTCGTTTTACAGAAAGTGGATACGAATC	M13F
AM		Complemen t-sre1 LR
Linlab8376/	GAACATACGGAGGAGGGAAGGTTTTAGAGCTAGAAATAGCA	sgrna1-
AM	AGTT	gRNAScaff old-F sre1
		promoter
Linlab8377/ AM	CTTCCCTCCGTATGTTCAACAGTATACCCTGCCGGTG	sgrna1- GnU6-R
Linlab8488/	CAACGCGGTAAGCATTAT	sre1 inside
AM		primer (pair
		with 5084
		or 4897)
Linlab9519/ AM	ACTTTACTTGGGCAGACC	Erg3 RTPCR F
Linlab9520/ AM	CCTGAGGAATAGGGTTCC	Erg3 RTPCR R
Linlab9478/ AM	aaacttcaaaggccggCCATGGACATCATCCTCGAA	FseI-Erg3 OE F
Linlab9479/ AM	actgtaaccettaATTAATCATTGTTCCTTCTCCC	PacI- Erg3 OR R
Linlab9474/ AM	GTGAAGCTTGTGAATGTG	Erg25 H272 and H187A
		R
		(Fragment
		$\begin{vmatrix} 1 \\ 1 \end{vmatrix}$
Linlab9475/	CACATTCACAAGCTTCACGCCGAGTTCTCTGCTCCTATT	Erg25 H272
AM		and H187A
		F (Fragment 2)
Linlab9476/	GTGGAAGTCGTGGTGCTC	Erg25 H272
AM		and H187A
		R
		(Fragment
		(2)
	1	1 /

Linlab9477/	GACCACCACGACTTCCACGCCGCCACTTTCACTTCTTGC	Erg25 H272
AM		and H187A
		F (Fragment
		3)
Linlab7308/ AM	ACAGGCCGGCCcgcaccccaacATG	Erg25
Linlab7309/ AM	GTATTAACTACTCGTTCTTTCCCCG	Erg25
Linlab8557/ AM	ctgtctatgctgaccaag	Erg27 RTPCR F
Linlab8558/ AM	ccagtctctccgaacagc	Erg27 RTPCR R
Linlab8559/	gettetettgeegagate	Erg26
AM	generations	RTPCR F
Linlab8560/	ctcattctgtctctccaac	Erg26
AM	- Crouncigiotocodulo	RTPCR R
Linlab6361/	ACGTCAGCGGAGGAGATAAG	Ure7
AM	ACCICACCOCACCACATAAC	RTPCR F
Linlab6361/	CGTCACGACGCATTACATCC	Ure7
AM	COTCACOACOCATTACATCC	RTPCR F
Linlab9581/	A TO COLOT COTO COTO LO	Ure7
	aaacttcaaaggccggccATGGCAGTGCCTGCTCAG	-
AM		cloning F
Linlab9582/	actgtaaccettaattaaTTATGCCTTAGCCTTACC	Ure7
AM		cloning R
Linlab5083/	ataggccggccatggcctcattacaggaca	Sre1
YZ		cloning
		Fwd
Linlab5085/	ATATTAATTAACTACAGTTCATCTAAATCGCCCT	Sre1
YZ		cloning Rev
Plasmids Use	d in this Study	
	Source	
pLinlab1059	88, 90	P _{GPDI} -cas9-
PEImacross	00,70	HYG
pLinlab1996	64	P_{GPDI} -
PLIMATION	T-0-1	ERG11-
		HYG
pLinlab1918	64	P _{TEFI} -
PLIIIa01918	04	ERG25-
		NEO
"T :"1 ₋ 1,01.40		
pLinlab2148	64	P _{TEFI} -
		ERG26-
		NEO
pLinlab2149	64	P _{TEF1} -
		ERG27-
		NEO
pLinlab2451	This manuscript	P _{TEF1} -
		$ERG25^{H187A}$
		^{H272A} -NEO

pLinlab2416	This manuscript	P _{TEF1} -
		ERG3-NEO
		P _{GPD1} -
		3xFlag-
pLinlab197		SRE1-
6	This manuscript	NEO
		P _{TEF1} -
pLinlab275		URE7-
6	This manuscript	HYG

CHAPTER 4

CONCLUSIONS

Cryptococcus neoformans is a ubiquitous environmental organism that needs to respond to the ever-changing external environment in order to survive. This fungus causes the deaths of hundreds of thousands of patients every year and thus poses a serious public health threat.

Understanding the cell biology of this organism and the mechanisms it employs to respond to external stimuli from the environment can help inform research involved in the clinical treatment of this pathogen. During graduate school I have focused my work on investigating the localization of ergosterol during mating (Chapters 2 respectively), as well as the mechanisms used by C. neoformans to tolerate Ni, a metal commonly found in soils. In the course of my study I discovered that ergosterol levels are heavily impacted by the presence of Ni as well as during the mating process.

In the presence of nutrient limitation, *C. neoformans* will undergo the mating process to produce stress-tolerate spores. These spores are resistant to many stressors such as UV-radiation, heat, and antifungal drugs. We found that spores and basidia in particular were enriched in ergosterol, compared to other cell types such as hyphae and yeast cells when stained with filipin. Thus, we were interested in investigating the role of ergosterol during sporulation (Chapter 2). Indeed, ergosterol is critical for the successful production of spores. Unilateral crosses involving a wild-type strain crossed to a mating partner lacking Sre1, a transcription factor that regulates ergosterol gene transcription, were incapable of producing spores. The basidia produced in these

crosses were capable of maturing to a size typically suitable for producing spores, but despite this were incapable.

Because $srel\Delta$ is involved in regulating the transcription of the ergosterol biosynthesis pathway (EBP) we hypothesized that overexpression of EBP genes would be able to restore sporulation of this mutant. Using $erg3\Delta$ and $erg4\Delta$ mutants we confirmed that disruption of the EBP causes a sporulation defect in unilateral crosses. Furthermore, in bilateral crosses of these mutants, mating overall is reduced. When we overexpressed the EBP genes we discovered that all overexpression strains tested with the exception of ERG27 overexpression were capable of restoring sporulation in the $srel\Delta$. The overall results of this project highlight the importance of ergosterol in the mating process of C. neoformans.

C. neoformans typically grows in soils and is exposed to many stressors in the environment. One of these is the presence of metals in the natural environment. Previous work has been done by several labs investigating how C. neoformans responds to several metals such as Cu, Fe, and Zn. However, the main question that I investigated during my time in graduate school was how C. neoformans responds to Ni (Chapter 3). Bacterial organisms are known to utilize Ni for many critical cellular functions and Ni is actually more abundant in soils compared to some well-studied metals (Zn and Fe).

Via a genetic screen to find mutants sensitive to Ni, I found one gene deletion mutant, sre1Δ. This mutant was sensitive to Ni supplemented into media but not other metals. The growth defect was not due to hyperaccumulation of Ni in this strain, which is known to be toxic. Rather, based on RNA-seq we found that Ni causes a high upregulation of ergosterol biosynthesis pathway (EBP) genes. This upregulation of EBP genes is due to the reduction of ergosterol at the cell membrane when cells are exposed to Ni. Sre1 is known to be the

transcription factor primarily involved in increasing transcription of EBP genes when cells are exposed to hypoxic (low oxygen) environments. A multicopy expression library done in the lab of Dr. June Kwon-Chung showed that ERG25 expression was capable of rescuing the growth of $sre1\Delta$ when exposed to cobalt chloride, a hypoxia mimetic.

When I overexpressed ERG25 in the $sre1\Delta$ mutant I found that it was also capable of restoring growth of the mutant on Ni. We also tested the overexpression of other EBP genes and found that only ERG25 overexpression was capable of causing growth restoration. Erg25 is one of two iron binding proteins in the EBP and contains a histidine enriched binding pocket. I found that site-directed mutagenesis of two of these histidine residues was capable of reverting the growth phenotype back to the $sre1\Delta$. Erg25 exists in abundance in the cell and we hypothesize that Erg25 may be capable of binding Ni, serving as an intracellular chelator. When Erg25 is able to bind Ni in the $sre1\Delta$ mutant, the cells are able to grow despite the presence of Ni in the media. However, if Erg25 is incapable of binding Ni in the mutant background, the cells will not be able to grow.

Erg25 is a highly conserved protein and ergosterol is produced in a similar pathway to cholesterol in mammalian cells. We wanted to see if Ni caused a conserved reduction in membrane sterols. Indeed, exposure to increasing concentrations of Ni reduced the cholesterol in the plasma membranes of lung epithelial cells. In all, we found that sterols are also a critical component of responding to Ni in both fungal and mammalian cells.

In conclusion, our findings in these studies advanced our understanding of the cellular requirements for ergosterol during sporulation and response to environmental Ni stress in *Cryptococcus*.